Small Extracellular Vesicles from Porous Templated Scaffold Resident Cells Modulate $CD4^+$ T Cell Subsets that Promote a Pro-Healing Host Response

Thomas Hady

A dissertation

submitted in partial fulfillment of the

requirements for the degree of

Doctor of Philosophy

University of Washington

2022

Reading Committee:

James D. Bryers, Chair

Kelly Stevens

David Koelle

Program Authorized to Offer Degree:

Bioengineering

University of Washington

Abstract

Small Extracellular Vesicles from Porous Templated Scaffold Resident Cells Modulate $CD4^+$ T Cell Subsets that Promote a Pro-Healing Host Response

Thomas Hady

Chair of the Supervisory Committee:

James D. Bryers

Bioengineering

Porous precision templated scaffolds (PTS) cause a differential foreign body reaction (FBR) dependent on pore size; 40μm pores generate a unique pro-healing response, while larger or smaller pores do not. The mechanisms behind this phenomenon remain unclear. The role of T cells within the host response to PTS is poorly understood, though previous research demonstrates their presence in the PTS microenvironment. Moreover, current cytokine signaling paradigms also cannot fully explain the unique host response to 40μm PTS. Thus, we investigated pore size dependent small extracellular vesicle (sEV) signaling within the PTS microenvironment. Here, we characterize the previously poorly understood properties of cells and sEVs from explanted PTS (pEVs). We then demonstrate that pEV treatment causes phenotypic differences in T cells by stimulating viability, upregulating T_{reg} activation, and modulating the TH1/TH2 ratio; further, T_{regs} significantly contribute to this T cell phenotypic homeostasis and are required for the unique host response to 40μm PTS. Finally, we identify the multiple regulatory roles of MyD88 dependent and independent TLR4 signal transduction in pEV-to-T cell signaling, and provide a detailed proteomic analysis of pEV cargo that details functional immunomodulatory signaling pathways of pEVs. Ultimately, these findings can be used to create engineered sEVs by using biomaterials to influence the phenotype of parent cells in order to create novel patient derived acellular biomedical therapies.

Contents

Table of Figures

Table of Tables

Table of Equations

List of Select Abbreviations

- FBR: Foreign body reaction
- FBC: Foreign body capsule
- PTS: Precision porous templated scaffold
- PMMA: Poly(methyl methacrylate)
- TEGDMA: Tetraethyleneglycol dimethacrylate
- HEMA: 2-hydroxyethyl methacrylate
- pHEMA: Poly(2-hydroxyethyl-methacrylate)
- SEM: Scanning electron microscopy
- M1: Classically activated macrophage phenotype
- M2: Alternatively activated macrophage phenotype
- BMDM: Bone marrow derived macrophage
- TH1: T helper 1 phenotype
- TH2: T helper 2 phenotype
- TH3: T helper 3 phenotype
- TH17: T helper 17 phenotype
- Tr1: Type 1 regulatory phenotype
- T_{reg}: Regulatory T cell
- EV: Extracellular vesicle
- sEV: Small extracellular vesicle
- pEV: sEVs isolated from PTS resident cells
- NTA: Nanoparticle tracking analysis
- TLR: Toll-like receptor
- HSP: Heat shock protein
- GRP: Glucose regulated protein
- PSM: Peptide spectral match
- NSAF: Normalized spectral abundance factor

Acknowledgements

Thank you to Dr. James D. Bryers and Dr. Billanna Hwang. This work would not have been possible without their tireless mentorship; they provided many hours of teaching and guidance on the subject matter of this work and training me as a scientist. Thank you to the current members of the Bryers and Mulligan/Hwang laboratories: Nathan Chan, Sarah Nick, Rachel Waworuntu, and An Tran for providing a wonderful work environment and experimental expertise. I would also like to thank the past members of the Bryers laboratory: Robyn Francisco, Alissa Bleem, and Ruying Chen for their guidance.

We would also like to extend our thanks to the funders of this research: the NIH and NIDCR, grant numbers 5 R01 DE 018701-10 and 5 R01 GM 128991-03. Members of the Bryers Laboratory and UW Dept. of Environmental & Occupational Health Services generated the PTS seeded BMDM transcriptomic data (Neal Beeman, Sengkeo Srinouanprachanh, and James Macdonald). Members of the Mulligan/Hwang Laboratory kindly provided the WT control data for the PTS implantation T cell panel (Rachel Waworuntu and An Tran). Members of the Diabetes Research Center Quantitative and Functional Proteomics Core (Tomas Vaisar) supported by grant P30 DK017047 performed the shotgun proteomic characterization by liquid chromatography mass spectrometry of pEVs. Part of this work was conducted at the Molecular Analysis Facility, a National Nanotechnology Coordinated Infrastructure (NNCI) site at the University of Washington, which is supported in part by funds from the National Science Foundation (awards NNCI-2025489, NNCI-1542101), the Molecular Engineering & Sciences Institute, and the Clean Energy Institute. BioRender helped to generate many figures in this work.

Dedication

This work is dedicated to those who have supported me before and during my dissertation. To my fiancée, Sarah Ianni, for your love and unending support through everything—even a difficult trek full of self-doubt and long hours. Knowing that my life partner has my back makes challenges surmountable and worth conquering. To my parents, Holly and Frank Hady, who raised me to be the person I am today, and now comprise some of my closest relationships. Your kind guidance instilled values and a love of science from a young age, and I value your wisdom in our friendship. To my sister, Joan Marie, for your kindness and dedication. Growing up together and closer as we grow older drives me to be the best person I can be. To Austin Ambrose and Jason Ye, for being the most genuine friends I could ask for. Our friendship has and continues to bring immense joy and fulfillment to life. To Charlie Leonard, Cody Wolterman, Jace Hanson, Liam Fleischmann, Matt Fernandez, Milan Thakkar, Steven Hawker, and Zach Shute, for your ability to pick me up at the end of a hard day. Your quick wits never struggle to bring a smile to my face. To Dr. J. Timothy Stout, for providing tremendous and selfless mentorship, and the opportunity to work in my first biomedical research laboratory during key formative years. With your support, I was lucky enough to find a career I'm excited to continue to pursue daily. Thank you, everyone—you make it all worth it.

Chapter 1: Introduction

1.1: Foreword: A question born of combined problems

Three separate fields contain mysteries that, when combined, form the fundamental question of the research presented herein. First, in biomaterials research, our understanding of the unique host response to 40μm precision porous templated scaffolds (PTS) is limited. Namely, we do not understand the mechanisms by which pore size alone can dictate the host response to an implanted biomaterial scaffold, and why 40μm pores lead to increased cellularization and vascularization in the implant microenvironment regardless of tissue type while other pore sizes lead to enhanced fibrosis in and around the implant. Second, from an immunological perspective, we incompletely understand the role of T cells in the host response to implanted materials. Research has been performed to study the role of different T cell subsets in wound healing, but studies investigating the role of T cells and their subsets in the host response are few and conflicting. Third, in small extracellular vesicle (sEV) research, non-antigen presenting sEV-mediated signaling to T cells is not well characterized. This is particularly true within the context of wound healing. Put together, our research question addresses all three issues synergistically: how do sEVs from PTS resident cells (pEVs) affect the phenotype of T cells to influence the host response to 40μm PTS (**Figure 1**)? Addressing this question has led to results that contribute to these broad issues in biomaterials, immunology, and EV research, but also provides the basis for investigation of a new technology: biomaterials as immunomodulatory EV engineering platforms to inform future therapeutics.

1.2: Specific Aims and Summary of Results

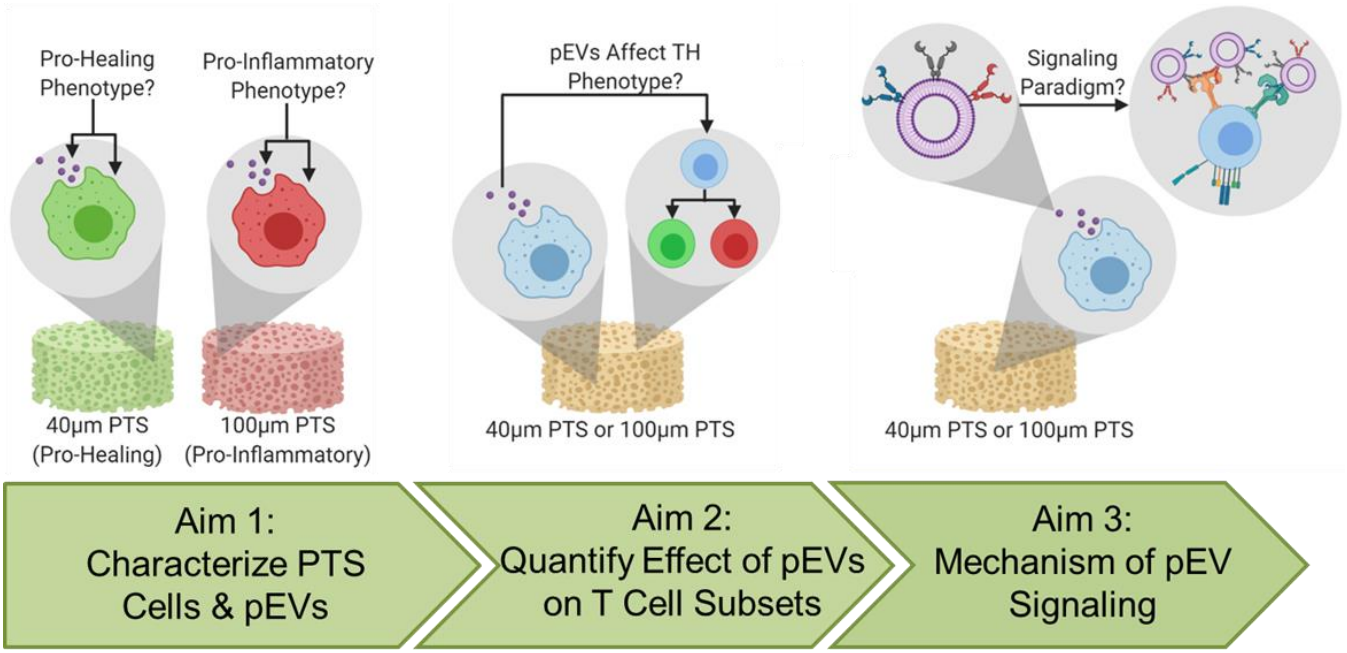

Figure 1: Graphical abstract

Specific Aim 1: Measure the effect of PTS pore size on resident leukocyte populations, crucial myeloid gene expression, and the nucleic acid cargo of pEVs.

Premise: PTS with 40µm pores elicit a pro-healing response upon implantation characterized by increased cellularization, improved vascularization, and decreased collagen deposition in the PTS microenvironment. Previous studies have shown unique macrophage responses to implanted 40µm PTS, but the phenotypes of these cells and associated pEVs remained poorly understood. We hypothesized that 40µm pores would influence macrophages, T cells, and pEVs to pro-healing (i.e. immunomodulatory) phenotypes.

Findings: While pore size barely affected resident leukocyte population profiles, which notably contained macrophages and lymphocytes, there were phenotypic differences between cells resident to 40µm PTS versus those of the 100µm PTS; 40µm PTS resident cells upregulated M2-like and T cell stimulatory markers. PTS residence and pore size also both induced unique changes in the transcriptomic profiles of resident macrophages. pEVs were a monodisperse EV

population 50-200nm in diameter that exhibited unique phenotypes from their parent cells, showing both unique transcriptomic cargo from their parent cells and upregulation of M1 and M2 markers. Moreover, pEVs displayed a disparate myeloid lineage when compared to PTS resident cells. Thus, our results indicated that PTS pore size affected cell phenotype and identified distinct pEV populations that were potential mediators of T cell signal transduction with the PTS microenvironment.

Specific Aim 2: Quantify the ability of pEVs to differentially influence T cell activation, transcription, and subtype based on PTS pore size.

Premise: Despite the crucial role of $CD4^+$ T cells in the determination of wound outcome, the role of T cells in the host response to PTS was previously unexplored. Moreover, biomaterial driven EV signaling to T cells was also under characterized. We hypothesized that pEVs would influence $CD4^+$ T cell phenotypes, affecting T_{reg} populations, in a pore size dependent manner. We also hypothesized that these T_{regs} were an integral part of the host response to PTS.

Findings: To demonstrate the interactions between T cells and pEVs, we visually confirmed that fluorescently labelled pEVs colocalized with T cells. Subsequently, treatment with pEVs from explanted 40μm and 100μm PTS induced phenotypic changes in both immortalized and primary T cells; the TH1/TH2 balance, T_{reg} activation and proliferative activation of primary T cells were all modulated by pEV signaling. These data demonstrated pEV-to-T cell signaling and implicated the adjustment of T cell homeostasis, particularly with respect to T_{regs}, by pEV signaling as potential mediators of the unique host response to 40μm PTS. We therefore characterized the role of T_{regs} in the host response to PTS. Our data indicated that T_{regs} were required to initiate the 40μm PTS specific pro-healing host response to 40μm PTS. Moreover, T_{reg} activation in PTS was dependent on pore size, and T_{reg} depletion prior to PTS implantation demonstrated their critical role in maintaining phenotypic differences in PTS resident T cells to drive differential FBR based on PTS pore size. Together these data demonstrated that pEVs

altered the TH1/TH2/T_{reg} equilibrium, which is modulated by T_{regs}, to determine the host response to PTS. These results further necessitated the explanation of mechanisms driving pEV signaling to $CD4^+$ T cells.

Specific Aim 3: Determine pathways by which pEV-to-T cell signaling may occur, specifically quantifying the role of TLR4-mediated signaling in this capacity.

Premise: While pEV-to-T cell signaling was potent, the specific signaling mechanisms behind this phenomenon were uncharacterized. TLR4 is often classified as a mediator of innate immunity, and has been shown to modulate macrophage phenotype in response to the physical properties of biomaterials; however, TLR4 may also affect $CD4^+$ T cell phenotypes in a manner consistent with the observed results of Specific Aim 2.

Findings: We therefore quantified the phenotype of and TLR4 downstream gene regulation in pEV treated T cells lacking MyD88 and TLR4, hypothesizing that the TLR4 pathway enabled certain aspects of pEV-to-T cell signaling. The MyD88 independent TLR4 pathway heavily regulated $CD4^+$ T cell differentiation driven by pEVs, particularly in those cells treated with pEVs from 40μm PTS, as well as downstream adaptor proteins potentially used in other inflammatory signaling pathways (e.g. the TCR and TLR2). Moreover, MyD88 dependent TLR4 signaling by pEVs caused a downregulation of type I interferons and enabled pEVs from 40μm PTS to downregulate PI3K mediated MyD88 independent responses. However, previously observed pEV induced T_{reg} and TH1 activation were independent of TLR4. Therefore, to further clarify the interactions involved in pEV-to-T cell signaling, we analyzed the proteome of pEVs via liquid chromatography mass spectrometry, hypothesizing that pEVs contained unique immunomodulatory cargo dependent on PTS pore size that may have impacted TLR4 signaling processes. Proteomic analyses of pEVs indicated that they contained immunomodulatory cargo that affected inflammatory signaling and cell adhesion, with significant functional differences between pEVs based on PTS pore size. Additionally, some pEV cargo (e.g. Rho GTPases) had

been previously characterized to contribute to aspects of TLR4 signaling. Finally, we characterized the potent, understudied, and somewhat controversial TLR4 modulating ligands GRP78, GRP94, Gal3, and Gal9 on the surface of pEVs with imaging flow cytometry, and determined that GRP78, GRP94, and Gal9 were all present on the surface of pEVs. These data demonstrated the multiple roles of TLR4 signal transduction in pEV-to-T cell signaling, as well as the unique and heterogeneous nature of immunomodulatory pEV cargo.

1.3: Significance and innovation

Quantifying the underlying mechanism of T cell activation within the context of implanted PTS will benefit the understanding of nontraditional immunological pEV signaling. Specifically, this immunomodulatory signaling modality could establish a misunderstood link between innate and adaptive immunity that may enhance clinical treatments for autoimmune diseases, the FBR, and transplant rejection. While certain types of biomaterials and EVs have been used to induce a pro-regenerative response in previous works, engineering an EV response from innate immune cells by using physical biomaterial characteristics to induce differential cellular phenotypes in adaptive immunity remains novel. In particular, this approach holds promise in affordably engineering individualized biological therapeutics. As pEVs can induce T cell responses, implanted PTS pore sizes could be manipulated to induce a desired effect. These pEVs could easily be used as patient derived, individualized, biologically relevant, low-risk therapeutics. Depending on pore size of the implanted PTS alone, a patient-derived adjuvant with fewer potential complications than current market solutions or a pro-regenerative pEV solution to resolve the FBR could modulate tolerance to medical implants or transplants. To realize these therapeutic developments, however, we had to characterize the pEVs from PTS of different pore sizes and their abilities to induce phenotypic responses in recipient cells.

Chapter 2: Characterization of the PTS and its resident cells

2.1: Introduction: A biomaterial context for the PTS

Medical implants are constantly at odds with the host's response to foreign biomaterials[1]. This response is commonly called the FBR, and it causes device failures in nearly every modern medical field— including, but not limited to, the treatment of cardiovascular[2], neural[3], aural[4], ocular[5], periodontal[6], arthroplastic[7], and dermal[8] pathologies. FBR mediated rejection of biomaterial implants endangers patient health in two ways: through device failure and biological complications of the FBR itself. These failures are costly, requiring an average of $50,000 in further medical care per incident[9–11]. Further, FBR mediated rejection of a medical implant is frustrating for patients due to requisite repeated medical procedures and the loss of regained biological function upon implant failure.

2.1.1: Cellular mechanisms of the FBR

Many different biological phenomena drive the FBR, but the immune system plays an indispensable role in both the genesis and perpetuation of the host response to foreign biomaterials (**Figure 2**). The FBR begins with an acute inflammatory phase upon biomaterial implantation initiated by classical plasma mediated wound healing responses[10,12]. Specifically, proteins are non-specifically adsorbed to the surface of the implanted biomaterial; these are often comprised of chemokines, growth factors, extracellular matrix (ECM) elements, complement proteins, and antibodies[10,13]. Clotting also occurs as platelets activate at the site of implantation[13]. This combination of tissue injury and concentrated blood proteins then causes the recruitment of phagocytes. Neutrophils are the first to arrive, undergoing degranulation to release reactive oxygen species (ROS) and enzymes upon failed phagocytosis of the implanted biomaterial[10]. After a number of days, neutrophils disappear, succeeded by tissue resident macrophages and recruited monocytes[10,13].

As the macrophages in the wound microenvironment attempt and fail to phagocytose the implant, chronic inflammation begins[12,14]. During this phase, lymphocytes and fibroblasts are recruited to the wound microenvironment[10]. These lymphocytes, particularly T cells, are thought to drive inflammation or fibrosis in the wound microenvironment respectively—though their exact mechanistic contributions are not well understood within the broader context of the FBR[10]. Fibroblasts are also activated, resulting in increased collagen deposition onto the surface of the implant[10,13]. Macrophages continue to become frustrated while failing to phagocytose the implanted biomaterial, causing the formation of foreign body giant cells[10,12,14]. This summative encapsulation of the biomaterial implant by both cells and ECM elements (principally collagen) results in the formation of a foreign body capsule (FBC)[10,13]. The FBR thus ultimately results in an equilibrium encompassing chronic inflammation, loss of tissue function, collagenous encapsulation, and inadequate vascularization.

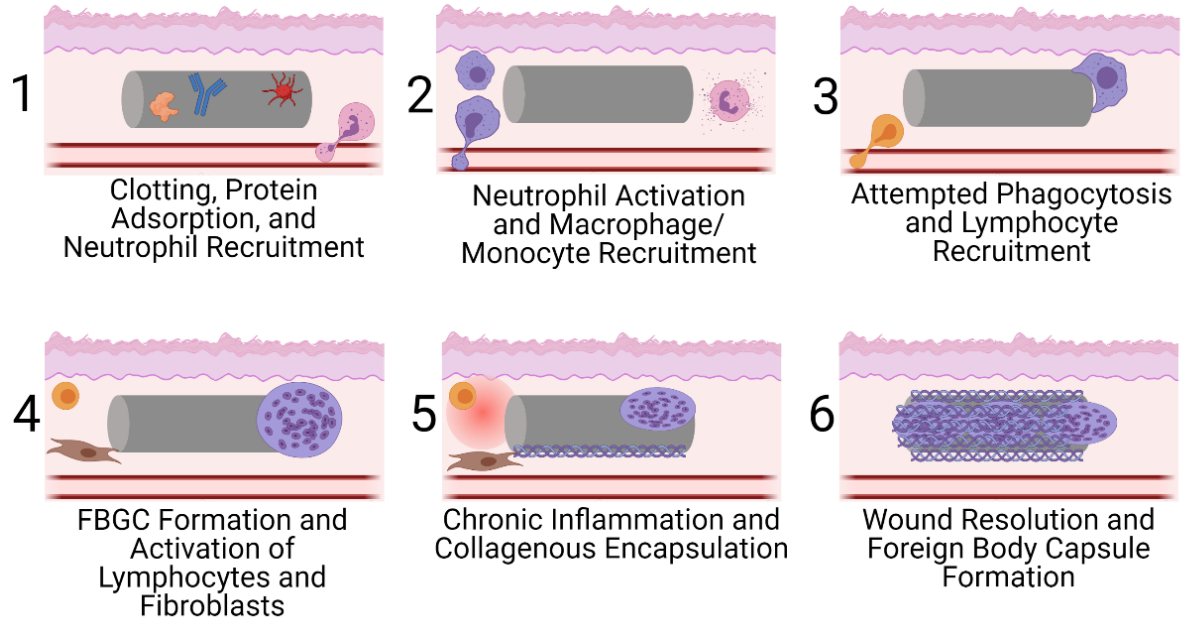

Figure 2: Stages of the foreign body reaction (FBR). This work primarily focuses on the activation of macrophages and lymphocytes, investigating their roles in chronic inflammation in the implant microenvironment.

Macrophage activation is therefore critical in determining the host response to implanted biomaterials[9,10,15]. As macrophages are activated during the FBR, they become polarized to one

of many phenotypes[10]. However, it must be noted that macrophage phenotypic classifications are highly controversial; recent research has demonstrated a rapidly expanding number of possible phenotypes, populations of macrophages that share properties of many different subtypes, and conflicting reports on subtype function[16–19]. Classically, non-polarized macrophages are considered to be M0 macrophages, classical inflammatory activation yields M1 macrophages, and alternative activation yields M2 macrophages[10,20]. M1 macrophages perpetuate type I inflammation, but also cause potent angiogenesis in the implant microenvironment through cytokine secretion[17]. While M2 macrophages generally oppose type I inflammation, they have several different subtypes[10]. Many of these M2 subpopulations induce an opposing type 2 immune response (M2a and M2b), whereas others initiate broad immunosuppression (M2c)[10]. M2 macrophages have also generally been shown to promote tissue remodeling and wound resolution, but also may lead to hypertrophic scarring due to excessive myofibroblast differentiation[18,19].

In addition to the controversies inherent to macrophage subtyping, the roles of M1 and M2 macrophages in wound healing and biomaterial implantation are contentious. Some researchers view M1 macrophages as the primary mediators of angiogenesis and reduced fibrotic encapsulation, while others view them as anti-angiogenic initiators of fibrosis[15,17,18]. Others consider M2 macrophages to be primarily fibrotic, while yet more researchers consider them to modulate fibrosis during acute activation[15,18]. We will therefore focus on the functional effects of individual “M1-like” or “M2-like” markers, while refraining from broad classifications of macrophage phenotype in our work.

2.1.2: Biomaterial development leading up to the PTS

Different aspects of the FBR lead to unique modalities of failure depending on the site and type of biomaterial implant. Implant sequestration by fibrotic encapsulation is particularly problematic for implants that deliver an electrical, mechanical, or chemical payload to the body[21]. The FBC

increases the electrical impedance of the tissue surrounding the implant, thereby partially or completely reducing the efficacy of pacemakers and neural implants[21,22]. The FBC also affects drug eluting implants through altered release kinetics[23]. On the other hand, chronic inflammatory responses can cause material damage to polymeric implants, resulting in implant degradation and worsened inflamamtion[24,25]. Mitigation of the FBR has therefore spawned a multi-billion dollar biomaterials industry dedicated to improving the viability of implanted biomaterials[26].

Efforts to engineer biomaterials to mitigate the FBR have so far undergone three distinct generations[27]. First generation biomaterials were designed to be biologically inert, while providing necessary physical characteristics (e.g. tensile strength)[27,28]. Specifically, first generation biomaterials were chosen to minimize the particulate release, toxic byproducts, and surface bound immunogenic contaminants[29]. Stable metals like stainless steel, high density porous ceramics like zirconia, and highly stable polymers like polymethylmethacrylate (PMMA) were popular materials during this era of biomaterial development[28,30]. As a result of their biological inertia, these passively biocompatible materials successfully avoided dangerous acute interactions with the host. However, the total lack of biological interaction exacerbated certain aspects of the FBR: specifically, chronic collagenous sequestration of the implant[10]. This understanding led to the realization that a total lack of host interaction rendered implanted biomaterials useless for long term therapies.

Second generation biomaterials were therefore engineered for active biocompatibility. These materials were characterized by forcing specific beneficial biological interactions to aid treatment efficacy and tissue integration[28]. Popular approaches to active biocompatibility included engineered biomaterials that were intentionally degradable, facilitated cellular recruitment, or drug eluting[2,27–31]. Materials such as hyaluronic acid, hydroxyapatite, and poly(2-hydroxyethyl-methacrylate) (pHEMA) were of particular interest during this generation of biomaterials research[29,30]. Additionally, functional surface modification of biomaterials was

heavily investigated during this time—the coating of first generation biomaterials (previously used as inert implants) was common to create bioactive, therapeutic materials[30]. Second generation biomaterials thus yielded an improvement in both long term biomaterial viability and pro-regenerative efficacy over first generation materials[28]. The active biocompatibility of second generation materials, however, still required the exploitation of relatively broad tissue-level processes upon implantation.

Third generation biomaterials induced highly specific responses from individual cells to improve wound regeneration (restoration of function)[27]. These materials were largely composed of heavily modified second generation materials: cocktails of growth factors and ECM components were biochemically anchored to the surface of degradable, resorbable materials to drive highly specific cellular functions[32]. Specifically, third generation biomaterials have so far successfully affected relatively late stage processes in wound resolution through cytokine sequestration[33], progenitor cell integration[34], and biomimetic scaffold engineering[35]. These therapies have thereby successfully incorporated tissue engineering strategies to improve pro-healing host responses[28].

2.1.3: The PTS and next generation biomaterials

While previous generations of biomaterials have realized significant progress in characterizing and mitigating the FBR, many critically important biomaterials are still rejected upon implantation[10]. We are currently at the dawn of the fourth generation of biomaterials research: engineering tunable materials that induce cascading and synergistic pro-healing processes in certain subsets of infiltrating cells. Specifically, development of biomaterials that affect the host response through modulation of early stage immune processes in the host are recognized as a key component of next generation of biomaterial therapies[10,20,36]. By manipulating immunologically driven processes within the FBR, next generation biomaterials can optimize both the pro-regenerative (functional restoration) and pro-resolution (wound closure)

components of a healthy pro-healing response. While underexplored, preliminary development of biomaterial mediated immune manipulation to control these immune interactions has proven promising, enabling phenotypic differentiation and polarization to demonstrate preliminary efficacy in mitigating the FBR[37].

The Bryers, Ratner, and Giachelli laboratories have developed the PTS. The PTS is composed of a homogeneous polymer forming uniformly sized, interconnecting pores[38–42]. These highly ordered pores are formed around tightly packed spherical templates, and the interconnections between each pore are roughly 25-33% of the pore size[9,43]. While the gross biomaterial structure remains consistent across all PTS, the polymer composition of the PTS is highly versatile; thus PTS have successfully been synthesized from a variety of different polymer compositions for different biological appliations[41,43,44]. Specifically, recent efforts have been directed towards using polymers in PTS that mimic the mechanical properties of the tissue surrounding the implant to reduce both inflammation and fibrotic encapuslation[45,46].

Remarkably, PTS pore size alone is responsible for FBR modulation and the subsequent determination of implant fate—controlling the development of fibrotic scarring, chronic inflammation, and acceptable healing[38–42]. Regardless of polymer composition, PTS made with 40µm diameter pores exhibited reduced chronic inflammation and elicited pro-healing responses in a diverse array of tissues: skin [39,40,47], cornea [44], heart muscle [42,48], vaginal wall [49], and bone [42]. However, pore sizes larger or smaller than 40µm completely abrogated the pro-healing effects observed in 40µm PTS, instead causing increased foreign body encapsulation and chronic inflammation while reducing implant vascularization[38,39,50].

While porous polymer scaffolds were originally popularized in the second generation of biomaterial development, the PTS has unique properties that necessitate a different generational classification[10]. Specifically, the PTS drives differential host responses consisting of tunable wound resolution and regenerative responses based on physical properties of the

biomaterial itself[10]. As this tunable immunomodulatory response occurs as a result of specific mechanical cues that elicit cellular responses in specific infiltrating leukocytes upon implantation, we view the PTS as a material that bridges the gap between previous and next generation biomaterials.

2.1.4: Current research in the cellular response to PTS

Previous studies have demonstrated that PTS with 30-40μm pores achieved their unique pro-healing response at least partially through immunomodulation. To date, macrophage recruitment and polarization to and around the PTS has been the primary area of study. In 2010, the Ratner group visualized an abundance of macrophages among infiltrating leukocytes and stromal cells in the pores of a 40μm PTS[39]. Subsequently, the Ratner and Murry groups demonstrated that porous templated scaffolds implanted into cardiac tissue increased macrophage recruitment to the implant[51]. Moreover, 40μm pores increased the relative percentage of canonical M2-like macrophages around the implant[51].

The Ratner lab then continued this research with a study that focused exclusively on macrophage polarization, and was therefore able to use more elaborate characterization methods[9]. Therein, the group demonstrated a greater M2-like macrophage presence around the implanted 30-40μm PTS, while macrophages inside of the implant were instead M1-like[9]. While seemingly contradictory, the M2-like macrophages around the implant likely contributed to the observed improved wound resolution, while the M1-like macrophages inside the implant aided in the observed FBC reduction and increased vascular density through the PTS[9,51]. These results indicated the importance of paying special consideration to myeloid cells within the PTS.

While immunomodulation through macrophage recruitment and polarization has recently been shown instrumental in the pore size mediated host response to the PTS, the functional mechanism for pore size mediated differences in the FBR remains unclear. Recent research by the Groll laboratory indicated that pores in fibrous scaffolds caused surrounding macrophages

to elongate based on size[52]. This elongation served as a biomechanical cue to cause M2-like macrophage differentiation, with the greatest efficacy seen in scaffolds with 40μm pores[52]. Work by Garg et al. indicated that the pore size of electrospun scaffolds influenced the phenotype of resident macrophages, and implicated the role of MyD88 (downstream of TLRs)[53]. While this study only investigated pore sizes smaller than 30-40μm in diameter, pore sizes closer to this range yielded higher expression of M2-like macrophage markers. Interestingly, another study implicated MyD88 dependent TLR4 signaling in macrophage responses to other biomaterial cues (substrate stiffness)[54]. However, all of these studies utilized primary macrophages or BMDM—meaning that the investigation of the biomechanical cues associated with macrophage driven differential host responses has historically been performed in isolation. Therefore, other cell types present in the Ratner group's work *in-vivo* are missing in these studies[39]. Thus, other mechanisms behind pore size mediated responses to implanted PTS remain poorly characterized.

2.2: Synthesis of the PTS

2.2.1: Significance

PTS synthesis and characterization before implantation are vital to investigation of the cells within implanted PTS. While PTS synthesis has been defined in previous research, the method has changed slightly in recent years[38,43,51]. Specifically, the commercial availability of monodisperse PMMA beads has eliminated the need for initial bead sieving, as well as changed bead sintering and storage conditions. As the pore and throat sizes of PTS are of critical importance to their viability as an implanted biomaterial, we herein demonstrated that our synthesized PTS met the physical requirements necessary to investigate the pro-healing response intrinsic to the 40μm PTS.

2.2.2: Materials and Methods

(Section adapted from Hady et. al, 2020)

2.2.2.1: *PTS synthesis*

A sphere-templating method (**Figure 3**) was used to create three dimensional porous polymer scaffolds with scalable, uniformly sized pores and pore interconnects[51,55,56] (Patent US208/075752A1). PTS were fabricated as previously described[57]. PMMA beads (40µm and 100µm OD) were obtained from Microbeads AS (Skedsmokorset, Norway). A mold was created by placing 1 mm thick Teflon strips (2 mm wide) to serve as a retaining gasket between two 75 mm x 25 mm x 1 mm glass slides. Beads of the desired pore size were poured into the cavity. Molds filled with beads were placed in a water bath sonicator for 2 hours to uniformly pack the beads. Beads were then sintered to each other by heating at 175°C (40µm) or 179°C (100µm) for 24 hrs. Sintering time and temperature were determined to create templates where interconnects between beads were 25-33% of the bead diameter. Poly(hydroxyethyl methacrylate) was selected over other polymers for its superior performance in histology dissection, biological inertness, and stability. HEMA monomer solution was made up of 5 mL 2-hydroxyethyl methacrylate (HEMA) (Polysciences, ophthalmic grade), 0.23 mL tetraethyleneglycol dimethacrylate (TEGDMA) (Polysciences), 2.0 mL deionized water, 3.6 mL ethylene glycol, and 20 mg 2, 2-dimethoxy-2-phenylacetophenone (Irgacure 651) (BASF, Freeport, LA). The PMMA bead template was infiltrated with monomer solution for 30 minutes under vacuum to ensure degassing. HEMA monomer was free-radical polymerized to pHEMA under a 450W broad-spectrum UV lamp for 15 minutes. The product was then removed from the glass slide mold, and immersed in acetone washes to dissolve the PMMA bead template. Acetone was changed when cloudy, and product was washed until acetone was clear. The pHEMA PTS were then separated into discs using a 5mm biopsy punch.

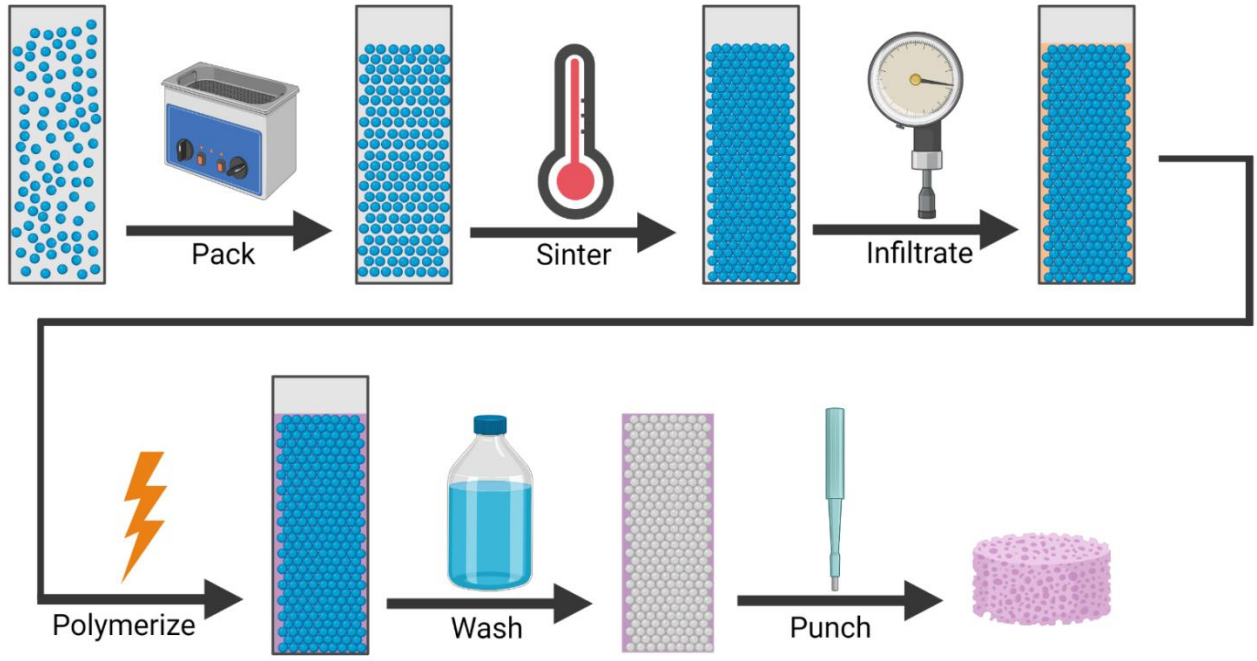

Figure 3: Precision porous templated scaffold (PTS) fabrication process. PMMA beads were first placed into a mold, and packed via manual force and sonicator. Beads were then sintered in an oven, and infiltrated with HEMA monomer solution. HEMA was then polymerized into pHEMA under UV light, and the PMMA beads were washed out using acetone washes. The resulting PTS were then punched into discs using a biopsy punch.

2.2.2.2: *PTS characterization*

To ensure correct pore and interconnect sizes, lyophilized PTS were analyzed via scanning electron microscopy (SEM). PTS were sputter coated for 120 seconds with gold/palladium to form a 20nm conductive layer. SEM was then performed on the scaffolds using an FEI SEM XL Siron at 5 kV. Cross sectional and surface views of the PTS were observed in order to ensure uniform pore and interconnect sizes; ImageJ was used to measure the pore and interconnect diameters.

2.2.3: Results

Upon determination of correct sintering conditions for 40µm and 100µm PMMA beads, tightly packed, ordered spherical templates were formed. Importantly, there appeared to be minimal plastic degradation of the bead structure, ensuring spherical pores in the subsequently formed

PTS (**Figure 4A-B**). It must be noted, however, that the sintering conditions of beads of both sizes were highly dependent on the batch and manufacturer of the beads. Moreover, quality control of beads via SEM was highly necessary—as certain batches of beads had “pinhole” defects, which drastically altered sintering time and bead size after sintering (**Figure 4C**). Finally, anecdotal evidence indicated that optimal sintering conditions for beads of both sizes became more mild (decreased time and/or temperature) the longer beads were stored. Periodic assessment of sintering conditions via SEM analysis of the spherical template is therefore necessary to create PTS with proper interconnect sizes.

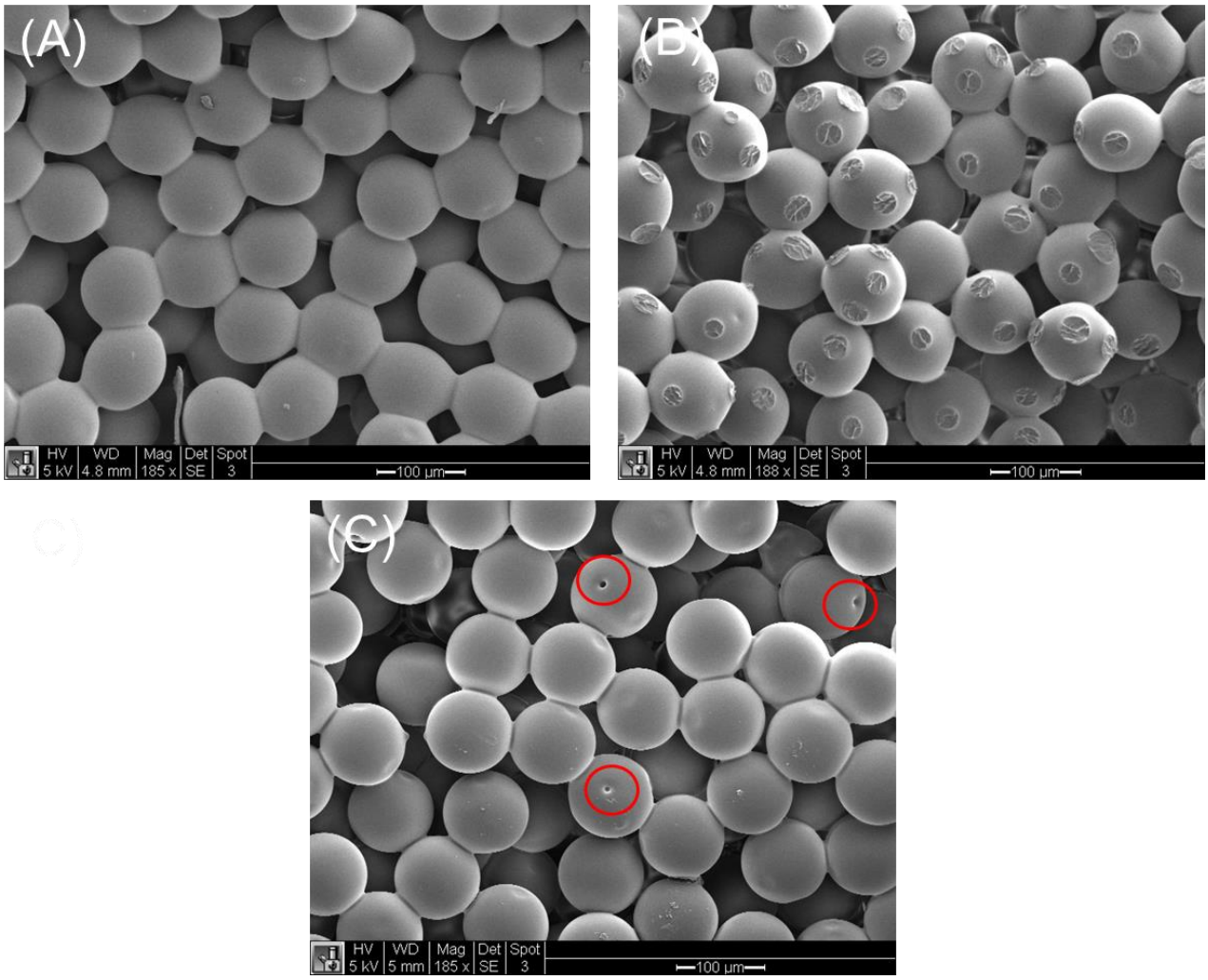

Figure 4: Scanning electron microscopy images of sintered 100µm bead templates. (A) top view of sintered 100µm bead template; (B) cross section of sintered 100µm bead template split with a razor blade; (C) defects in specific batch of 100µm beads in sintered bead template (red circles).

PTS with both 40µm and 100µm pore sizes demonstrated uniformly sized and interconnected pores with a highly ordered structure (**Figure 5**). Moreover, there were no remaining PMMA beads within or leftover solid pHEMA skin on the surface of the finished PTS. The final pore sizes of three representative PTS of both pore sizes were within specifications: PTS formed with 40µm PMMA beads had pores just under 40µm in diameter [31.54-38.49µm], and PTS formed with 100µm beads had pore sizes just under 100µm in diameter [79.19-92.78µm]. The interconnect sizes of these representative PTS were also correct, as they were 25-33% the diameter of the pores for both 40µm PTS [9.84-13.04µm] and 100µm PTS [25.26-35.49µm].

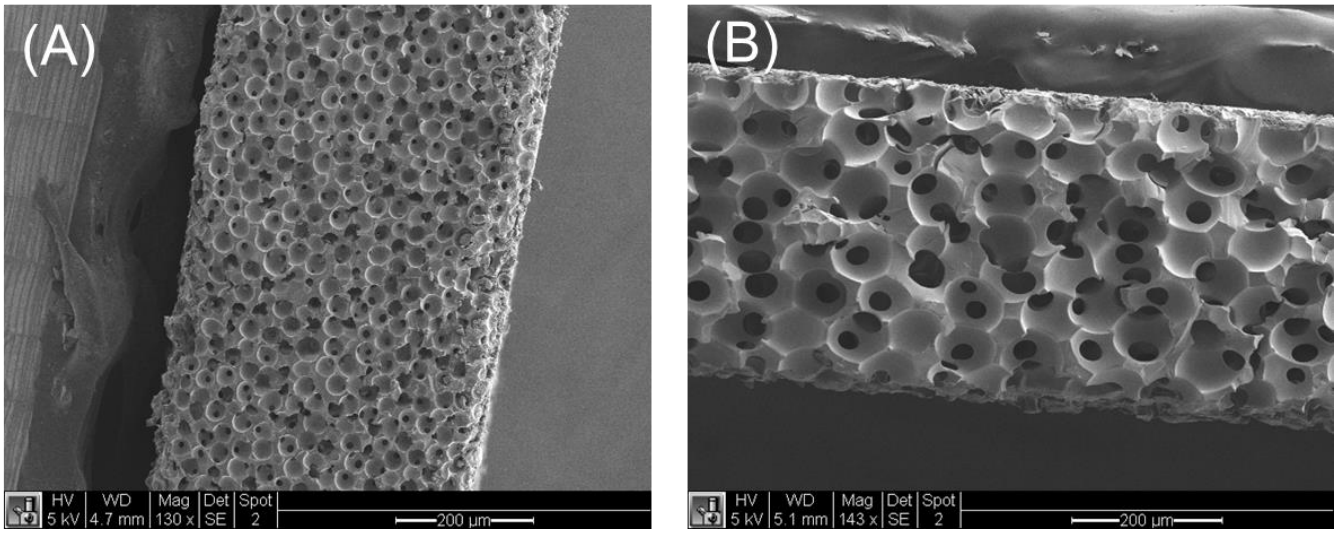

Figure 5: Scanning electron microscopy images of PTS. (A) 40µm PTS; (B) 100µm PTS.

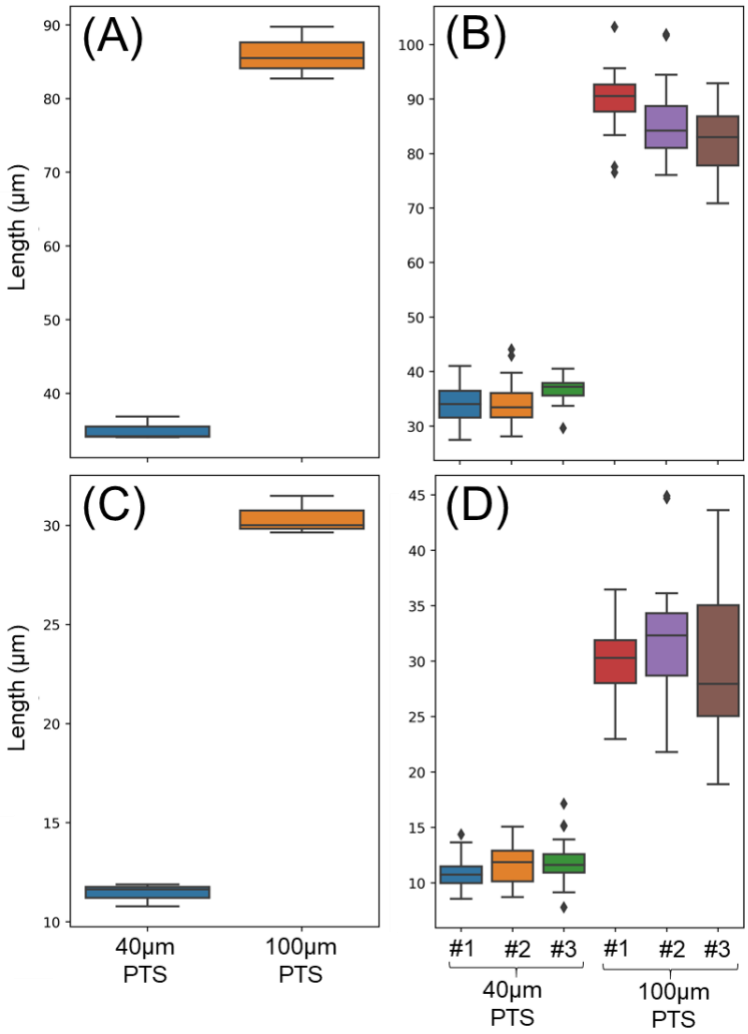

Figure 6: Measurements of pore and interconnect size from scanning electron microscope images of 40µm and 100µm PTS. (A) Average measured PTS pore size in µm (25 pores per PTS, N=3); (B) Individual pore size measurements from each representative PTS; (C) Average measured PTS interconnect size in µm (40 interconnects per PTS, N=3); (D) Individual interconnect size measurements from each representative PTS. Box plot whiskers represent the minimum (Q1-1.5*IQR) and maximum (Q3+1.5*IQR), the box boundaries represent the IQR, and the line bisecting the box the median; outliers (greater than maximum or less than the minimum) are represented as diamonds. These notations are consistent through the document.

2.3: Investigation of PTS resident cells

2.3.1: Significance

The cellular response to implanted PTS is still not well understood. While previous work has demonstrated that macrophages were both abundant and required to elicit the pro-healing response to implanted 40µm PTS, an understanding of what other cells resided within implanted

PTS remained lacking. Previous research has also focused on designation of PTS resident cells as M1-like or M2-like macrophages[9]. While this research excellently demonstrated the complex interplay between M1-like and M2-like macrophages necessary for the unique host response to 40µm PTS, describing whole macrophages as either M1-like or M2-like is an oversimplification of macrophage biology that necessitates a more detailed explanation of individual gene regulation (those of which may still be designated as M1-like or M2-like phenotypic indicators) to explicate underlying macrophage processes within this context. We therefore investigated the lineage, phenotype, and the transcriptome of PTS resident cells, paying special attention to macrophages, in order to better understand the mechanisms driving differential responses between implanted 40µm and 100µm pore size PTS.

2.3.2: Materials and Methods

(Section adapted from Hady et. al, 2020)

2.3.2.1: *In-vivo PTS implantation and explant sample collection*

PTS were rehydrated in PBS and implanted subcutaneously in male and female C57/Bl6 mice (strain #000664) 6-8 weeks of age. Using aseptic technique, mice were anesthetized with isoflurane and a mid-sagittal dorsal incision 1.5cm long was made. PTS were inserted on both sides of the incision under the skin, ensuring that the scaffold laid flat and did not fold. The wounds were sealed with wound clips. The scaffolds were removed after one week and cultured for two days in RPMI 1640 containing 10% FBS and 1% penicillin streptomycin in 12-well plates. Cells recovered from the scaffold were separated by centrifugation.

2.3.2.2: *PTS resident cell population profiling*

First, cells recovered from the PTS were hemolyzed and separated from debris with a 40µm cell strainer. The cells were then counted with a trypan blue live/dead cell stain to assess viability and total cell number. White blood cell differentials were then performed on the cells recovered

from PTS. Briefly, 200µL of cells were put into a Simport plastic funnel (ThermoFischer) with an attached slide, and spun for 5 minutes at 750rpm on a Cytospin3. The cells were then fixed with methanol and stained using Hema 3 Stat Pack (Fisherbrand). The number of macrophage, lymphocytes, basophils, eosinophils, and neutrophils were quantified until 200 total cells were counted. To assess the number of viable PTS resident cells of each type, the proportion of each cell type was multiplied by the total number of live cells recovered from the PTS.

2.3.2.3: *Transcriptomic analysis of PTS resident cells*

Cell samples recovered from explanted PTS were processed with RNeasy Mini kit as per manufacturer's protocol (Qiagen) and used to generate cDNA as per manufacturer's protocol (Applied Biosciences). qPCR was performed with SYBR green probes on an ABI 7900HT. Thermal cycling parameters were as follows: 50°C for 2 minutes, 95°C for 10 minutes, then 40 cycles of 95°C for 15 seconds followed by 60°C for 1 minute. The macrophage characterization panel included PPIA, ARG-1, CD86, CD206, FIZZ-1, IL-10, iNOS, TGF-β1, TNFα, and YM1 (primer sequences available in **Table 1**). Rationale for this panel can be seen in **Table 1**. Ct was considered undetermined if one or both replicates failed to amplify. Results were expressed in relative fold expression by normalizing against housekeeping genes (PPIA) and expressed as $2^{(-\Delta Ct)}$ where $-\Delta Ct$ is Ct_{target}-$Ct_{housekeeping}$.

Gene	Macrophage Phenotype	Primer Sequences
ARG-1	M2-like	F: TTTTAGGGTTACGGCCGGTG R: CCTCGAGGCTGTCCTTTTGA
CD86	M1-like	F: AACTTACGGAAGCACCCACG R: CTCCACGGAAACAGCATCTGAG
CD206	M2-like	F: TTCAGCTATTGGACGCGAGG R: GAATCTGACACCCAGCGGAA
FIZZ-1	M2-like	F: ACTTCTTGCCAATCCAGCTAAC R: CAAGCACACCCAGTAGCAGT
IL-10	M2-like	F: TGCAGGACTTTAAGGGTTACTTG R: TCAGCTTCTCACCCAGGGAA
iNOS	M1-like	F: GCCACCTTGGTGAAGGGACT R: ACGTTCTCCGTTCTCTTGCAGT
TGF-β1	M2-like	F: AGCTGCGCTTGCAGAGATTA R: AGCCCTGTATTCCGTCTCCT
TNFα	M1-like	F: GTCCCCAAAGGGATGAGAAGT R: TTTGCTACGACGTGGGCTAC
YM1	M2-like	F: CTGTGGAGAAAGACATTCCAAGG R: CAAGAGACTGAGACAGTTCAGGG
PPIA	Housekeeping	F: GTCTCCTTCGAGCTGTTTGC R: GCGTGTAAAGTCACCACCCT

Table 1: Macrophage gene expression panel. Genes of the macrophage RT-qPCR panel and their associated macrophage phenotypes.

2.3.2.4: *BMDM isolation, culture, and microarray analysis*

BMDM culture and RNA isolation performed by the Bryers Laboratory, Clariom S Microarray and processing of raw .CEL data was performed by the Department of Environmental and Occupational Health Sciences.

The femur, tibia, and fibula were removed from euthanized WT C57Bl/6 mice and separated from the muscle. The ends of each bone were cut on both sides to reveal the marrow, which was rinsed out of the marrow pocket with DPBS. The pellet was then resuspended in 15mL of medium (RPMI 1640 with GlutaMax, 10% FBS, 1% penicillin/streptomycin) and plated onto a 100mm^2 non-TC treated petri dish. Recombinant murine MCSF (Peprotech, cat. #315-02) was added to the medium and mixed thoroughly at a concentration of 20ng/mL. After 4 days of incubation with minimal disturbances, 10mL of medium with 20ng/mL of recombinant murine

MCSF was added to the culture. Three days later, the medium was discarded and the differentiated macrophages were removed from the bottom of the plate via a cold DPBS wash.

PTS were first rehydrated. BMDMs were then seeded in PTS with 40μm and 100μm pores as previously described[58]. Briefly, BMDMs were resuspended at a concentration of 10 million cells/mL in PBS. Rehydrated PTS were placed on an autoclaved KimWipe folded twice, and 50μL of BMDM cell suspension was added to the top of the PTS. Once there was no liquid visible on the top of the PTS, another 50μL of cell suspension was added to the top of the PTS. The PTS was then inserted into a PTFE transwell (Millicell, cat. #PICM03050) in a 6 well plate with 3mL medium. After 2 weeks of culture, the PTS was removed, rinsed in DPBS, and placed against a piece of filter paper. The PTS was then placed into TRIZOL (Ambion) and frozen at -80°C. The sample was then ground using a pestle, sonicated for 5 minutes in ice water, and subjected to chloroform extraction. The RNA was then isolated from the aqueous phase with RNeasy Mini with DNase digestion kit as per manufacturer's protocol (Qiagen). RNA was run on an Agilent 2100 bioanalyzer to ensure RINs were between 9.6 and 10 for each sample. 200ng of RNA was then hybridized to a Clariom S Microarray (Affymetrix) for 17 hours and scanned on a Fluidics 450 and 7500G scanner. The RMA algorithm of the Bioconductor package in R was used to normalize expression data.

The expression data was then subjected to a 3 dimensional principal component analysis (PCA) using Python's SKLearn package. The 95% confidence interval for each sample group was then quantified, and mapped on each 2 dimensional representation of the 3 dimensional PCA in order to assess sample homogeneity. The gene expression data of those genes differentially regulated as a function of treatment condition were then subjected to a 2 dimensional PCA. This PCA was used to assess the uniqueness of transcriptomic differences between treatment conditions.

2.3.2.5: *Statistical analyses*

First, a Shapiro-Wilk test was performed in order to assess data normality at $\alpha=0.10$ (determined via Q-Q plot examination). If the data was determined to be normal and the comparison was pairwise, a two-sided Student's t-test was performed at $\alpha=0.05$. If the data was normal and the comparison was between 3 or more conditions, an ANOVA at $\alpha=0.05$ with a subsequent Tukey-Kramer posthoc test was performed if $p<0.05$. If the data was non-normal and a pairwise comparison was performed, a two-sided Mann-Whitney U test was performed at $\alpha=0.05$. If the data was non-normal and the comparison was between 3 or more treatment conditions, a Kruskal-Wallis at $\alpha=0.05$ with a subsequent Conover-Iman posthoc test (using a two-stage Benjamini Hochberg correction for FDR) was performed if $p<0.05$.

2.3.3: Results

The number and viability of PTS resident cells from 40μm and 100μm PTS was first quantified via cell count. The total number of cells and the total number of live cells were not significantly different between cell populations from 40μm and 100μm PTS. However, significantly more dead cells were recovered from the 100μm PTS compared to the 40μm PTS (**Figure 7**, $p=0.024$, $N=5$). Differential blood counts on PTS resident cells revealed that leukocyte populations within the PTS after one week of implantation did not appear to be a function of pore size, as the total number of viable leukocytes of each type observed were not significantly different between cell populations from 40μm and 100μm PTS (**Figure 8**). Both 40μm and 100μm PTS displayed a predominant (~85%) macrophage population, and similar smaller populations of lymphocytes (~3%), eosinophils (~6%), and neutrophils (~6%) (**Figure 9**). While there were slightly proportionally more neutrophils in 100μm PTS ($N=5$, $p=0.0453$), this result is not supported by the more important total viable neutrophil cell count in the PTS.

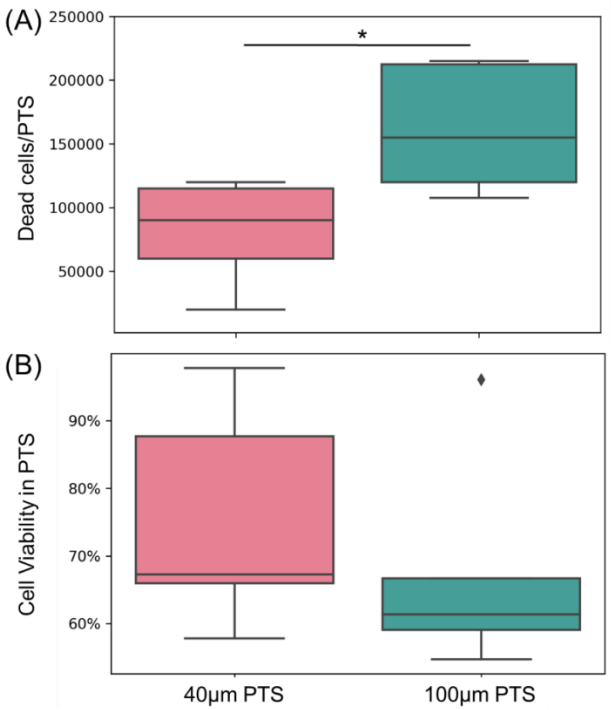

Figure 7: Comparison of cellular viability in implanted PTS. Number of dead cells (A) and cell viability (B) in PTS resident leukocytes after 1 week of subcutaneous murine implantation (*, p>0.05, N=5; significance was determined via two-sided T or Mann-Whitney U test based on normality assessed by Shapiro-Wilk test, see 2.3.2.5: for details).

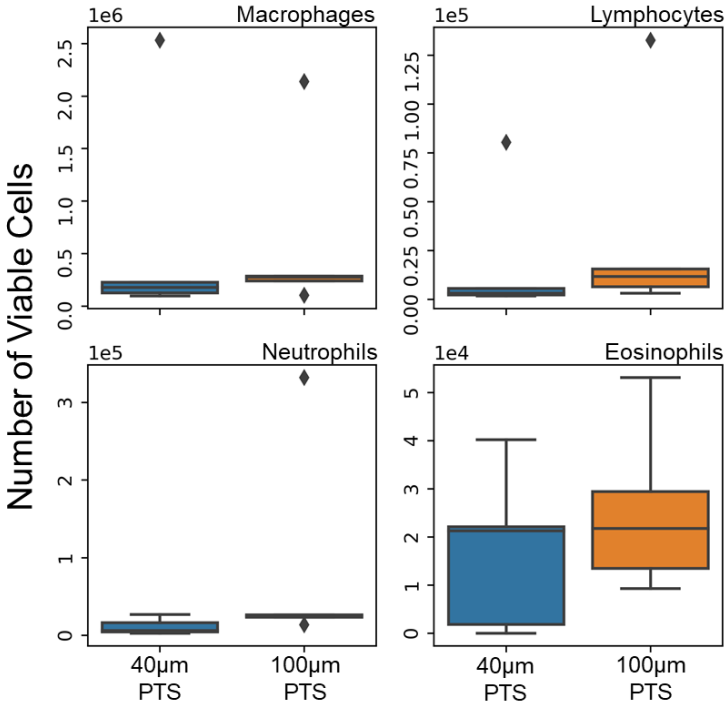

Figure 8: Classification of viable PTS resident leukocytes. Cells resident to PTS were classified by a WBC differential after 1 week of subcutaneous murine implantation in 40µm PTS (A) and 100µm PTS (B)

(*, p>0.05, N=5; significance was determined via two-sided T or Mann-Whitney U test based on normality assessed by Shapiro-Wilk test, see 2.3.2.5: for details).

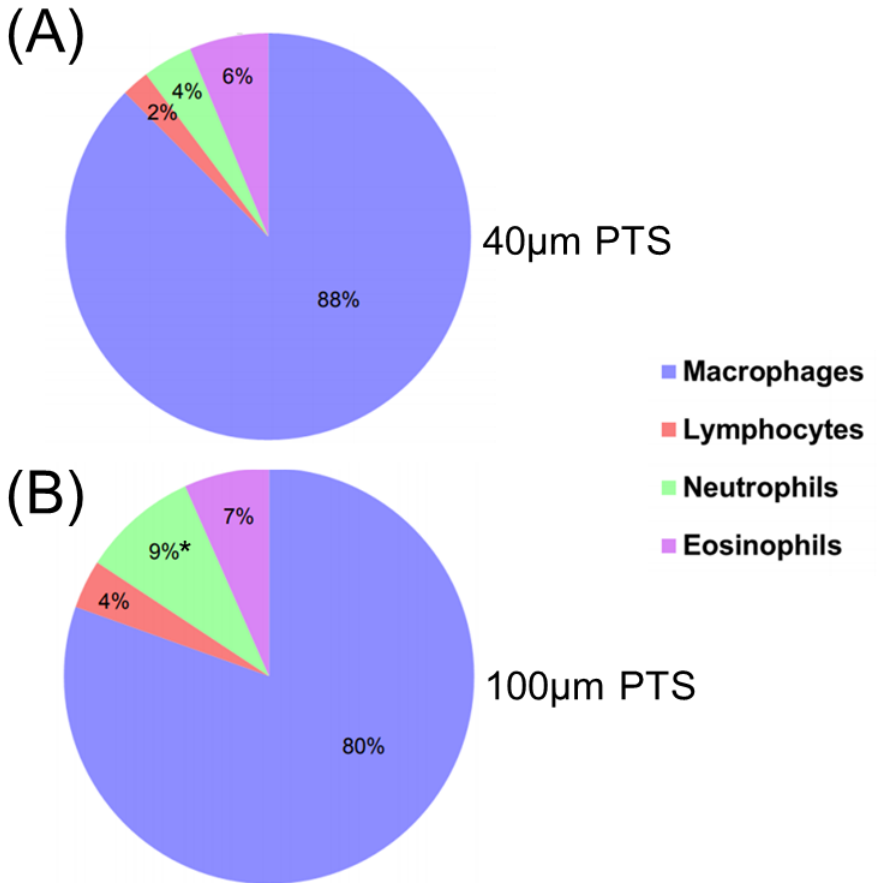

Figure 9: Proportion of PTS resident leukocyte populations. Leukocytes were characterized by a WBC differential after 1 week of subcutaneous murine implantation in 40µm PTS (A) and 100µm PTS (B) (*, p>0.05, N=5; significance was determined via two-sided T or Mann-Whitney U test based on normality assessed by Shapiro-Wilk test, see 2.3.2.5: for details). Average leukocyte proportions are displayed.

The phenotypic differentiation and activation within specific leukocyte subpopulations further aided in explaining the differential host responses between 40µm and 100µm PTS. RT-qPCR of PTS resident cells (**Figure 10**) demonstrated that the phenotypes of macrophages resident to explanted PTS were affected by pore size. 40µm PTS resident cells obtained after 1 week of implantation significantly upregulated the M2-like markers ARG-1 and FIZZ-1, as well as the M1-like marker CD86 (ARG-1 p=0.041, FIZZ-1 p=0.03, CD86 p=0.023, 40µm PTS N=6 and 100µm PTS N=5). Regulation of critical macrophage polarization markers and genes capable of T cell activation in PTS resident cells were thus a function of PTS pore size.

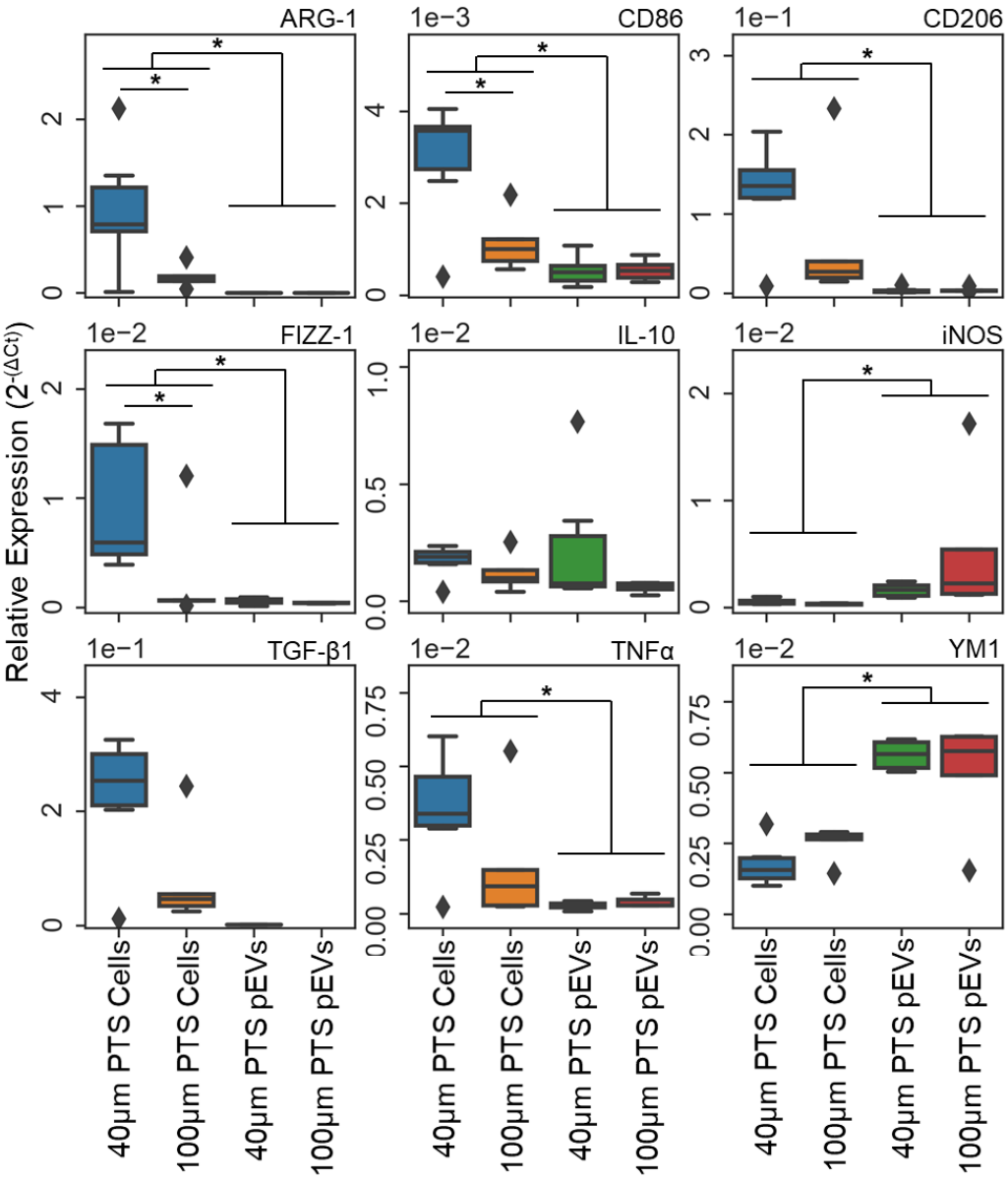

Figure 10: Macrophage gene expression in PTS resident cells and pEVs. RT-qPCR was run on mRNA from cells and pEVs from implanted 40µm and 100µm PTS. Gene targets were contained in the macrophage panel denoted in **Table 1** (*, $p<0.05$, N=6 for 40µm PTS and N=5 for 100µm PTS; significance was determined via two-sided T or Mann-Whitney U test based on normality assessed by Shapiro-Wilk test, see 2.3.2.5: for details). Pairwise comparisons were drawn between the following groups: 40µm PTS cells vs. 100µm PTS cells, 40µm PTS pEVs vs. 100µm PTS pEVs, and all PTS cells vs. all PTS pEVs.

The transcriptome of PTS resident macrophages (the predominant cell type within the PTS) was then analyzed via microarray to assess the phenotypic differentiation induced by PTS residence (microarray data provided courtesy of the Bryers laboratory). Specifically, the phenotypes of

BMDMs seeded within the PTS for 2 weeks were analyzed via principal component analysis (PCA) of the gene expression data (**Figure 11A**). The 3 dimensional PCA encapsulated 62% of the differences between each sample group: BMDMs resident to 40μm PTS, 100μm PTS, and TC plastic. PC1 captured 25.3% of the differences, PC2 19.5%, and PC3 17.2% (N=3). The PCA demonstrated highly distinct clustering based on sample group, indicating distinct macrophage phenotypes as a function of PTS residence and pore size. In order to assess the uniqueness of differences between each sample group, a 2 dimensional PCA on genes that were differentially expressed in any one of the three treatment groups was performed (**Figure 11B**). This PCA captured 76% of the differences between each sample group, with PC1 capturing 45.6% of the differences and PC2 31.2%. This PCA demonstrated extremely distinct clustering, especially along PC1, which indicated that the differences between each sample group were unique to each treatment condition.

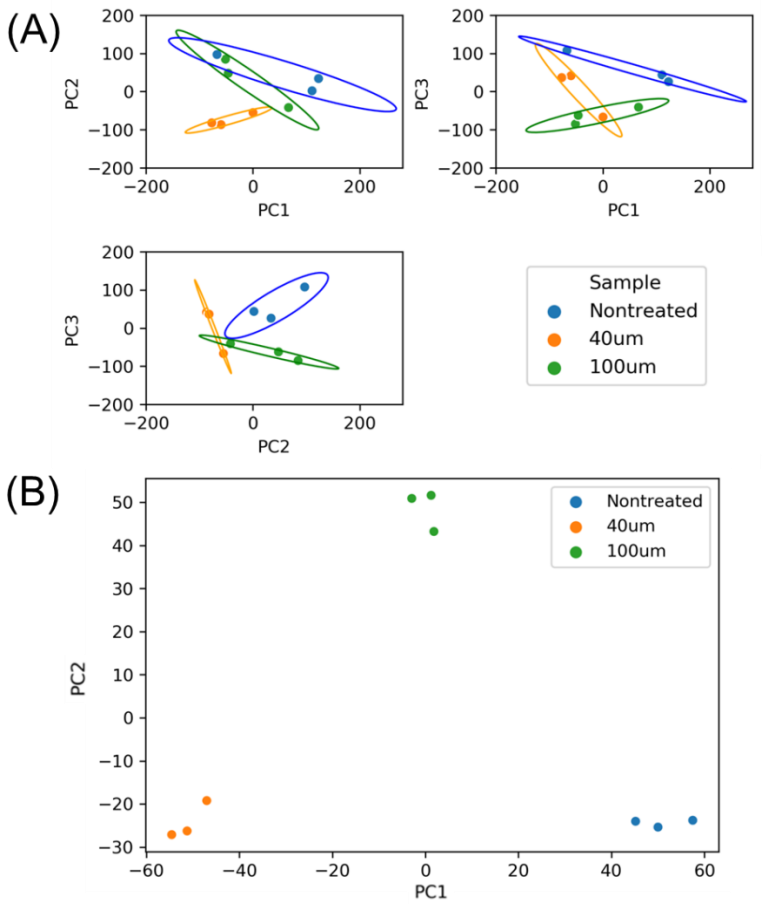

Figure 11: Principal component analyses of Clariom-S microarray run on bone marrow derived macrophage (BMDM) seeded in 40µm and 100µm PTS for 14 days. (A) 3 dimensional PCA of all genes expressed in the microarray; 62% of differences were captured (PC1: 25.3%, PC2: 19.5%, PC3: 17.2%); circles represent 95% CI. (B) 2 dimensional PCA of differentially expressed genes in the microarray; 76% of differences captured (PC1: 45.6%, PC2: 31.2%). Microarray data provided courtesy of the Bryers laboratory.

2.4: Discussion: Characterization of the PTS and its resident cells

The characteristics of synthesized PTS with both 40µm and 100µm pores were consistent with those of prior works[39,56]. Specifically, PTS pore sizes were just under 40µm and 100µm in diameter, and the interconnects between each pore were between 25% and 33% the size of each pore. While some previous studies have relied on sifting beads through a sieve mesh to obtain a population of correctly sized PMMA spheres, off-the-shelf monodisperse PMMA beads provided similar results[9]. However, these results do reinforce the need for periodic SEM-based

QC of beads, sintered templates, and resulting PTS generated using this method. Regardless, the manufactured PTS were within specifications for further experimentation.

PTS resident leukocyte profiles were nearly identical, regardless of pore size—particularly with respect to macrophage and lymphocyte populations. Given our current understanding of the FBR and host response to implanted PTS, these cells (along with neutrophils and a small population of eosinophils) are expected to be present in the PTS microenvironment, particularly within the first week of the FBR. However, pore size did affect the number of dead cells in and around the PTS; while the cellular viability was not significantly different as a function of pore size, the increased number of dead cells recovered from 100μm PTS may implicate the participation of non-40μm pores in the induction of certain inflammatory processes (e.g. reactive oxygen species release or cellular apoptosis).

The phenotypes of macrophages recovered from the PTS were dependent on pore size. Specifically, cells resident to 40μm PTS upregulated traditionally M2-like pro-regenerative macrophage polarization markers ARG-1 and FIZZ-1 when compared to cells resident to 100μm PTS. In addition to being an M2-like macrophage marker, ARG-1 participates in wound healing processes and inhibits the inflammatory iNOS via the hydrolysis of its substrate L-arginine[59]. Additionally, both ARG-1 and FIZZ-1 downregulate inflammatory and fibrotic responses caused by T Helper 2 (TH2) cells[60,61]. Although it is traditionally an M1-like marker, 40μm PTS resident cells upregulated CD86 expression. As CD86 is a CD28 ligand, these cells may be predisposed to the activation of T cells, as CD28 binding is part of the costimulatory signaling paradigm necessary for T cell activation. Thus, 40μm PTS resident macrophages displayed a unique phenotype via the upregulation of markers and signaling molecules implicated in increased pro-regenerative and T cell stimulatory processes. These observations corroborate and expand upon those of prior studies from the Ratner laboratory, which demonstrated the simultaneous

upregulation of M2-like macrophage markers around and M1-like macrophage markers within the 40μm PTS microenvironment[9].

Transcriptomic data gathered from PTS resident BMDMs via microarray also demonstrated unique macrophage phenotypes as a function of pore size. According to the PCA, residence in a PTS of either pore size induced unique phenotypes in resident cells. Moreover, 40μm pores and 100μm pores also induced distinct cellular phenotypes. The differences between each sample group were also highly dissimilar, as each sample group formed tight clusters upon examination of differentially regulated genes. Additional overlap between PTS resident sample groups in both PCAs would be expected if differential macrophage phenotype was simply a result of 3 dimensional versus 2 dimensional tissue culture conditions. Thus, PTS residence itself induced unique phenotypic differentiation in macrophages, and 40μm pores further adjusted this phenotype.

Chapter 3: Characterizing the role of T_{regs} in the host response to implanted PTS

3.1: Introduction: T cells in the unique host response to PTS

(Partially adapted from Hady et. al, 2020)

The Ratner group first identified T lymphocytes in explanted PTS, and our recent observations corroborated their findings[39]. While T cells have been well characterized within the context of classical wound healing, the specific functions of T cells in FBR modulation remain poorly understood[62]. Due to their potent moderation of the wound microenvironment, we will herein focus on $CD4^+$ T cells as opposed to $CD8^+$ T cells. Prior studies have shown that $CD4^+$ T cells are abundant in implanted synthetic biomaterial scaffolds and may be crucial in facilitating pro-healing aspects of these host responses[63–65]. Despite $CD4^+$ T cells' presence and dramatic effect on wound healing outcome, we do not yet understand their role in the unique host response to implanted PTS[66,67]. Investigation of $CD4^+$ T cell phenotype within the implanted PTS was therefore crucial, as these cells exhibit powerful subtype dependent inflammatory or regenerative effects to determine implant fate [68]. Each T_{helper} subtype plays a unique role within the context of wound healing and has a suspected contribution to the FBR, summarized in **Figure 12**.

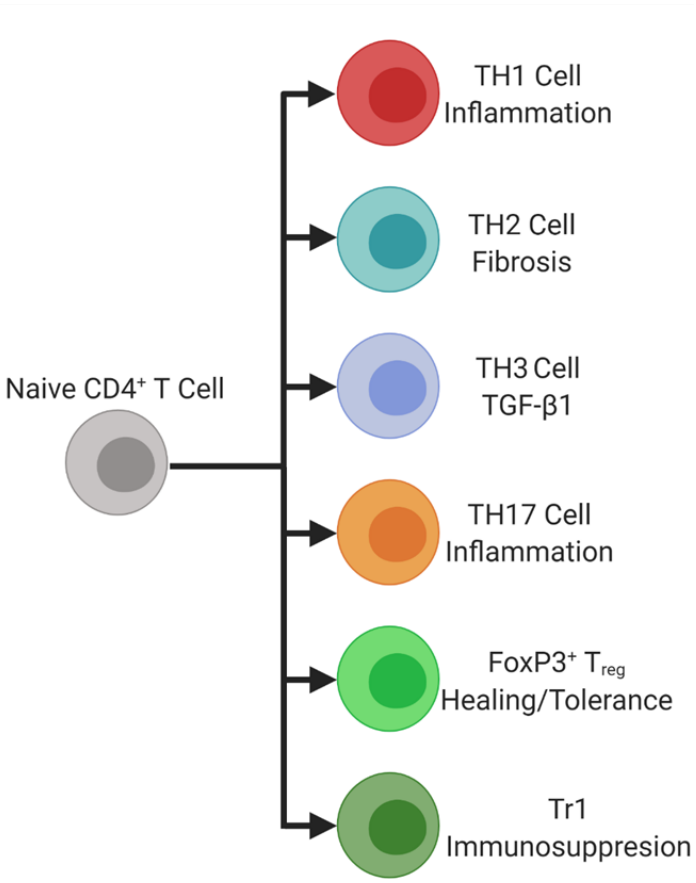

Figure 12: Different roles of CD4$^+$ T cell phenotypes in wound healing responses. T_{regs} play a unique role in maintaining unique CD4$^+$ T cell equilibriums in wound healing, thereby making them crucial to the host response to foreign biomaterials.

3.1.1: T_{regs} in wound healing and FBR modulation

Regulatory T cells (T_{regs} often indicated by IL-10 secretion and FoxP3 expression) are instrumental in initiating and maintaining anti-inflammatory pro-healing responses[68,69]. T_{regs} may either be natural T_{regs} (nT_{regs}) recruited from the thymus or peripherally induced T_{regs} (iT_{regs}), though the exact role of this distinction in wound healing is not completely understood[70]. While nT_{regs} always express FoxP3, iT_{regs} may or may not: T regulatory 1 cells (Tr1) are iT_{regs} that do not express FoxP3, but still exert immunosuppression through IL-10 secretion[70]. Both nT_{regs} and iT_{regs} affect effector T cell subtype and modulate neutrophil, macrophage, and local progenitor cell phenotype and recruitment, making them indispensable in both wound resolution and regeneration[71–77].

T_{regs} are powerful enhancers of pro-healing responses in tissue engineering, but our understanding of their impact on the host response to implanted biomaterials remains limited[78,79]. To date, T_{reg} differentiation has been largely attributed to biomaterial induced M2-like macrophage cytokine signaling[62,79]. However, T_{regs} may also be induced or recruited by type I inflammatory responses and other environmental cues relevant to biomaterial implantation[80,81]. The limited scope of current research has primarily demonstrated the ability of organic (decellularized) scaffolds to cause T_{reg} differentiation associated with pro-healing outcomes; though the ability of chemokine laden synthetic polymer scaffolds to induce systemic T cell upregulation has also been characterized[80,82]. Therefore while T_{regs} aid in pro-healing responses to biomaterial implantation, the specific roles of T_{regs} in this capacity remain uncharacterized.

3.1.2: TH1 and TH2 cells in wound healing and FBR modulation

T Helper 1 (TH1, indicated by TNFα, TBX21, and IFN-γ expression) cells are classically inflammatory: they inhibit wound resolution by reducing collagen deposition, downregulating other T helper responses, and releasing inflammatory cytokines[68]. T Helper 2 cells (TH2, indicated by GATA3 expression) modulate classical TH1 driven inflammation while enhancing wound closure, eosinophil activation, and IgE mediated responses[83]. However, an excess of TH2 cells causes fibrotic scarring and allergic reaction[81]. The correct balance between TH1 and TH2 populations is therefore necessary to avoid both fibrosis and chronic inflammation for optimal wound healing[84]. This phenomenon resembles the observations of the Ratner group, where the balance between M1 macrophages throughout and M2 macrophages outside the PTS led to optimal healing[9].

A large majority of biomaterial mediated T cell signaling has focused on TH2 responses. Though TH2 cells may be potentially fibrotic in wound healing, the Ellisseeff laboratory's recent evidence indicates that TH2 cells are required to elicit the pro-resolution response intrinsic to certain biomaterial scaffolds [37]. Utilizing a RAG1 knockout model, the group demonstrated an

mTOR mediated pathway that caused a TH2 response, subsequently inducing M2-like macrophage differentiation[37]. Although this data has demonstrated the importance of TH2 signaling within the implant microenvironment, older research questions this paradigm. The Anderson laboratory demonstrated that while cellular infiltration greatly decreases upon thymic T cell ablation, TH2-associated cytokines remain present within the implant microenvironment[85]. Further, the Gonzalez-Juarrero laboratory observed that T cells within the wound microenvironment were likely not close enough to the foreign body capsule to enable direct cell to cell signaling to result in TH2 cytokine secretion[11]. Confoundingly, the Klinge group has recently disputed this claim by showing a mixed population of T cells and macrophages close to an implanted polypropylene mesh[65]. Additional research on the effect of TH2 cells in the FBR is therefore necessary.

3.1.3: TH3 and TH17 cells in wound healing and FBR modulation

T Helper 3 and T Helper 17 (TH3 and TH17 indicated by TGF-β1 and RORγ) cells can be ambiguous within the context of wound healing. TH3 cells are iT_{regs}, which downregulate both TH1 and TH2 cellular responses[86]. Specifically, TH3 cells release varying amounts of IL-10 and the paradoxical TGF-β1 depending on external stimuli[87]. TH17 cells are broadly considered to be pro-inflammatory within the context of wound healing, though they can also aid in the induction and maintenance of pro-healing responses[62,88]. However, depending on their environment and activation state, TH17 cells release inflammatory cytokines (e.g. IL-17 and TNFα), anti-inflammatory cytokines (e.g. IL-10), and cytokines that may be both inflammatory and anti-inflammatory (e.g. IL-22)[88].

The role of TH3 cells in the FBR is not yet known; TH3 cells have not yet been observed within the biomaterial implant microenvironment, and there is a lack of data indicating their potential function. However, TH17 cells are characterized as inhibitors of a pro-healing response to implanted foreign biomaterials[62,89]. Recent evidence by the Ellisseeff laboratory suggests that

TH17 cells are instrumental in enabling inflammatory aspects of the FBR[90]. They identified that an initial IL-17 secretion by innate immune cells induced an upregulation of TH17 cells, which caused a subsequent upregulation in inflammatory macrophage populations to create a positive feedback loop[91]. This cell signaling paradigm has thus been attributed to a worsened FBR, driving both inflammation and fibrosis in synthetic biomaterial implant microenvironments[90,91].

3.2: Visual and quantitative characterization of the role of T_{regs} in the host response to PTS

3.2.1: Significance

Although T cells have been observed in the PTS microenvironment, little is known about their role in determining the host response upon implantation[39]. Given their powerful role in determining the scope of the FBR, the phenotypes of T cells within the PTS are important to characterize. The role of T_{regs} in determining the host response to PTS is of particular interest due to their unique immunomodulatory abilities. We therefore investigated the FBR and transcriptional expression of $CD4^+$ T cell phenotypic indicators within the PTS after 1 week of implantation in the presence and absence of $FoxP3^+$ T cells.

3.2.2: Materials and methods

(Section adapted from Hady et. al, 2020)

3.2.2.1: *$FoxP3^+$ cell depletion*

$FoxP3^{DTR}$ homozygous mice expressing human diphtheria toxin (DPT) receptor and eGFP genes at the Foxp3 locus were obtained (Jackson Labs strain B6.129(Cg)-Foxp3tm3(DTR/GFP)Ayr/J). Endogenous FoxP3 expression was not affected by this addition, but DPT treatment ablates FoxP3+ cell populations upon IP injection. These mice were treated with 1µg of diphtheria toxin (Sigma Aldrich) in 100µL of sterile saline via intraperitoneal injection once every 3 days. Scaffolds were implanted one day post-injection to allow adequate time for initial cell depletion. Mice were weighed daily to ensure no more than 15% of body weight was

lost during treatment. Scaffold implantation and explantation were performed as previously described.

3.2.2.2: *Tissue histology*

Explanted PTS were embedded in OCT (Tissue-Tek Sakura, VWR), and snap frozen using liquid nitrogen. OCT blocks were cut with a cryotome into 5-10µm sections. The tissue sections were then stained for collagen (blue), nuclei (black), and cytoplasmic spaces (red) using a Trichrome stain (Abcam) as per manufacturer's protocol. Histo-Clear II (National Diagnostics) was used as a clearing agent, the slides were mounted using Omnimount (National Diagnostics), and covered with a 1.5mm cover slips.

3.2.2.3: *T cell transcriptional analysis*

Control (WT) PTS implantation and T cell panel qPCR was performed by the Mulligan/Hwang laboratory.

PTS resident cells were processed with RNeasy Mini kit as per manufacturer's protocol (Qiagen) and used to generate cDNA as per manufacturer's protocol (Applied Biosciences). qPCR was performed with FAM (T Cell Panel) probes on an ABI 7900HT (thermal cycling parameters as previously described). The T cell panel included GAPDH, FOXP3, IL-10, IFN-γ, TGFb1, TNFa, RORC, GATA3, and TBX21 (primer/probe IDs available in **Table 2**). Rationale for this panel can be seen in **Table 2**. We do recognize, however, that no gene is perfectly indicative of a singular cell phenotype (e.g. macrophages may also secrete TNFα). Ct was considered undetermined if one or both replicates failed to amplify. Relative fold expression was calculated as previously described normalizing against the housekeeping gene GAPDH.

Gene	$CD4^+$ T cell Phenotype	Probe ID
FoxP3	T_{reg}	Mm00475162_m1
IL-10	Tr1	Mm01288386_m1
IFN-γ	TH1	Mm01168134_m1
TNFα	TH1	Mm00443258_m1
TBX21	TH1	Mm00450960_m1
GATA3	TH2	Mm00484683_m1
TGF-β1	TH3	Mm01178820_m1
RORC	TH17	Mm01261022_m1
GAPDH	Housekeeping	Mm99999915_g1

Table 2: T cell gene expression panel. Genes of the T Cell RT-qPCR panel and their associated $CD4^+$ T cell phenotypes.

3.2.3: Results

(Partially adapted from Hady et. al, 2020)

There were significant histological differences in sectioned PTS as a result of both pore size and $FoxP3^+$ cell depletion (**Figure 13**). Consistent with prior research, the 40µm PTS exhibited a high degree of cellularization when implanted into WT mice. However, the 100µm PTS implanted into WT mice exhibited a reduction in cell recruitment and morphological spreading in favor of the less uniform influx of less spread cells. Cellular infiltration was also lessened in $FoxP3^+$ cell depleted PTS of both sizes. Further, $FoxP3^+$ cell depletion altered the morphology of PTS resident cells, particularly those close to the surface of the 40µm PTS. These cells tended towards a denser, darker shape similar to the response observed in the 100µm PTS—but the changes were more dramatic, as the nuclei were only barely distinguishable in these PTS resident cells. In the control PTS of both sizes, the cytoplasm and nucleus were highly distinct from one another.

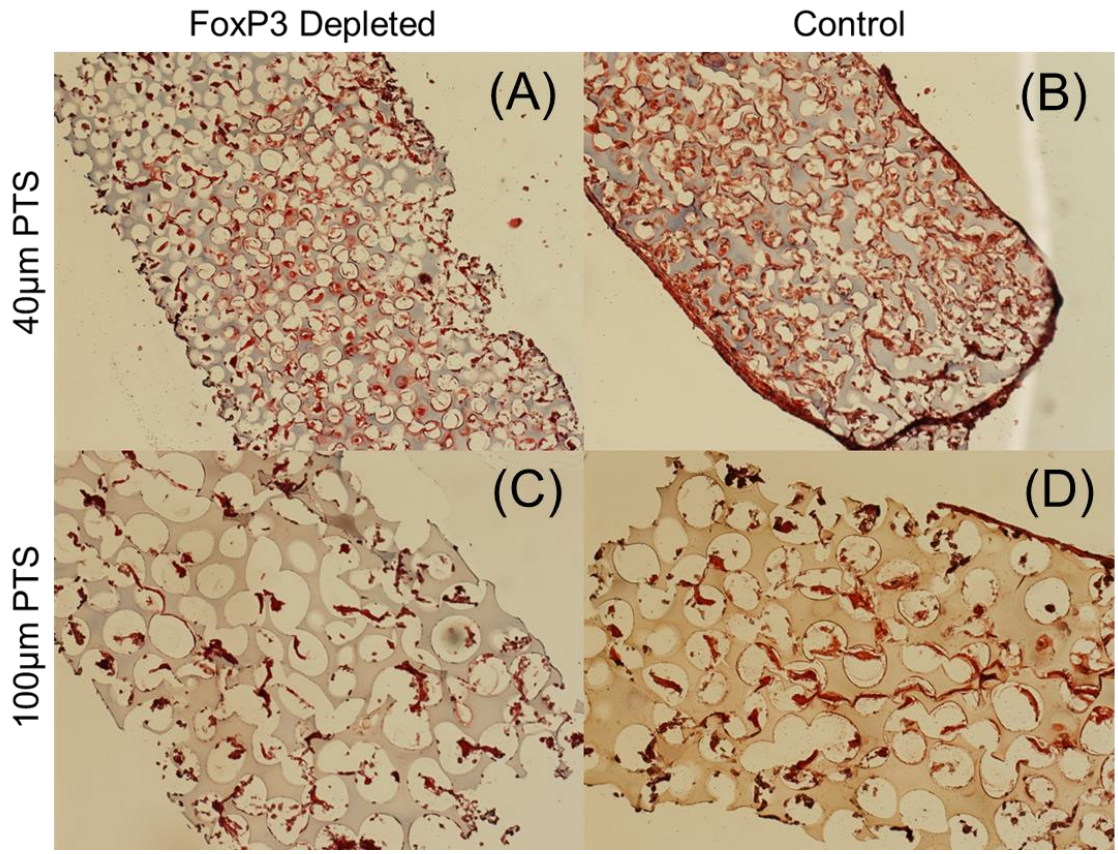

Figure 13: Trichrome stain of cryosections obtained from explanted PTS after 1 week of implantation in WT and FoxP3$^+$ cell depleted mice. (A) is a representative image of a FoxP3- 40µm PTS implant, (B) a WT 40µm PTS implant, (C) a FoxP3- 100µm PTS implant, and (D) a WT 100µm PTS implant. Red denotes cytoplasm, blue collagen, and black nuclei.

40µm pores caused the upregulation of the TH1 marker TBX21 (p=0.0055, N=8 for 40µm PTS and N=7 for 100µm PTS), the TH2 marker GATA3 (p=0.0043), and the T_{reg} marker FoxP3 (p=0.041) in wild type (non-FoxP3$^+$ cell depleted) PTS resident cells (**Figure 14**) (control data provided courtesy of the Mulligan/Hwang Laboratory). FoxP3$^+$ cell depletion downregulated TBX21 expression in PTS resident cells (p=0.00015 and p=0.0055, N=4 for T_{reg} depleted 40µm and 100µm PTS) and abrogated the differences in TBX21 and GATA3 expression between 40µm and 100µm PTS resident cells. While not statistically significant (p=0.074), FoxP3$^+$ cell depletion may have caused GATA3 expression to tend towards upregulation in 100µm PTS resident cells. Finally, FoxP3$^+$ cell depletion caused a significant downregulation of IL-10 in cells

resident to both 40µm and 100µm PTS (40µm PTS p=0.0022 and 100µm p=0.016). PTS pore size and FoxP3^{+} cells therefore both played a role in T cell homeostasis within the PTS.

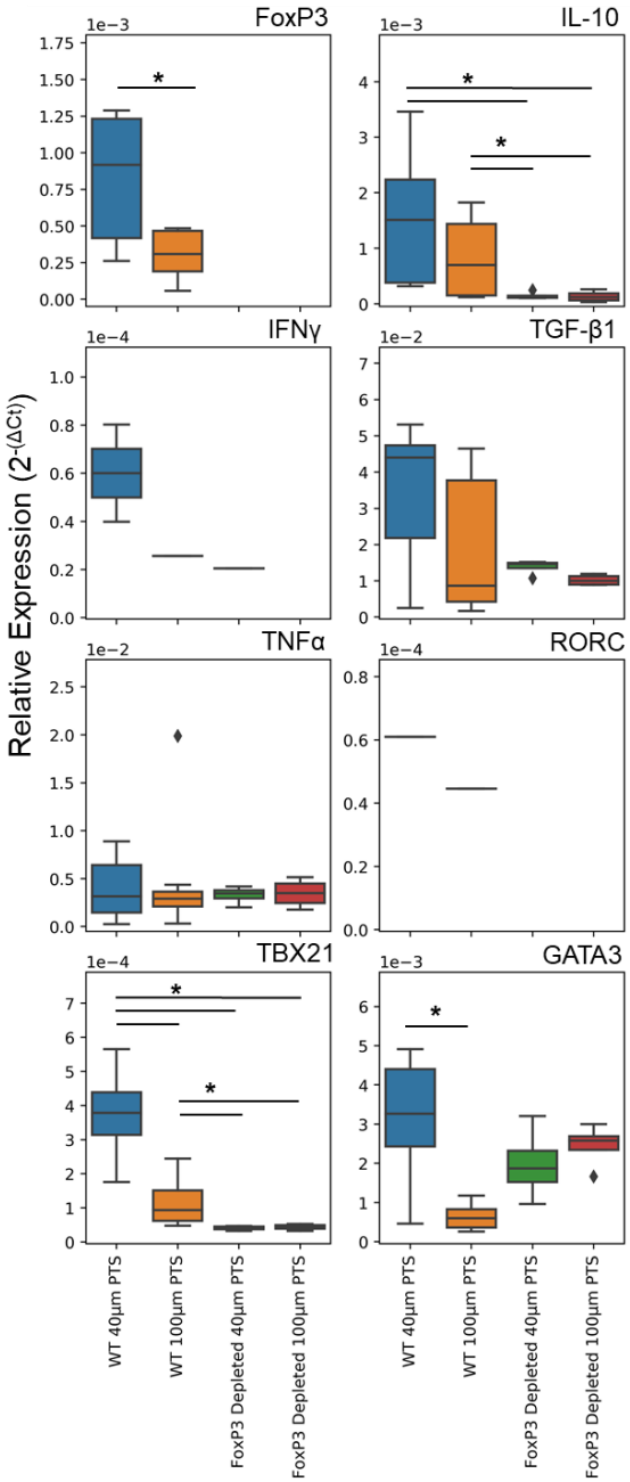

Figure 14: T cell gene expression of 40µm and 100µm PTS resident cells after in WT and FoxP3^{+} cell depleted mice. The RT-qPCR T cell gene panel in **Table 2** was run on PTS resident cells from PTS

explanted from wild type and FoxP3^{DTR} mice treated with diphtheria toxin after 1 week (*,p<0.05, N=8 for WT 40μm PTS, N=7 for WT 100μm PTS, and N=4 for FoxP3^{DTR} PTS of both pore sizes; significance was determined via ANOVA or Kruskal-Wallis tests followed by Tukey or Conover-Iman posthoc tests respectively based on normality assessed by Shapiro-Wilk test, see 2.3.2.5: for details). WT Control data provided courtesy of the Mulligan/Hwang laboratory.

3.3: Discussion: characterizing the role of T_{regs} in the host response to implanted PTS

Consistent with previous studies, cellular infiltration and morphology in 40μm PTS implanted into wild type mice was improved over implanted 100μm PTS. However, this difference was abrogated upon T_{reg} depletion, as the cellular infiltration and morphology in 40μm and 100μm PTS implanted in FoxP3^{+} cell depleted mice do not look remarkably different. These results indicated that T_{regs} that express FoxP3 drove the healing response intrinsic to 40μm PTS, as only implanted non-depleted 40μm PTS displayed a dramatically improved cellularization compared to the other treatment conditions. Corroborating our histological data, CD4^{+} T cells from 40μm PTS significantly upregulated the T_{reg} marker FoxP3. Together, these data indicated not only that there was additional FoxP3^{+} T_{reg} activity among 40μm PTS resident cells, but also that these T_{regs} were crucial to the unique host response to 40μm PTS.

As expected, T_{reg} depletion led to a downregulation of the key anti-inflammatory regulator IL-10 and an absence of FoxP3 expression in PTS resident T cells. While there were significant differences in phenotype between CD4^{+} T cells from 40μm and 100μm PTS implanted in wild type mice, these differences were lost upon T_{reg} depletion. Specifically, the upregulation of TH1 and TH2 markers TBX21 and GATA3 in 40μm PTS resident T cells were lost. As T_{regs} play a key role in maintaining T cell homeostasis in wound healing environments, these data indicated that a unique T cell phenotypic equilibrium maintained by T_{regs} was necessary for the unique pro-healing response to 40μm PTS. Moreover, as TBX21 was downregulated upon T_{reg} depletion in PTS of both pore sizes while GATA3 was not, we posit that T_{regs} were paradoxically responsible for the maintenance of the TH1 response responsible for counteracting potential excessive TH2 activation that may otherwise lead to additional fibrosis. Additionally, due to the

trending upregulation of GATA3 in 100μm PTS upon T_{reg} depletion, we also hypothesize that T_{regs} may be responsible for dampening the TH2 response upregulated by the 100μm PTS, which would cause further fibrosis. However, additional experimentation is required to validate these hypotheses. Regardless, $FoxP3^{+}$ T_{regs} appeared to be indispensable in the unique host response to 40μm PTS.

Chapter 4: Isolating and characterizing pEVs

4.1: Introduction: A cell signaling context for EVs

EVs are lipid bilayer bound particles released by nearly every cell in the human body that may range from 30-6000nm in diameter[92,93]. EVs contain cargo comprised of functional lipids, proteins, and nucleic acids (**Figure 15**)[94]. Nucleic acids within EVs are diverse, consisting of DNA, messenger RNA, long noncoding RNA, and microRNA[94]. EVs may have membrane bound or intravesicular proteins, thereby encompassing a wide variety of transcription factors, surface receptors, growth factors, and antigens[92,94,95]. EV associated lipids are less well characterized, but include membrane bound lipid rafts (i.e. cholesterols and glycosphingolipids) to aid protein sorting and cellular uptake[96,97], as well as intravesicular functional lipids (i.e. eicosanoids) to affect cell signaling[98]. These lipids, proteins, and nucleic acids propagate EV mediated cell signaling through both surface interactions with and uptake by recipient cells[94,96]. It is important to note that the specific method of signal transduction depends on the properties of the recipient cell (e.g. ability of the recipient cell to phagocytose EVs)[96].

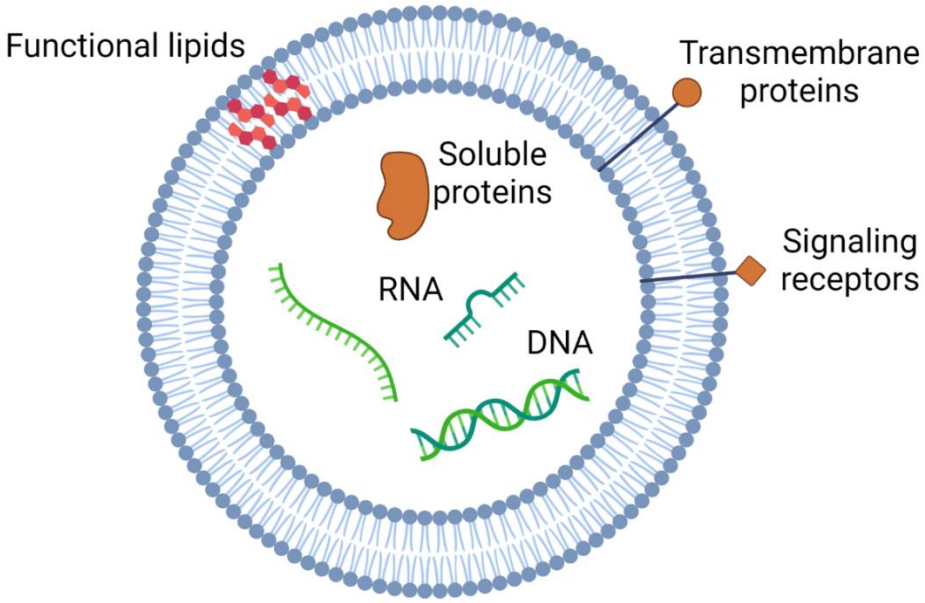

Figure 15: Contents of EVs. Lipids, proteins, and nucleic acids of many different varieties are contained inside and on the surface of EVs.

4.1.1: Defining the relevant EV population

EVs are further subclassified to differentiate their wide variety[92,93]. EV populations are primarily determined based on their size, though due to the novelty of the field, the exact name and size cutoff of each EV population varies[93,99,100]. Large EVs (lEVs) are also called apoptotic bodies, and are the largest (in size) EV subcategory, generally accepted to be larger than 800-1000nm in diameter[92,93]. Medium EVs (mEVs) are also called microvesicles, and are larger than 100-200nm but smaller than 1000nm in diameter[92,93,101]. Small EVs (sEVs), colloquially called exosomes, are larger than 30nm but smaller than 150-200nm in diameter[92,93,101]. The naming conventions of EVs are currently contentious, and further confused by the innate heterogeneity of EVs. While lEVs, mEVs, and sEVs have been historically called apoptotic bodies, microvesicles, and exosomes based on their size, some researchers argue that these terms should require additional proof of specific biogenic pathways[92,93,101].

We are particularly interested in EVs 30-200nm in diameter. While many consider these small EVs to be exosomes, the International Society for Extracellular Vesicles disagrees with this

classification with their “MISEV” guidelines, instead opting to classify EVs based on their size[101]. While we appreciate their commitment to standardization, due to the inherent heterogeneity of EVs we respectfully dispute these rules for classification. Specifically, the MISEV requirements cite specific protein expression (e.g. the tetraspanins CD9, CD63, and CD81) as requisite for exosome designation; we view these guidelines as unrealistic and artificially restrictive. For example, some or all tetraspanins may not be present on exosomes isolated from progenitor cells, but these EVs are still considered to be exosomes[102,103]. We thus consider EVs between 30-200nm in diameter as exosomes, but will herein designate EVs of this size sEVs to avoid unnecessary distraction.

4.1.2: Key characteristics of sEVs

The biogenesis of sEVs is highly distinct. While mEVs and lEVs are generally singular vesicles resulting from the budding of the plasma membrane, sEVs may utilize the endocytic pathway[92,104]. Specifically, sEVs are generated from budding of the endosomal membrane to form intraluminal vesicles inside of a multivesicular body to form many sEVs concurrently[104]. This process is thought to be at least partially mediated by unique proteins (i.e. ESCRTs, RABs, and tetraspanins)[104]. However, previous studies have shown that a lack of these proteins does not preclude sEV production, and that different methods of intraluminal vesicle formation may lead to sEV heterogeneity[104]. Further, these methods of sEV biogenesis allow for an additional discretionary step during vesicle formation, yielding yet more heterogeneous vesicles with unique cargo[104]. It must also be noted that components of sEVs are often recycled upon the initiation of signal transduction with the recipient cell, thereby potentially rendering the sEVs released by the recipient cell a reflection of both the recipient and parent cells[105]. sEVs are thus important and unique cell signaling participants that share biochemical properties with their (potentially multiple) parent cells—enabling powerful, novel, and unconventional methods of cell signaling[106].

Principally, there are two categories of sEV signaling to consider: those occurrences where the sEV remains extracellular, and those where the sEV is cytoplasmic. Extracellular sEV signaling is thought to be substantially more limited in scope than methods of intracellular sEV signaling. When an sEV is extracellular, proteins decorating the sEV may bind cellular surface receptors to initiate transduction[107]. This process may also occur after proteolysis releases a ligand from the surface of an sEV[107]. However, receptor mediated signaling may also lead to sEV endocytosis via receptor internalization[107].

Intracellular sEV signaling is achieved through a wide variety of different methods dependent on cell type[96]. Most obviously, phagocytes (e.g. macrophages and dendritic cells) may phagocytose sEVs, where they fuse with the membrane of the phagosome[96]. While naturally occurring in phagocytes, non-myeloid cells may also macropinocytose sEVs in the presence of certain cytokines[107–109]. Many cells may also initiate endocytosis by utilizing lipid rafts, caveolin, and clathrin to create intracellular compartments that facilitate endosomal membrane fusion with the sEV[96]. Finally, sEVs may also undergo membrane fusion with the recipient cell to deliver the intravesicular cargo to the cytoplasm[96]. While many methods of cell signal transduction have been elucidated thus far, there are many unexplored methods of potentially impactful cell signaling still to be discovered. For example, some believe that trogocytosis allows for the exchange of sEVs across neighboring cells[110]. By utilizing these mechanisms of cell signaling, sEVs change the phenotype of recipient cells to drive important physiological effects[94,95].

4.1.3: sEV signaling in wound healing

Due to their versatile, complex, and powerful cell signaling capabilities, sEV signaling plays an indispensable role in many different key physiological functions—many of which remain undiscovered or poorly characterized. These processes can be physiologically beneficial, such as sEVs driving embryonic development of organs, osteogenesis, antigen presentation, and tissue repair[111–113]. However, these processes may also be pathological, leading to

atherosclerosis, kidney stones, cancer development, and viral transduction[111–114]. It is therefore important to understand the context and mechanism involved in each individual sEV signaling circumstance.

The pro-healing abilities of sEV include the enhancement of both wound resolution and tissue regeneration, rendering sEVs a promising therapeutic vehicle in the modulation of immune and tissue engineered responses[95,115]. The majority of previous studies have focused on the ability of progenitor (i.e. stem-like) derived sEVs to improve wound healing outcomes, specifically demonstrating the efficacy of stem-like cell derived sEVs in driving angiogenesis, wound closure, anti-inflammation, and restoration of tissue function[95,100,102,116,117]. However, recent evidence also demonstrates that non-progenitor cell derived sEV signaling is integral to wound healing processes[94,95,118–120]. Specifically, immunomodulation has been recognized as a means to initiate and maintain regenerative wound healing responses[68]. As sEVs have recently been shown to contribute to or detract from inflammatory host immune responses, sEV based immune signaling may be used to explain previously confounding immunological phenomena that may result in a pro-healing response[95,121,122]. We have therefore explicated the roles of sEVs in wound healing processes to understand the contextual role and potential immunomodulatory signaling abilities of sEVs in the PTS microenvironment.

sEVs effectively modulate inflammation. A wide variety of cells including leukocytes, progenitor cells, parenchymal cells, and stromal cells may both produce and receive immunomodulatory sEVs[123]. However, macrophages, dendritic cells, neutrophils, and T cells are the principle leukocytes of interest, as they are powerful immunomodulators that both release and receive sEVs to affect inflammation[123]. Immunomodulatory sEVs may induce both pro-inflammatory and anti-inflammatory effects in recipient cells depending on the phenotype of the parent and recipient cells[123,124]. While this field of study is in its infancy, the role of these sEVs has been largely characterized within the context of aberrant immune regulation. Broadly, sEVs from

(largely stromal) tissue resident cells have been shown to contribute to the inflammatory components of autoimmune and kidney diseases, bowel and neural inflammation, and cancer[125]. Conversely, sEVs from other (largely progenitor) cell types have been shown to cause potent anti-inflammatory immunomodulation of leukocytes[126–128]. Macrophage derived sEVs have received special attention as potent immunomodulatory signaling mediators. While an oversimplification of macrophage biology, sEVs isolated from M1-like macrophages may progress inflammation in recipient cells while sEVs isolated from M2-like macrophages reduce inflammation in recipient cells[124,129–132]. The pathological regulation of M2-like macrophage derived sEV signaling has been particularly well detailed within the context of cancer, where these sEVs enabled the enhanced motility and migration of tumor cells[130,133]. M1-like macrophage derived sEVs, however, have recently been shown to perpetuate autoimmune reactions during aberrant regulation[134]. While the moderation of inflammation is a classical immunomodulatory phenomenon, sEV mediated immunomodulation also broadly enables other pro-healing consequences of sEV signaling.

Angiogenesis is a principle mechanism by which sEVs initiate a pro-healing response[94,135]. Modulation of angiogenic processes by sEVs primarily occurs as a result of their signaling to endothelial cells[135]. Currently, sEVs from progenitor cells are well documented to direct angiogenesis in the recipient tissues[135]. However, sEVs from both mature cells (especially during hypoxia) and platelets also played a key role in the induction of angiogenesis[135,136]. sEV signaling to endothelial cells may occur in a number of different ways: through micro-RNA (miRNA) delivery (e.g. miR-125a and 214), protein delivery (e.g. PDGF), signaling pathway transduction (e.g. ERK1/2, WNT4, and NF-κB), and transcription factor delivery (e.g. STAT3)[135]. Angiogenic activity may also be modulated by sEVs to decrease blood vessel formation, such as in cases of oxidative tissue stress[118,135]. Immunomodulation by sEVs plays a crucial role in angiogenesis; macrophage sEVs have been shown to facilitate both positive and negative

regulation of angiogenesis by signaling to endothelial cells and other macrophages[129]. Finally, while angiogenesis within the context of wound healing is generally positive, sEVs may lead to aberrantly regulated angiogenesis in tumors to perpetuate their growth[111].

sEVs have recently been found to facilitate wound closure. Progenitor cell derived sEVs are best characterized in this role—though research investigating sEVs derived from mature cells in wound closure is highly novel at the time of publishing[137–139]. sEVs from progenitor cells influence wound closure in a number of different ways: by initiating cellular migration and proliferation, stimulating ECM deposition, and inducing phenotypic differentiation[137–139]. Specifically, progenitor cell derived sEVs caused the recruitment and proliferation of fibroblasts and keratinocytes to cutaneous wounds, aiding in closure[137,138]. These sEVs also induced the deposition of ECM elements, namely collagen, in the wound microenvironment[138]. Finally, sEVs may have utilized conventional cell signaling mechanisms (e.g. CD73) to affect the phenotype of surrounding cells, potentially inducting macrophages to an M2-like phenotype[137,139]. Progenitor cell derived sEV mediated effects are likely caused by similar signal pathway transduction phenomena as sEV mediated angiogenesis (i.e. ERK, AKT, and STAT3)[138]. However, recent evidence also indicates that non-progenitor cell sEV signaling may be key to wound closure, as sEV signaling within the wound environment between mature cells also drove a pro-healing response[140]. Macrophages in particular received cues from wound-resident keratinocytes to induce M2-like phenotypic differentiation, causing improved wound closure responses[140]. Thus, immunomodulatory sEV signaling plays an important role in driving the wound closure aspect of a pro-healing response.

sEVs also participate in the tissue regeneration—specifically, the successful differentiation of wound resident cells into parenchyma to restore tissue function. Recent studies have demonstrated that progenitor cell derived sEVs may have led to regeneration in a variety of tissues, including bone, cartilage, skin, lung, liver, and heart[103,141,142]. sEV mediated neural

regeneration has been particularly successful; progenitor cell derived sEVs have induced both neuronal differentiation and remodeling, which has been shown to restore cognitive function after traumatic brain injury[102,103]. Though sEVs derived from mature cells are not as well characterized within the context of tissue regeneration, bone marrow derived M2-like macrophage sEVs have demonstrated efficacy in improving motor function after spinal cord injury[143]. While many mechanisms of sEV induced tissue regeneration remain unknown, miRNA mediated signal transduction may play a critical role in this phenomenon[103,143].

While the investigation of sEVs within the context of wound healing is a burgeoning field, the role of sEV signaling to determine the wound healing outcome of implanted biomaterials remains poorly understood. Current research has primarily focused on loading EVs onto or inside of biomaterials to serve as controlled release mechanisms, but the role of sEV signaling induced by biomaterials themselves requires additional investigation[144]. As of the time of publishing, an extremely limited number of laboratories have investigated the influence of biomaterial cues on the content of released sEVs, with the most prominent study focusing on progenitor cell sEVs[145]. Given that cells release potentially unique sEV populations in response to environmental cues, we believe this area of research to be both important and understudied.

As the pores of PTS provide unique environmental cues based on their size to cause immunomodulation in resident cell populations, we viewed PTS resident cell derived sEVs as a potential tunable signaling modality. Moreover, as conventional cell signaling mechanisms (i.e. cytokine signaling) cannot fully explain the differential host response to PTS of different pore size, we believed that sEV signaling may play a significant role in the PTS FBR. We have herein described sEVs derived from PTS resident cells as “pEVs”.

4.2: Optimization of sEV isolation

4.2.1: Significance

There are currently a variety of accepted techniques for sEV isolation. Ultracentrifugation, ultrafiltration, size exclusion chromatography, immunosorting, and precipitation are all recognized as valid methods of sEV isolation[101]. Each method, however, has varying degrees of specificity and yield[101]. We chose to use sEV precipitation as our isolation method. As we are investigating non-specific populations of pEVs (i.e. all sEVs harvested from PTS resident cells), precipitation's high yield of non-specific particles was preferable to other options[101]. However, there are many different methods of sEV precipitation.

We investigated the differences between Invitrogen's Total Exosome Isolation (from cell culture) reagent and SBI's ExoQuick-TC isolation solution. As non-specific sEVs were the isolation target, we were principally interested in comparing the difference in size distributions between sEV populations using the two isolation buffers. A previous study investigating the sEV populations between the two kits revealed a similar particle size and purity in both populations[146]. However, this was performed in HeLa cells, and the most common cells within the PTS are macrophages. Therefore, we measured the modal particle size, size variability, and concentration of sEVs isolated from RAW 264.7 macrophages seeded in 40μm and 100μm PTS.

4.2.2: Materials and methods

4.2.2.1: *Tissue culture*

RAW 264.7 cells (ATCC) were cultured in high glucose DMEM (Gibco, cat #11965092) with 10% FBS and 1% penicillin streptomycin. A suspension of $1*10^7$ cells/mL was prepared in PBS, and seeded in PTS using capillary action as previously described herein[58]. Conditioned medium was collected from RAW 264.7 cells after 24 hours in culture.

4.2.2.2: *sEV isolation and characterization*

In order to isolate sEVs using Invitrogen's reagent, conditioned medium from RAW 264.7 cells was spun at 2000xg for 30 minutes in order to remove cells and debris. The supernatant was then combined with 0.5 volumes of Total Exosome Isolation Reagent (from cell culture media) (Invitrogen, cat. #4478359) and mixed thoroughly by pipetting and vortexing. The samples were then incubated at 4°C overnight, and centrifuged at 10,000xg for one hour at 4°C. The supernatant was aspirated, and the sEV pellet was resuspended in PBS.

In order to isolate sEVs using SBI's reagent, conditioned medium from RAW 264.7 cells was centrifuged at 3000xg for 15 minutes to remove cells and debris. The supernatant was then combined with 0.2 volumes of ExoQuick-TC reagent (SBI, cat. #EXOTC10A-1) and mixed thoroughly by tube inversion. The samples were then incubated at 4°C overnight, and centrifuged at 1500xg for 30 minutes at 4°C. The supernatant was then aspirated, and the sample was centrifuged at 1500xg for 5 minutes at 4°C, and any remaining supernatant was removed. The sEV pellet was then resuspended in PBS.

Upon final PBS resuspension, EV quality and concentration were assessed via Nanoparticle Tracking Analysis (NTA) (NanoSight™, Malvern Panalytical Inc.). NTA was performed using three 60 second captures per sample after vigorous vortexing. Particles were diluted to reach the acceptable concentration range of NTA quantification.

4.2.3: Results

NTA characterization indicated the viability of both Invitrogen's and SBI's sEV isolation reagents. The modal size of sEVs isolated overnight with both reagents were not significantly different, and both were of acceptable size to be considered sEVs, as the average modal diameters were 66.95nm [51.46-82.43nm] and 94.6nm [35.91-153.28nm] for Invitrogen's and SBI's reagents, respectively (**Figure 16**) (N=2, one 40µm PTS and one 100µm PTS, p=0.585).

The average intrasample standard deviation was 38.05nm for Invitrogen's reagent and 52.35nm for SBI's reagent. Although the average intrasample size variability in sEVs isolated with SBI's reagent was higher, this difference was not statistically significant (p=0.171). Additionally, the concentration of sEVs isolated with both kits were not significantly different (p=0.735). Thus, it appeared that there was not a significant difference between sEVs isolated with Invitrogen's or SBI's isolation kits. However, our data did indicate a trend towards higher intrasample variability in sEVs isolated with SBI's ExoQuick-TC reagent.

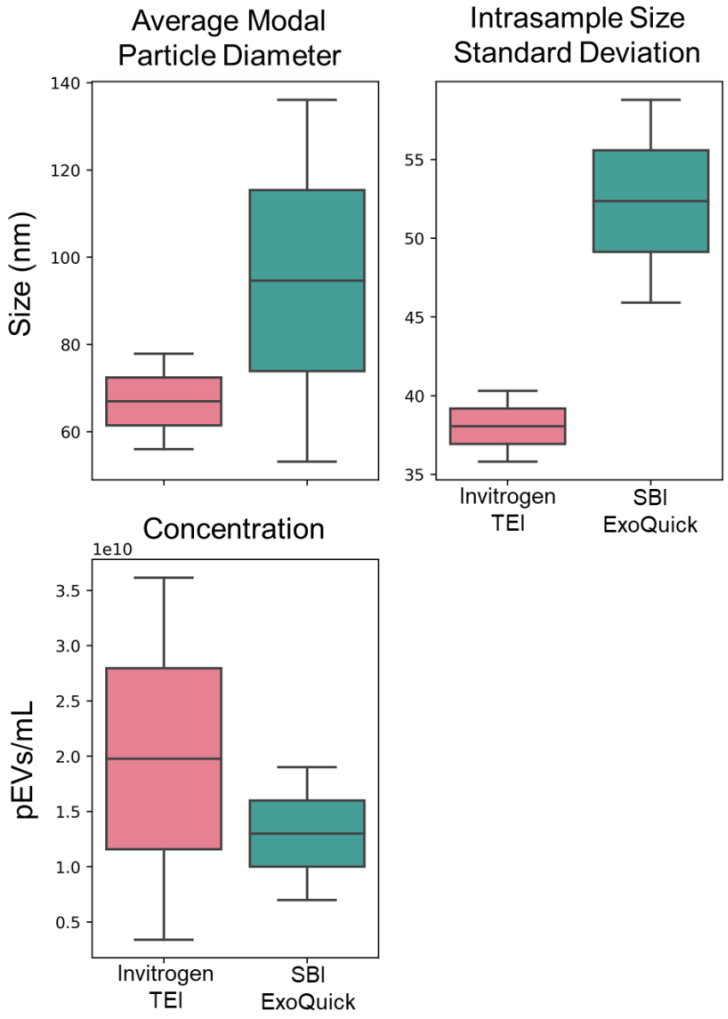

Figure 16: NTA analysis of sEVs isolated from PTS seeded RAW 264.7 cells. Cells were seeded in 40μm and 100μm PTS and pEVs were isolated using Invitrogen's Total Exosome Isolation or SBI's ExoQuick reagents (*, p<0.05, N=2, 1 40μm PTS and 1 100μm PTS; significance was determined via two-sided T or Mann-Whitney U test based on normality assessed by Shapiro-Wilk test, see 2.3.2.5: for details).

4.3: Characterization of pEVs

4.3.1: Significance

While prior research has investigated the cells resident to implanted PTS, pEVs remained understudied. Characterization of pEVs may explicate previously unknown signaling phenomena in the host response to PTS, as the underlying cell signaling mechanisms that cause the pro-healing response intrinsic to 40μm PTS may be partially driven by sEVs. Moreover, the characterization of pEVs within the context of tunable implanted biomaterials leads to an improved understanding of the influence of environmental cues on sEV cargo and release. Therefore, by explicating the role of these physical cues on the characteristics of released sEVs compared to the phenotype of their parent cells, biomaterials may be used to engineer specific cellular responses that consistently generate specific desired sEV populations.

We initially evaluated the physical properties of pEVs in order to classify them by particle size and monodispersity within the context of EV research. Subsequently, we examined the expression of select genes in these pEVs in order to ascertain their potential functionality. Due to the abundance of macrophages within implanted PTS, we then developed a double transgenic mouse model (mTmG/LysMCre) where myeloid pEVs express eGFP and used it to assess pEV lineage. Finally, we compared the phenotypes and lineages of these pEVs with those of their parent cells.

4.3.2: Materials and methods

(Section adapted from Hady et. al, 2020)

4.3.2.1: *pEV isolation and size verification*

PTS were explanted after 1 week and placed in EV-free medium for 48 hours. EV-depleted FBS was generated via overnight ultracentrifugation at 100,000xg, and used in tissue culture medium from which pEVs were to be harvested. EVs were isolated using Invitrogen's Total Exosome

Isolation Kit (Catalog number 4484450) after centrifugation of the conditioned medium at 2000xg for 30 min to eliminate cell debris as per manufacturer instructions; however, instead of using a 1:2 ratio of TEI:conditioned medium as specified, a 1:5 ratio was used. Upon final PBS resuspension, EV quality and concentration were assessed via Nanoparticle Tracking Analysis (NTA) (NanoSight™, Malvern Panalytical Inc.) and ImageStream® imaging flow cytometric analysis. NTA was performed as previously described. EV presence and sample integrity were based on measured particle size (under 150-200nm in diameter without contaminating medium EVs [mEVs] or large EVs [lEVs]).

4.3.2.2: *Double transgenic mouse model for myeloid characterization*

NIH guidelines for the care and use of laboratory animals (NIH Publication #85-23 Rev. 1985) have been observed. All breeding, genotyping, and PTS implantation experiments were carried out in accordance with the National Institute of Health Guide for the Care and Use of Laboratory Animals and were approved by the Institutional Animal Care and Use Committee of the University of Washington.

A double transgenic mouse strain was developed to quantify in vivo myeloid phenotypes within implanted PTS. Cells of myeloid origin express the fluorescent protein eGFP (green) while cells of non-myeloid lineage express mTomato (red). This recombination is irreversible and extracellular vesicles (EVs) also retain their parent cell's fluorescence, allowing quantitative lineage tracking of cells and EVs. To create this strain, LysM-Cre on C57Bl/6 background mice (Jackson labs, stock number 004781) were bred with mT (mTomato) / mG (eGFP) mice on C57Bl/6 background (Jackson labs, stock number 007676). Briefly, breeding trios utilizing female C57Bl/6 and homozygous male transgenic mice to generate heterozygous (either LysM-Cre +/0 or mTmG +/0) were established, and then heterozygous LysM-Cre and heterozygous mT/mG mice were bred to produce offspring of all genotypes for further study. All mice were on a C57Bl/6 background to minimize strain difference. Cell type specific expression of mG was

confirmed in resident tissue macrophages in multiple organs. To verify model efficacy, lungs were retrieved from LysM-Cre+/0:mTmG+/0 mice and processed for fluorescence microscopy; no synthetic fluorochromes were applied. mT/mG reporter mice contain a single copy of the transgene integrated into the ROSA26 locus (R26R). The transgene cassette consists of a chicken β-actin promoter with a CMV enhancer, which causes a floxed membrane localized Tomato tandem dimer (mT) to be expressed. Cre-mediated recombination excises the mT transgene, driving expression of membrane-localized eGFP (mG). Genotyping was carried out via fluorescence imaging and PCR genotyping.

DNA for genotyping was prepared from ear biopsies. Litters were ear-tagged and clipped at 7-12 days post-birth. PCR products were electrophoresed on a 1.5% agarose gel containing ethidium bromide, and amplified fragments were visualized under UV trans-illumination.

4.3.2.3: *pEV lineage characterization*

Imaging flow cytometric analysis of EVs from double transgenic PTS explants was performed on an Amnis ImageStream® (Luminex, Inc. Austin, TX). EVs at an average concentration of approximately $3.57*10^{10}$ pEVs/mL were diluted 1:100 in sterile filtered PBS. All events were recorded in each sample. Fluidics were set to slow, sensitivity to high, and observations were taken at 60x. Compensation matrices were generated based on results from control fluorescent beads. pEVs were gated on size and fluorescence signal obtained from calibration beads and analyzed for the presence of EGFP and mTomato in order to assess myeloid or non-myeloid origin. While signal from non-myeloid (mTomato) EVs was too weak for meaningful analysis due to ImageStream laser limitations, the myeloid (EGFP) signal was strong.

4.3.2.4: *pEV transcriptional analysis*

pEVs were lysed in 2.5% Triton X-100 and 0.05% Tween-20^{100}. RNeasy Mini kits were used as per manufacturer's protocol to isolate the RNA from lysed pEVs (Qiagen). cDNA was then

generated via RT as per manufacturer's protocol (Applied Biosciences). qPCR was performed with SYBR green (macrophage panel available in **Table 1**) primers on an ABI 7900HT (thermal cycling parameters as previously described). Ct was considered undetermined if one or both replicates failed to amplify. Relative fold expression was calculated as previously described by normalizing against the housekeeping gene PPIA. Statistics were performed as previously described.

4.3.3: Results

(Partially adapted from Hady et. al, 2020)

Our experiments first quantified the size distribution of pEVs from 40μm and 100μm PTS using NTA. pEVs isolated from cells resident to 40μm and 100μm PTS implanted for 1 week were not significantly different in size. The average modal sizes of 40μm and 100μm PTS pEVs from wild type mice were under 150nm in diameter, at 106.56nm [96.97-116.14nm] and 106.7nm [90.89-122.5nm] respectively (**Figure 17** and **Figure 18**). The intrasample standard deviation of measured diameter for pEVs isolated from wild type mice were 59.56nm and 61.7nm for 40μm and 100μm PTS pEVs. The average modal sizes of 40μm and 100μm PTS pEVs from double transgenic mice were 120.7nm [74.6-166.79nm] and 143.74nm [111.43-176.04nm] respectively. The intrasample standard deviation of measured diameter for these samples was 87.54nm and 73.1nm for 40μm and 100μm pEVs. These results demonstrated that the pEVs from implanted PTS of both pore sizes were monodisperse populations free of contaminating EVs of other sizes or cellular debris.

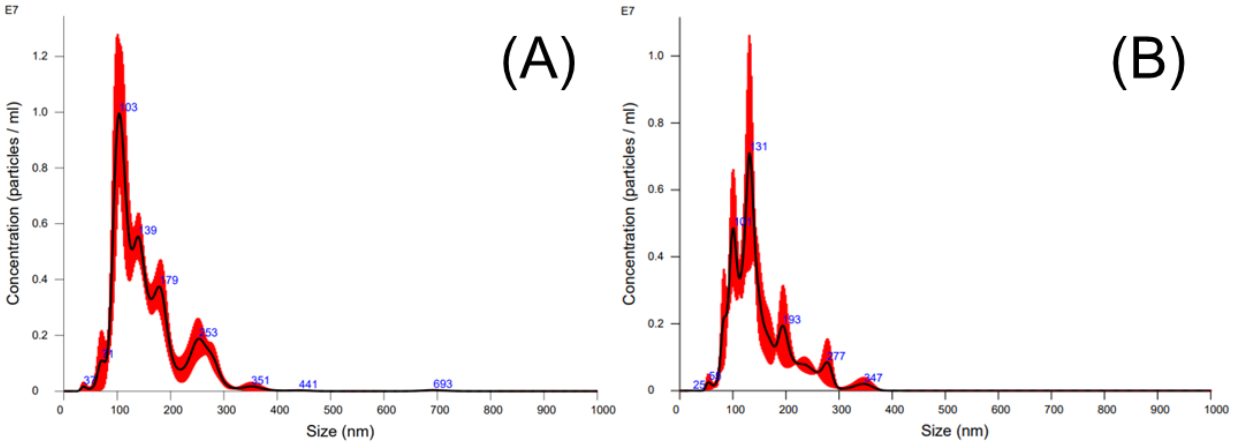

Figure 17: Representative plots of nanoparticle tracking analysis (NTA) performed on pEVs from (A) 40µm PTS and (B) 100µm PTS implanted in WT mice.

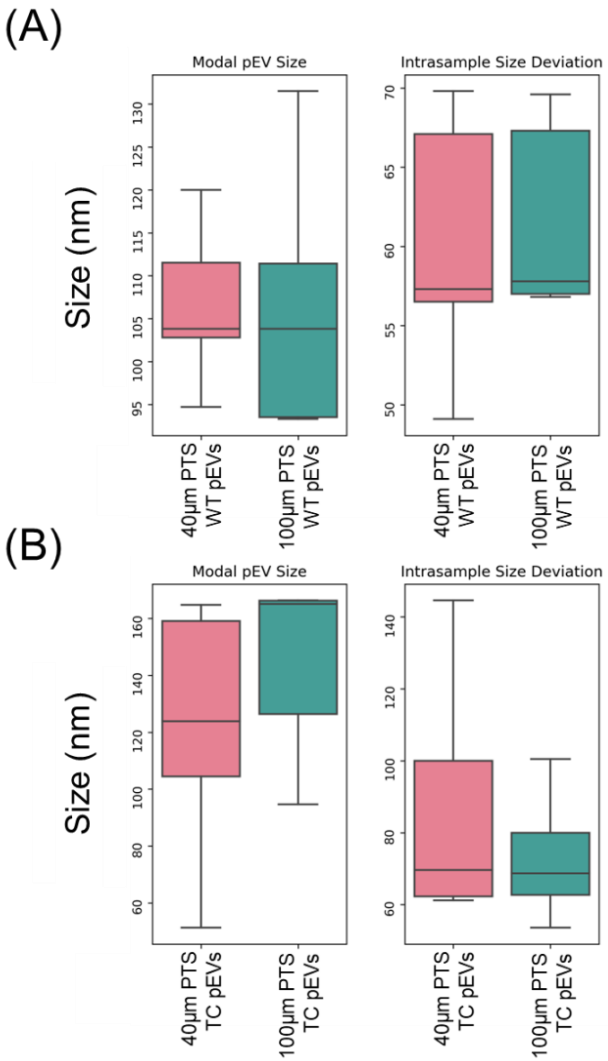

Figure 18: Size of pEVs determined via NTA from PTS implanted in (A) WT and (B) double transgenic (MtMg/LysMCre, abbreviated to TC) mice (*, p<0.05, N=5; significance was determined via

two-sided T or Mann-Whitney U test based on normality assessed by Shapiro-Wilk test, see 2.3.2.5: for details).

Imaging flow cytometry analyses were then performed to measure the cellular origin of pEVs from 40µm and 100µm PTS. These data contrasted earlier observations: where myeloid cells comprised ~95% of cells in the PTS, pEVs from double transgenic mice indicated that about ~60% of the pEVs produced were of the myeloid lineage regardless of pore size (**Figure 19**). These results indicated a disparity between cell and pEV lineage.

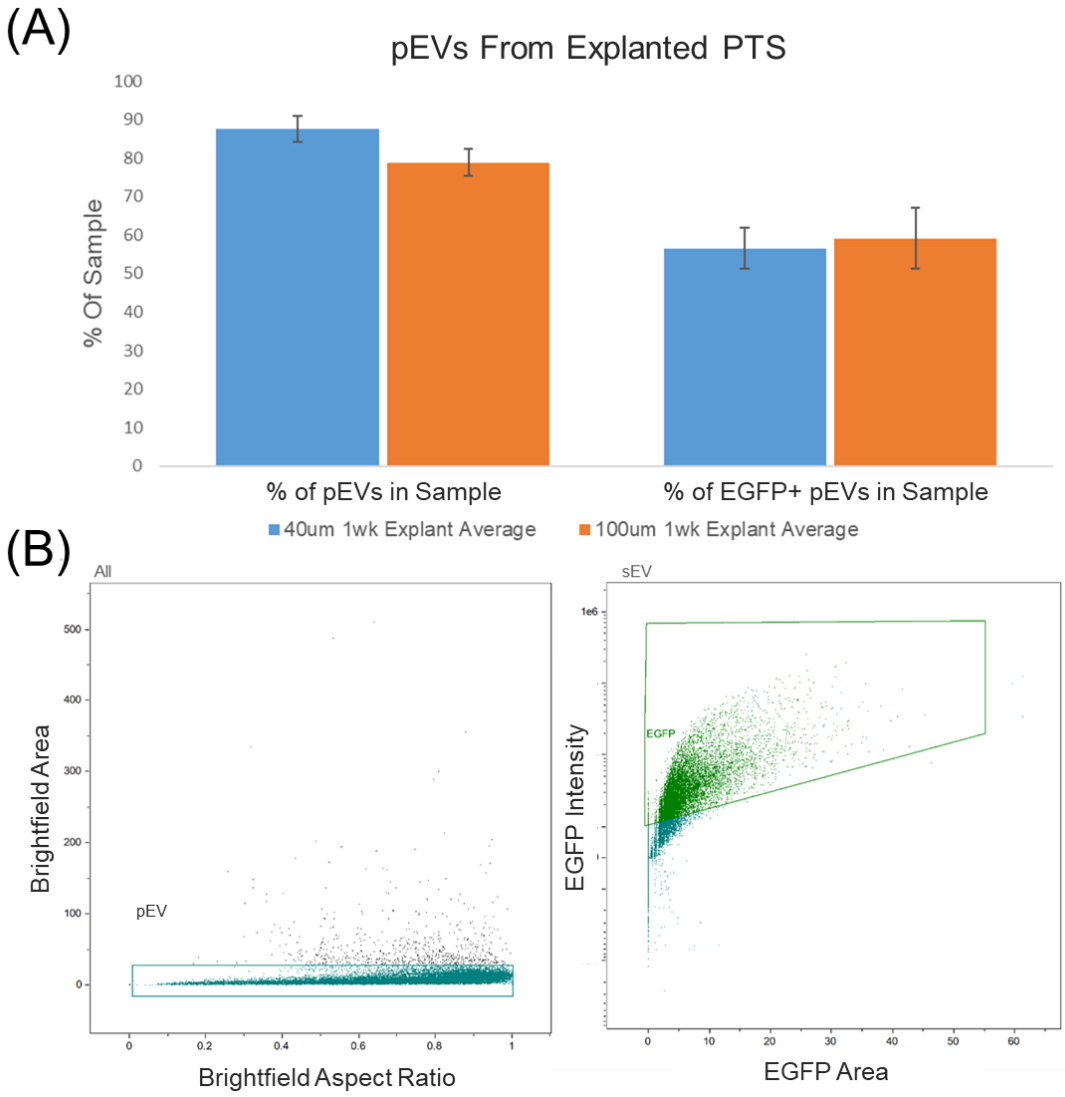

Figure 19: Imaging flow cytometry quantification of pEV lineage. The percentage of single pEVs contained in each sample's total particle reads and percentage of EGFP+ pEVs were measured (A) (N=6 for 40µm and N=5 for 100µm PTS pEVs). Gating strategy (B) first gated out aggregates and the debris field fractions, then the percentage of eGFP+ pEVs (myeloid lineage) from double transgenic mice.

RT-qPCR then quantified phenotypic differences between pEVs from 40μm and 100μm PTS, in addition to those of their parent cells. There were significant phenotypic differences between pEVs from 40μm and 100μm PTS and their parent cells. pEVs exhibited an increased abundance of iNOS (indicative of M1-like macrophages) and YM1 (indicative of M2-like macrophages) transcripts compared to their parent cells (YM1 p=0.00025, iNOS p=0.000069, 40μm PTS N=6 and 100μm PTS N=5) (**Figure 10**). Conversely, FIZZ1, CD206, ARG-1, CD86, and TNFα expression were upregulated in PTS resident cells versus their pEVs (FIZZ-1 p=0.022, CD206 p=0.000053, ARG-1 p=0.00004, CD86 p=0.0012, and TNFα p=0.0092). These results demonstrated preferential loading of certain nucleic acids by PTS resident cells into their released pEVs.

4.4: Discussion: sEV isolation and characterization

While the sEV populations isolated with SBI's ExoQuick-TC and Invitrogen's Total Exosome Isolation (from cell culture) reagents were not significantly different, our preliminary findings indicated a possible trend towards higher intrasample size variability in sEVs isolated with SBI's reagent. Moreover, at the time of publishing, SBI's reagent was significantly more expensive than Invitrogen's. SBI's reagent costs $6.54/mL of conditioned medium to isolate sEVs, whereas Invitrogen's reagent costed roughly $3.88/mL of conditioned medium. Modification of Invitrogen's protocol as implemented in primary cell pEV isolations further brought the cost of sEV isolation down to $0.78/mL of conditioned medium. Therefore, due to affordability and potentially better sEV size monodispersity, we used Invitrogen's Total Exosome Isolation (from cell culture) reagent for pEV isolation.

Although an official size limit is yet to be agreed upon, the average modal size of pEVs isolated from 40μm and 100μm PTS from both double transgenic and wild type mice were under 150μm in diameter; this demonstrated that they were sEVs. Moreover, the relatively low intrasample particle diameter standard deviation indicated that the pEVs were largely free of contaminating

EV populations: namely mEVs and lEVs. Therefore, some would consider pEVs to traditionally be called exosomes that are free of microvesicles and apoptotic bodies, although these definitions are still highly contentious.

EVs are generally thought to reflect the contents of their parent cell—however, PTS resident cells presented unique transcriptomic contents when compared to their pEVs demonstrated through greater expression of highly relevant, FBR-related transcripts: ARG-1, CD86, CD206, FIZZ-1, and TNFα. pEVs also contained unique transcriptomic contents, as demonstrated by the increased abundance of YM1 and iNOS transcripts compared to their parent cells. These results indicated that certain nucleic acid cargo is likely preferentially loaded into sEVs, as opposed to loading a random sampling of the parent cell's transcriptome. Interestingly, the differences in transcriptional regulation observed between cells and pEVs were not exclusively classical M1 or M2 markers, as separate M1 and M2 markers were both uniquely upregulated in cells and pEVs. Therefore the M1/M2 dichotomy of macrophage classification seems inadequate to characterize sEV signaling, even from a parent cell population of predominantly macrophages. Finally, while ~95% of cells observed within 40µm and 100µm PTS were myeloid, they produced only ~60% of the observed pEVs. These results indicated that pEVs are not necessarily produced at the same rate by all cell populations within the PTS. Taken together, we concluded that pEVs are characteristically distinct from their parent cells.

Chapter 5: Investigation of pEV mediated T cell signaling

5.1: Introduction: sEVs as a T cell signaling modality

The specific signaling mechanisms driving T cell differentiation and activation within the FBR to implanted synthetic biomaterials remain poorly understood and highly controversial. Prior literature describing the $CD4^+$ T cell response to implanted synthetic biomaterials focused on characterizing conventional cell signaling methods within the implant microenvironment, which do not fully explain $CD4^+$ T cell signaling therein. As sEVs are potent and unconventional mediators of immunomodulatory cell signaling, they merit further study within this context. Specifically, we believed pEVs to be important in determining the $CD4^+$ T cell response of the FBR upon PTS implantation. However, prior research characterizing immunological sEV-to-T cell signaling, even outside of the context of implanted biomaterials, is sparse.

The physical mechanics of sEV-to-T cell signaling are not well characterized, although some previous studies provide possible explanations. Signal transduction from dendritic cell-derived sEVs to $CD4^+$ T cells is the most well understood within this context, providing unique insights as to the physical processes of sEV-to-T cell signaling[147]. $CD4^+$ T cells have been shown to interact with dendritic cell sEVs via surface receptor binding; this occurred specifically through antigen presentation via MHC II, and also made use of CD80 and CD86 as T cell costimulators[147]. Additionally, $CD4^+$ T cells have also demonstrated the ability to endocytose or perform membrane fusion with dendritic cell-derived sEVs. This phenomenon was shown to induce the transfer of multiple surface receptors from the surface of sEVs to the surface of $CD4^+$ T cells, citing sEV bound ICAM-1 binding to T cell bound LFA-1 leading to the transfer of CD80 and MHC I to the T cell surface[148]. Yet other work demonstrates the transfer of MHC II from dendritic cell-derived sEVs to $CD4^+$ T cells, and noted that dendritic cell-derived sEV surface receptors may undergo trogocytosis by $CD4^+$ T cells[149]. There are therefore many different methods by which sEVs may initiate communication with $CD4^+$ T cells, although additional work

must be performed to more fully characterize this phenomenon: namely the examination of the physical mechanisms of sEVs derived from non-dendritic cells signaling to $CD4^+$ T cells.

While the characterization of the physical mechanisms driving non-dendritic cell-derived sEV signaling to $CD4^+$ T cells remains poorly understood, there are studies detailing the functional effects of this phenomenon. sEV signaling affects $CD4^+$ T cell phenotype, and macrophage-derived sEVs play a unique role in this phenomenon. This is highly relevant to our work, as macrophages are the most common type of cell in implanted PTS, and we have demonstrated that myeloid sEVs represent a significant population of pEVs. Early research by the Schoery group demonstrated that macrophages infected with a variety of pathogens release sEVs containing pathogen associated molecular patterns that initiate inflammatory responses in a wide variety of cells—particularly triggering MyD88 dependent TLR2 and TLR4 responses [150,151]. While TLR2 and TLR4 are not T cell specific, they are present on the surface of T cells, and play a role in $CD4^+$ T cell differentiation. Further studies by the Schoery group indicated that infected macrophage derived sEVs caused a TH1 response in $CD4^+$ T cells, acting synergistically with signals from other antigen presenting cells; however, it is therefore unclear whether the initial macrophage sEV signaling was MHC mediated within this context[152]. Recent literature provides a more defined role for macrophage sEV signaling to $CD4^+$ T cells by demonstrating that macrophage sEVs induced inflammatory TH1 and TH17 activation in $CD4^+$ T cells during aberrant inflammatory disease, and induced anti-inflammatory T_{reg} activity during cancer[153,154].

Although macrophages are the most common type of cell within implanted PTS, other myeloid and non-myeloid cells may also play a role in pEV signaling to $CD4^+$ T cells. Dendritic cells have been observed in the PTS, and their sEVs have been shown to activate $CD4^+$ T cells[43,147]. We have also demonstrated the presence of $CD4^+$ T cells within the PTS, which may also release sEVs that signal to other $CD4^+$ T cells; in some cases this triggers T_{reg} activation and

downregulation of TH1 responses[155]. Additionally, while not specifically yet observed in the PTS, recent evidence also indicates that mesenchymal stem cell and endothelial cell derived sEV signaling increased T_{reg} abundance and efficacy and immunomodulatory miRNA signaling respectively[155,156]. Thus, immunomodulatory sEV signaling is a potent mediator of the $CD4^+$ T cell equilibrium, and requires further study—particularly within the context of wound healing and the host response to implanted biomaterials.

5.2: Demonstration of pEV signaling to T cells

5.2.1: Significance

While $CD4^+$ T cell mediated modulation of the FBR within synthetic biomaterial implants and EV signaling to affect $CD4^+$ T cell phenotype have been separately and partially characterized to varying degrees, the role of sEV signaling to T cells within the implant microenvironment remains notably absent. This lack of understanding was particularly concerning due to the expectedly large role of bystander signaling within the PTS microenvironment. Our PTS have tunable biomaterial properties that impact resident cell phenotype, making them the ideal candidate for the study of biomaterial mediated sEV signaling to resident T cells. Moreover, the investigation of $CD4^+$ T cell subsets driven by PTS pore size will aid in the explanation of the unique pro-healing response intrinsic to 40μm PTS. Thus, we assert that sEV immune signaling to T cells within the PTS microenvironment is responsible for T cell phenotype and pore size dependent implant fate. In order to investigate this hypothesis, we examined the effects of pEVs on the stimulation and phenotype of $CD4^+$ T cells.

5.2.2: Materials and methods

(Section adapted from Hady et. al, 2020)

5.2.2.1: *Tissue culture and primary cell isolation*

Immortalized T lymphocytes (EL4 Cells, ATCC) were cultured according to manufacturer guidelines. Briefly, EL4 cells were cultured in T-75 culture flasks with DMEM (containing 4.5mg/mL, 4mM L-glutamine, 1mM sodium pyruvate, and 1.5mg/mL sodium bicarbonate, Gibco) with 10% horse serum and 1% penicillin streptomycin. The cells were kept at a concentration between $1x10^5$ and $1x10^6$ cells/mL.

Primary splenic T cells were isolated using CD3+ immunomagnetic separation. Briefly, spleens were removed from euthanized C57Bl/6 mice and homogenized in PBS. The homogenized spleen cells were placed in 15mL of hemolytic buffer and incubated at room temperature for 15 minutes and strained through a 40µm cell strainer. The cells were exposed to biotinylated CD3+ antibody and streptavidin coated magnetic beads and run through an LS column as per Miltenyi's instructions. Primary splenic T cells were cultured in RPMI 1640 (10% FBS, 1% penicillin streptomycin).

5.2.2.2: *In-vitro visualization of EV signaling*

EL4 cells were treated with pEVs from double transgenic mice. pEVs were added to affect an average final concentration of $5.93x10^8$ pEVs/mL. EL4 cells in a 12-well plate were exposed to EVs for one hour in medium as described above. Cells were then centrifuged at 300xg for 15 minutes, and the pellet was resuspended in PBS. The cell suspensions were analyzed with the ImageStream. The SPOT tool was then used to determine colocalization of fluorescent EVs with the EL4 cells.

5.2.2.3: *Primary splenic T cell viability assessment*

To test the effect of pEVs on viability, primary splenic T cells were loaded into a 6 well plate stimulated for 48 hours in stimulatory (CD3 and CD28 antibody coated plate) or non-stimulatory conditions (PBS without antibodies). As an aside, due to the use of positive immunomagnetic

selection to isolate primary T cells, T cells in non-stimulated culture conditions may have been affected by anti-CD3 conjugated microbeads. The cells were then loaded into a 96 well plate at a concentration of $1x10^5$ cells/well and treated with PTS cell derived EVs at an average concentration of $1.78x10^8$ pEVs/mL or PBS. 48 hours later the cells they were stained with trypan blue (Gibco). The live and dead cells were counted.

5.2.2.4: *T cell transcriptional analysis*

EL4 cells were divided equally into 12 well plates. The cells were then treated with pEVs from 40μm or 100μm PTS for 48 hours at an average final concentration of $7.14x10^8$ pEVs/mL. After 48 hours, the cells were collected and stored at -80°C until RNA isolation.

Primary T cells were resuspended in medium (RPMI1640 with 10% FBS and 1% penicillin streptomycin) with 100IU/mL IL-2 (ProLeukin from Novartis) and cultured in a plate coated with CD3 and CD28 antibodies for costimulation. After 48 hours the cells were split equally into 24 well plates, and treated with an average of $7.14x10^8$ pEVs/mL from 40μm or 100μm PTS for 48 hours. The cells were then collected and stored at -80°C until RNA isolation.

T cells treated with pEVs were processed with RNeasy Mini kit as per manufacturer's protocol (Qiagen) and used to generate cDNA as per manufacturer's protocol (Applied Biosciences). qPCR was performed with FAM (T Cell Panel) probes on an ABI 7900HT (thermal cycling parameters as previously described). The T cell panel included GAPDH, FOXP3, IL-10, IFN-γ, TGF-β1, TNFα, RORC, GATA3, and TBX21 (Probe IDs available in **Table 2**). Rationale for these panels can be seen in **Table 2**. Ct was considered undetermined if one or both replicates failed to amplify. Relative fold expression was calculated as previously described by normalizing against the housekeeping gene GAPDH.

5.2.3: Results

(Partially adapted from Hady et. al, 2020)

Initial imaging flow cytometry experiments examined the colocalization of myeloid pEVs to immortalized T cells in order to judge potential interactions between the two. Upon treatment of EL4 cells with pEVs from 40μm or 100μm PTS, pEVs colocalized upon the plasma membrane of EL4 cells when examined with imaging flow cytometry (representative image in **Figure 20**). Imagestream SPOT colocalization analysis determined that roughly 11.7% and 8.6% of EL4 cells were colocalizing with one or more myeloid pEVs from 40μm or 100μm PTS respectively (N=1) (**Figure 21**). These findings suggested a potential interaction between T lymphocytes and myeloid pEVs.

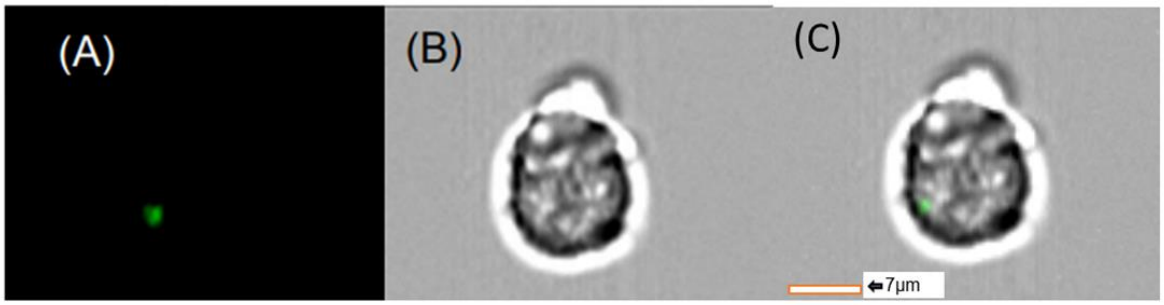

Figure 20: Imaging flow cytometric images of EL4 immortalized T cells co-cultured with pEVs from PTS explanted from double transgenic mice. Green myeloid pEVs can be seen co-localized with EL4 cells; GFP channel (A), brightfield (B), overlay (C).

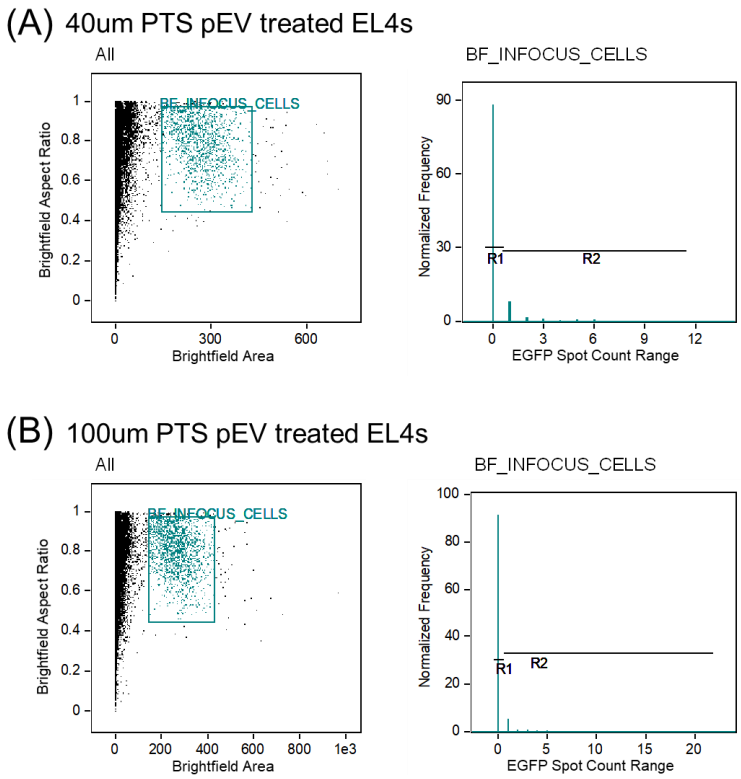

Figure 21: Imaging flow cytometric measurements of EL4 immortalized T cells co-cultured with pEVs from PTS explanted from double transgenic mice. pEVs were isolated from 40μm PTS (A) and 100μm PTS (B). The cell population was gated from the debris field, and the Spot Count tool in the IDEAS software was used to quantify pEV/EL4 colocalization.

Next, the effect of pEV-to-T cell interaction on T cell phenotype was examined; EL4 phenotype was quantified via RT-qPCR after treatment with pEVs from 40μm and 100μm PTS. Remarkably, immortalized T cells treated with pEVs significantly upregulated the T_{reg} marker IL-10 ($p=0.00012$ and $p=0.000043$ for 40μm and 100μm) and the TH1 marker IFN-γ ($p=0.001$ and $p=.001$ for 40μm and 100μm) regardless of PTS pore size (**Figure 22**) (N=4 (pEV treated cells) and N=10 (untreated cells)). However, only EL4 cells treated with 100μm PTS pEVs upregulated the TH1 marker TBX21 when compared with the untreated control ($p=0.0086$). Regrettably, the expression of T_{reg} indicating FoxP3 could not be quantified in this experiment as both a CD3 agonist and TGF-β1 treatment are required for EL4 cells to express it[157].These results demonstrated that pEVs stimulated the T cell transcriptome independent of pore size, particularly with regard to T_{reg} and TH1 phenotypes. Furthermore, these results indicated that

treatment with 100µm PTS pEVs may have led to an increased type I inflammatory response in recipient T cells observed via the upregulation of TBX21.

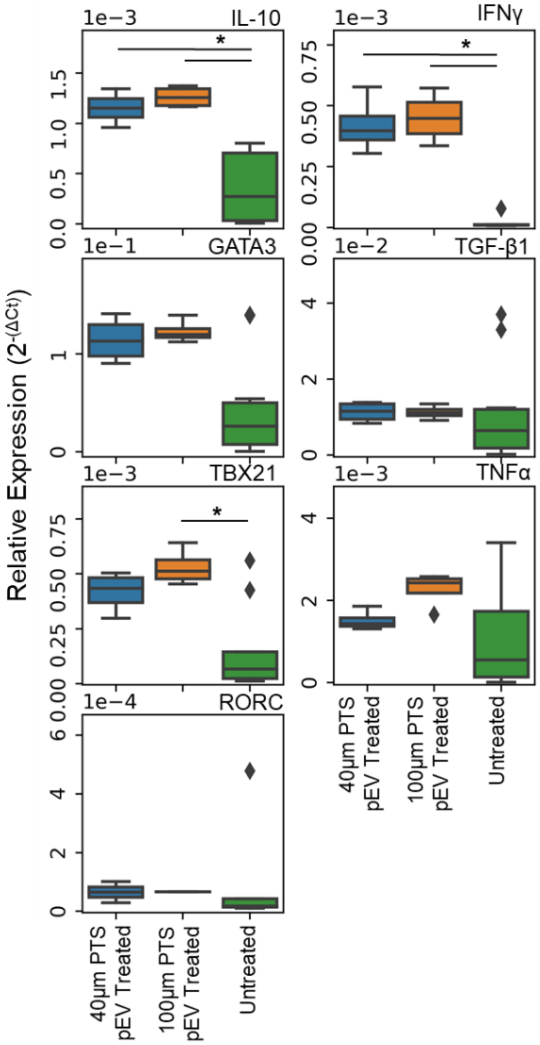

Figure 22: CD4$^+$ T cell phenotype of EL4 cells treated with pEVs. Differential gene expression CD4$^+$ T cell markers in EL4 cells treated with pEVs was measured by RT-qPCR using the T cell gene targets in **Table** 2: T cell gene **expression panel. Genes** of the T Cell RT-qPCR panel and their associated CD4+ T cell phenotypes.(*,p<0.05, N=4 for pEV treated and N=10 for untreated; significance was determined via ANOVA or Kruskal-Wallis tests followed by Tukey or Conover-Iman posthoc tests respectively based on normality assessed by Shapiro-Wilk test, see 2.3.2.5: for details).

The effect of pEV treatment on naïve splenic T cell phenotype was then assessed via the same method. 40µm and 100µm PTS pEV treatment caused naïve splenic T cells to upregulate the T_{reg} marker FoxP3 when compared to untreated cells (**Figure 23**) (N=5, p=0.035 and p=0.027 respectively). Moreover, pEVs from both 40µm and 100µm PTS caused primary T cells to

upregulate the TH1 marker TBX21 when compared to untreated cells (N=5, p=0.014 and p=0.001 respectively). These data corroborated the upregulation of T_{reg} and TH1 markers in immortalized T cells upon pEV treatment, and demonstrated that pEVs mediate unique phenotypic differentiation and transcriptomic stimulation of primary T cells (although these primary T cells potentially included $CD8^+$, γδ, and NK T cell populations as well).

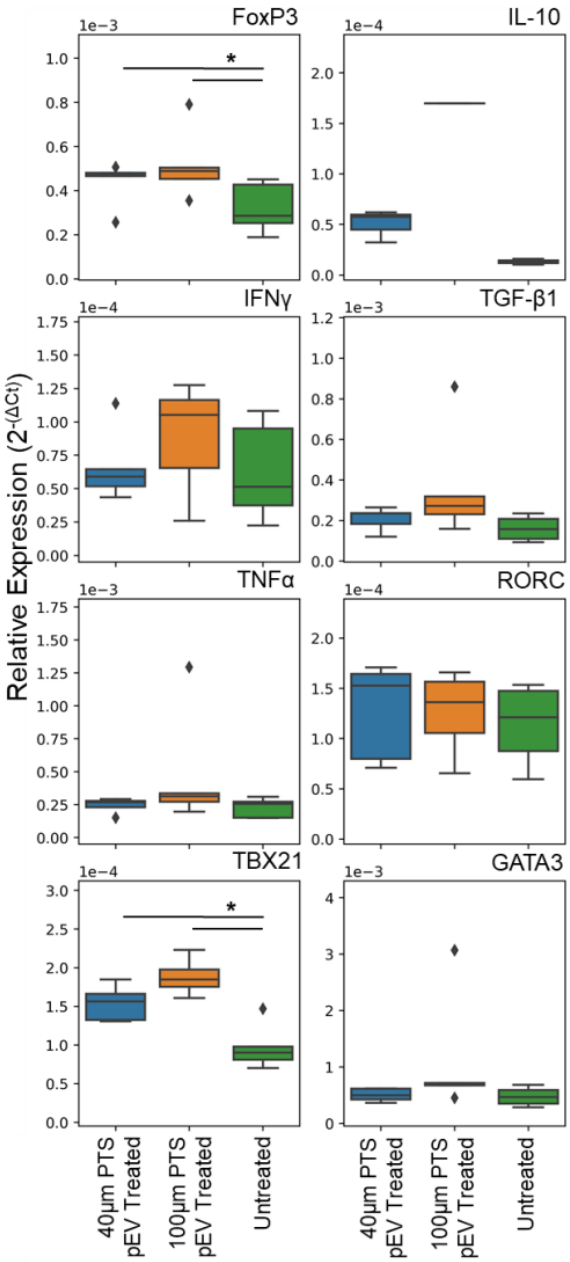

Figure 23: $CD4^+$ T cell phenotype of naïve splenic T cells treated with pEVs. Differential gene expression of $CD4^+$ T cell markers in costimulated IL-2 treated splenic T cells treated with pEVs was measured by RT-qPCR using the T cell gene targets in Table 2 (*,p<0.05, N=5; significance was

determined via ANOVA or Kruskal-Wallis tests followed by Tukey or Conover-Iman posthoc tests respectively based on normality assessed by Shapiro-Wilk test, see 2.3.2.5: for details).

The effect of pEV treatment on the viability of primary T cells was next examined; pEVs from 40µm and 100µm PTS were applied to costimulated (CD3 and CD28 antibody treated without IL-2) and unstimulated primary splenic T cells. Upon cell counting after a live/dead stain to determine cellular viability, costimulated primary T cells treated with pEVs were significantly more viable than unstimulated, untreated primary T cells (p=0.007 and p=0.0051 for 40µm and 100µm PTS pEV treated, N=12 (co-stimulated) and N=4 (non-co-stimulated)) (**Figure 24**). These data further support our assertion that pEVs from both 40µm and 100µm PTS stimulated primary T cells.

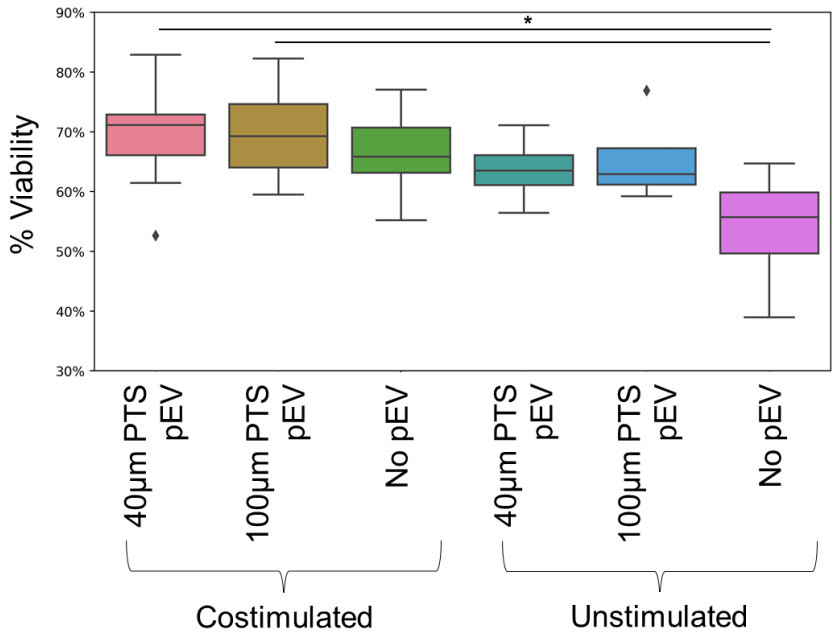

Figure 24: *In-vitro* effects of CD3/CD28 antibody stimulation and pEV treatment on splenic T cell viability. Viability was measured via cell counts. No significant difference in the total number of cells was noted (*,p<0.05. N=12 for stimulated and N=4 for unstimulated; significance was determined via ANOVA or Kruskal-Wallis tests followed by Tukey or Conover-Iman posthoc tests respectively based on normality assessed by Shapiro-Wilk test, see 2.3.2.5: for details).

5.3: Discussion: Investigation of pEV mediated T cell signaling

Immortalized $CD4^+$ T cells appeared to visibly interact with myeloid pEVs based on their colocalization in culture. While the colocalization of these cells and pEVs would not provide

sufficient evidence of interaction on its own, the significant differences in phenotypic expression in and activation of pEV treated T cells provided the necessary evidence to demonstrate pEV-to-T cell signaling interactions. In immortalized T cells, pEV treatment led to broad transcriptional upregulation through the upregulation of IL-10 and IFN-γ, T_{reg} and TH1 indicators. Moreover, 100μm pEV treatment caused the upregulation of TH1 indicator TBX21, while 40μm pEV treatment did not. These data thus indicated that pEVs caused specific transcriptional upregulation in immortalized T cells, while 100μm pEVs may have induced a more inflammatory T cell equilibrium than 40μm pEVs. While the concomitant upregulation of IFN-γ and IL-10 was initially counterintuitive, this phenomenon has been observed in bystander T_{reg} populations in chronic inflammation[158].

Primary T cells also demonstrated transcriptional upregulation as a result of pEV treatment. Specifically, the upregulation of T_{reg} and TH1 markers FoxP3 and TBX21 occurred as a result of both 40μm and 100μm PTS pEV treatment. Thus, in both immortalized and primary T cells, T_{reg} and TH1 markers were upregulated as a function of pEV treatment independent of PTS pore size. Moreover, the transcriptomic stimulation in primary T cells was corroborated by the upregulation of T cell viability as a result of pEV treatment. However, unlike in EL4 cells, IL-10 and IFN-γ were not differentially regulated as a result of pEV treatment, and TBX21 was not differentially regulated depending on the pore size of the PTS the pEVs were isolated from. As EL4 cells are unable to express FoxP3 in culture unless properly stimulated with a CD3 agonist and TGF-β1, we believe that these transcriptional discrepancies between pEV treated immortalized and primary T cells may be due to the lack of $FoxP3^+$ T_{regs} in EL4 cells; this conclusion is consistent with our findings that demonstrated the key role $FoxP3^+$ T_{regs} play in maintaining the $CD4^+$ T cell equilibrium within implanted PTS. While the upregulation of both FoxP3 and TBX21 in recipient T cells was confounding, $FoxP3^+/TBX21^+$ T cells have recently been shown to play a key role in reducing type I inflammation[159]. However, additional

experimentation is required to investigate whether pEV treated primary T cells co-express FoxP3 and TBX21, or if these are two distinct cell populations. Regardless, T_{reg} and TH1 populations are partially responsible for the attenuation of potentially fibrotic TH2 responses, which may indicate an anti-fibrotic role for pEV-to-T cell signaling in primary T cells.

Chapter 6: The role of TLR4 in pEV mediated T cell signaling

6.1: Introduction: TLR4 plays a key role in determining $CD4^+$ T cell phenotype

TLRs are best characterized as modulators of innate immunity—and as previously discussed, MyD88 dependent TLR4 signaling plays a role in determining the response of macrophages to the physical properties of biomaterials, including pore size[53,54]. However, TLRs have also demonstrated the ability to affect the adaptive immune system through T cell signaling[160]. TLR4 has specifically been shown to affect $CD4^+$ T cell activation and phenotype[161–163]. Although TLR4 mediated T cell signaling has been characterized by previous research, the mechanisms of this signaling have not yet been well defined. Moreover, the potential roles of sEVs within the context of TLR4 signaling are understudied.

6.1.1: Cell signaling regulators downstream of TLR4

TLR4 mediated signaling in $CD4^+$ T cells is a potent driver of their activation and phenotypic differentiation[161–163]. TLR4 signaling is either MyD88 dependent or independent, both of which exhibit different effects on $CD4^+$ T cell phenotype (**Figure 25**). One primary mechanism of MyD88 dependent signaling relies on TRAF6 to induce signaling cascades that activate AP-1, IRF5, and NF-κB via mitogen-activated protein kinase (MAPK)[164]. This signaling cascade results in elevated IL-6, TNFα, and IL-12 expression[164]. TRAF6 mediated MyD88 dependent signaling may thereby cause the upregulation of TH1 and TH17 responses[163]. While not in T cells, further evidence indicated that sEVs are capable of immunomodulation through the initiation of TLR4 mediated MyD88 dependent signaling in monocytic cells[165].

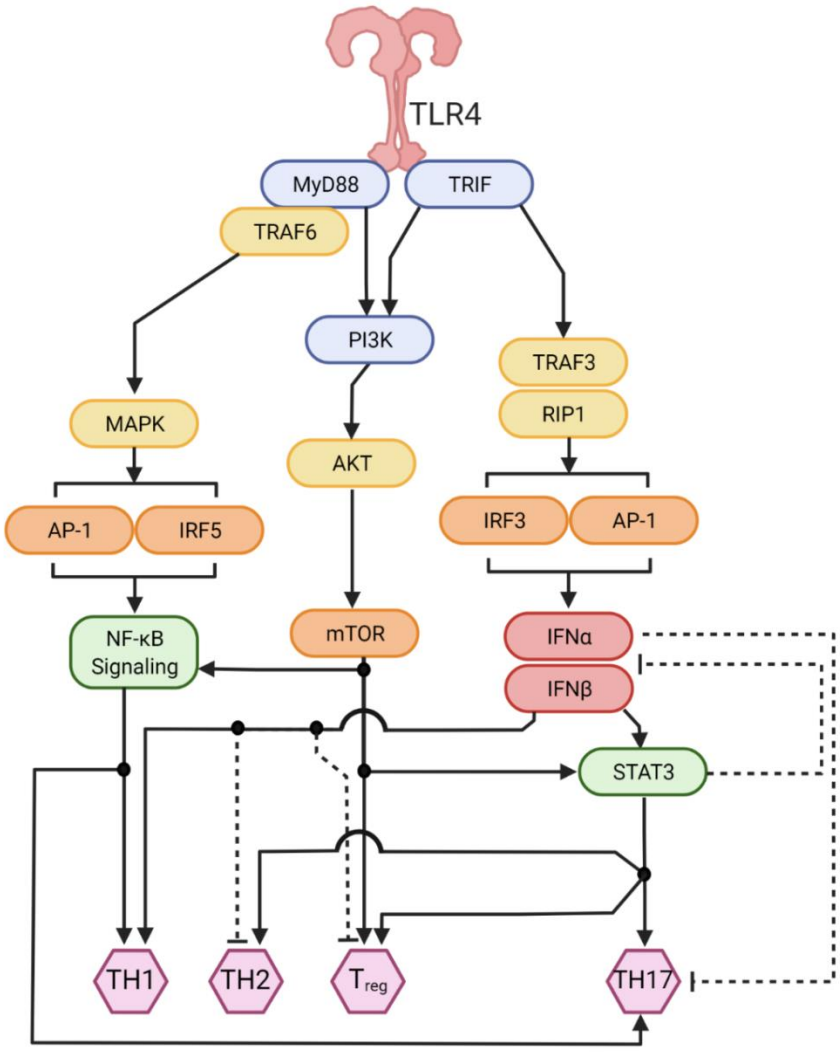

Figure 25: Simplified TLR4 pathway summary. TLR4 may affect $CD4^+$ T cell differentiation through the MyD88 dependent, MyD88 independent, or PI3K mediated pathways. Solid arrows indicate activation; dashed lines with flat heads indicate inhibition.

MyD88 independent TLR4 signaling relies on TRIF and TRAF3 to cause the upregulation of AP-1, IRF3, and NF-κB, which thereby induce IFNα and IFNβ production[164,166]. These cytokines upregulate TH1 responses while downregulating TH2, TH17, and T_{reg} responses[167,168]. On the other hand, these type I interferons and other TLR4 mediated signaling cues lead to changes in STAT3 regulation[169,170]. STAT3 upregulation inhibits type I interferon responses and causes the differentiation of TH2 and TH17 cells, while also modulating T_{reg} populations[171,172]. Increased TH1 stability and the modulation of T_{reg},TH2, and TH17 responses are therefore affected by MyD88 independent TLR4 signaling[167,173–176]. While not fully understood, previous research

demonstrated that sEV mediated MyD88 independent TLR4 signaling was immunomodulatory and dependent on TRIF in macrophages from obese mice[177].

Recent evidence has also demonstrated that PI3K signaling is upregulated as a result of both MyD88 dependent and MyD88 independent signaling[178]. These interactions are well known to upregulate AKT and subsequently mTOR activity. As PI3K and mTOR upregulation may initiate further MyD88 dependent or MyD88 independent signaling pathways, PI3K mediated signal transduction serves as a mechanism of cross-talk between these two methods of TLR4 signaling[179]. Functionally, PI3K and mTOR signaling play a complex regulatory role in TLR4 signaling. For example, recent evidence indicated that MyD88 dependent TLR4 signaling enhanced T_{reg} activation[180,181]; this phenomenon may have occurred as a consequence of MyD88 dependent, TRAF6 independent PI3K signaling, as the subsequent induction of mTOR (which may also theoretically be mediated by TRIF) led to upregulated proliferation of existing FoxP3$^+$ T_{regs}[182]. mTOR induction may also confoundingly induce an upregulation of inflammatory CD4$^+$ T cell subtypes and cause a downregulation of FoxP3 expression in naïve T cells[182]. Finally, recent evidence indicated that sEVs from macrophages polarized to an M2-like phenotype affected the PI3K to mTOR signaling pathway in a rat model of osteoarthritis[183].

TLR4 is thus a complex regulatory mechanism that influences CD4$^+$ T cell phenotype. Moreover, other studies indicated that a variety of different TLR4 signaling pathways were immunomodulatory targets of sEV signaling. It was therefore important to consider the specific components of the TLR4 pathway involved in the induction of immunomodulatory responses to pEVs. Additionally, the functional downstream effects of TLR4 signaling affect CD4$^+$ T cells in ways consistent with our findings that demonstrated activation as well as TH1 and T_{reg} marker upregulation as a result of pEV treatment[184].

6.2: The role of TLR4 in pEV-to-T cell signaling

6.2.1: Significance

TLR4 plays an important role in determining the $CD4^+$ T cell phenotypic equilibrium in inflammation, but research investigating sEV-to-T cell signaling via TLR4 was extremely limited. Given that pEV-to-T cell signaling induces $CD4^+$ T cell phenotypic differentiation in a manner consistent with the modulation of TLR4 cell signal transduction, we aimed to characterize this potential pathway. In addition to $CD4^+$ T cell differentiation induced by pEV mediated TLR4 signaling, we characterized the specific portions of the TLR4 signaling pathway (i.e. MyD88 dependent or MyD88 independent) that affect these changes. We hypothesized pEVs were interacting with TLR4 in order to affect $CD4^+$ T cell phenotype in a MyD88 independent manner. In order to investigate this phenomenon, we treated MyD88-deficient and TLR4-deficient splenic T cells with pEVs generated ex-vivo from cells inhabiting explanted 40μm and 100μm PTS, and examined the resulting effect on $CD4^+$ T cell phenotype via RT-qPCR. We also examined the expression of specific downstream effectors, both MyD88 dependent and MyD88 independent, downstream of TLR4 via RT-qPCR. Effectors were chosen to determine the mechanism of TLR4 signaling affected by pEVs: TRAF6 expression quantified classical MyD88 dependent TLR4 signaling, mTOR expression quantified PI3K mediated signaling, TRAF3 expression quantified classical MyD88 independent signaling, and type-I interferon and STAT3 expression quantified the specific portion of MyD88 independent signaling being upregulated.

6.2.2: Materials and methods

(Section adapted from Hady et. al, 2022 (in preparation))

6.2.2.1: *Tissue culture and primary cell isolation*

Primary splenic T cells from wild type C57Bl/6, MyD88ko C57Bl/6, and TLR4ko C57Bl/6 mice were isolated using CD3+ immunomagnetic separation as previously described. The positive

fraction was resuspended in culture medium containing 100IU/mL IL-2 (ProLeukin from Novartis)) then cultured in a plate coated with CD3 and CD28 antibodies for costimulation. After 48 hours the cells were divided equally into 24 well plates. pEVs were then added to affect a final average concentration of $7.14x10^8$ pEVs/mL. The pEV treated T cells were then frozen at -80°C until RNA isolation.

6.2.2.2: *T cell transcriptional analysis*

T cells treated with pEVs were processed with RNeasy Mini kit as per manufacturer's protocol (Qiagen) and used to generate cDNA as per manufacturer's protocol (Applied Biosciences). qPCR was performed with FAM (T Cell Panel, **Table 2**) probes on an ABI 7900HT (thermal cycling parameters as previously described). Additionally, qPCR for TLR4 effector genes was performed with SYBR green on the same thermocycler and thermal cycling parameters. The TLR4 effector gene panel included STAT3α, STAT3β, IFNα, IFNβ, TRAF3, TRAF6, and mTOR (primer sequences available in **Table 3**). Rationale for these panels can be seen in **Table 2** and **Table 3**. Ct was considered undetermined if one or both replicates failed to amplify. Relative fold expression by normalizing against the housekeeping gene GAPDH was calculated as previously described. Statistical analyses were performed as previously described.

Gene	Role in TLR4 Pathway	Affected T Cell Phenotype	Primer Sequences
STAT3α	MyD88 Independent & mTOR Signaling Effector	TH2, T_{reg}, TH17	F: ACCAACGACCTGCAGCAATA R: TCCATGTCAAACGTGAGCGA
STAT3β	MyD88 Independent & mTOR Signaling Effector	TH2, T_{reg}, TH17	F: TACCTCTACCCCGACATTCCC R: CATCAATGAATGGTGTCACACAGA
IFNα	MyD88 Independent Signaling Effector	TH1, TH2, T_{reg},TH17	F: CCTGTGTGATGCAGGAACC R: TCACCTCCCAGGCACAGA
IFNβ	MyD88 Independent Signaling Effector	TH1, TH2, T_{reg},TH17	F: ATGAGTGGTGGTTGCAGGC R: TGACCTTTCAAATGCAGTAGATTCA
TRAF3	MyD88 Independent Signaling Effector	TH1, TH2, T_{reg}, TH17	F: TGAGCTGGAGAGCGTAGACA R: AGATCAGCACCCCGTTGTAG
TRAF6	MyD88 Dependent Signaling Effector	TH1, TH17	F: GCAGTGAAAGATGACAGCGTGA R: TCCCGTAAAGCCATCAAGCA
mTOR	PI3K Signaling Effector	TH1, TH2, T_{reg}, TH17	F: TGTCTGATTCTCACCACGCA R: CTCTTTGGCCAGGGTCTCAT
GAPDH	N/A	Housekeeping	F: GCGGCACGTCAGATCCA R: CATGGCCTTCCGTGTTCCT

Table 3: Genes of the TLR4 Effector RT-qPCR panel, their role in the TLR4 pathway, and their affected $CD4^+$ T cell phenotypes.

6.2.3: Results

(Section adapted from Hady et. al, 2022 (in preparation))

We first investigated MyD88 dependent TLR4 mediated pEV-to-T cell signaling by treating splenic T cells from MyD88 knockout mice with pEVs from 40μm and 100μm PTS. Upon pEV treatment of naïve MyD88 deficient T cells (**Figure 26A**), a significant upregulation of FoxP3 was observed (N=5 for sEV treated and N=4 for untreated, p=0.00517). This result was consistent with the upregulation of FoxP3 in wild type naive T cells treated with pEVs. Additionally, TBX21 was significantly upregulated in MyD88 deficient T cells treated with pEVs from 40μm PTS (p=0.0264), but not significantly in those treated with pEVs from 100μm PTS. This slightly contrasted the upregulation of TBX21 as a result of both 40μm and 100μm PTS

pEV treatment in wild type naive T cells. However, TBX21 in MyD88 deficient T cells treated with pEVs from 100µm PTS still trended upwards when compared with untreated MyD88 deficient T cells. We thus concluded that MyD88 dependent pEV mediated TLR4 signaling did not play a significant role in the regulation of $CD4^+$ T cell phenotypic homeostasis.

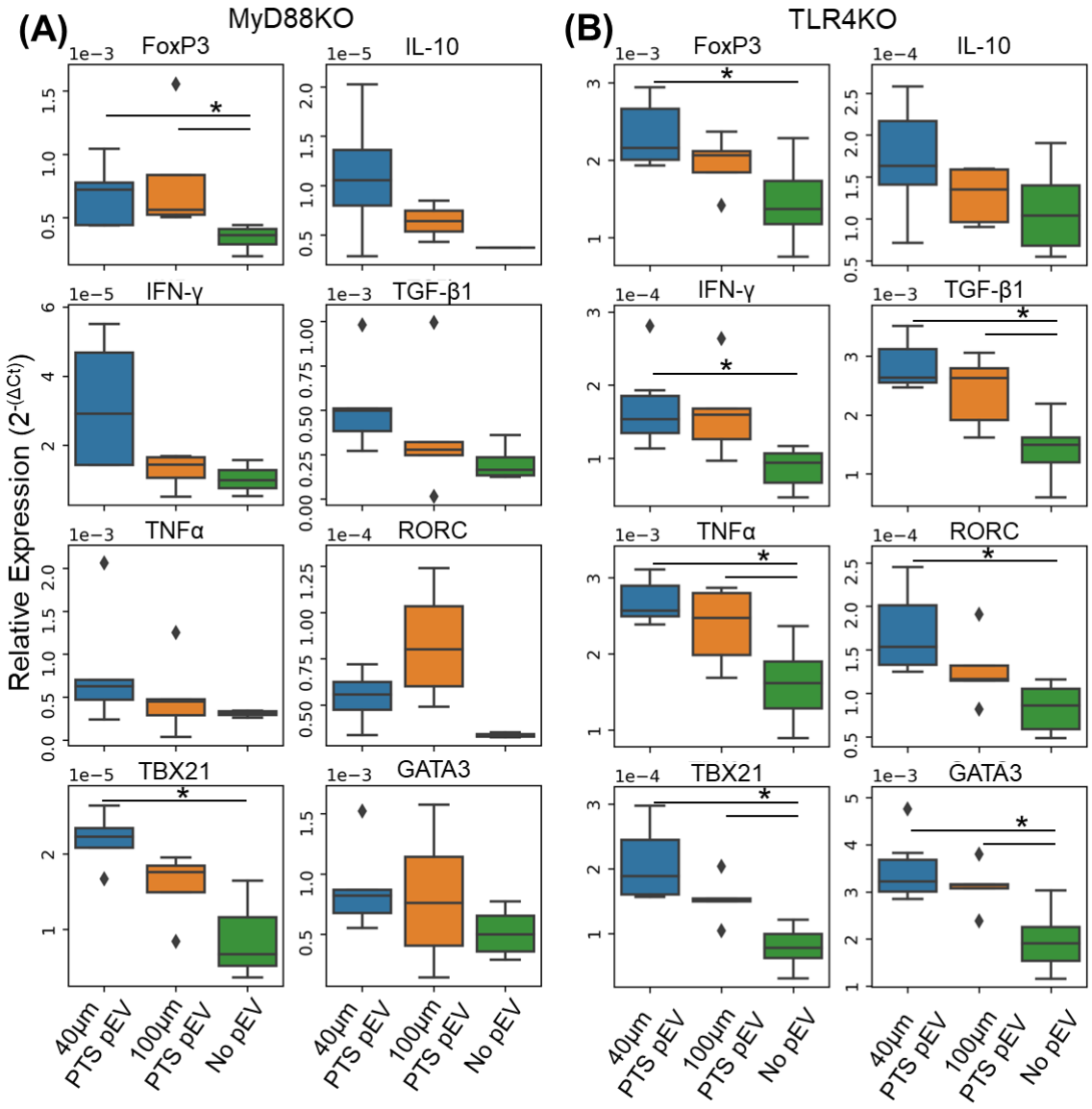

Figure 26: Quantification of the role of MyD88 and TLR4 in pEV treated T cell phenotype. $CD4^+$ T cell markers (**Table 2**) measured by RT-qPCR on pEV treated primary splenic T cells from (A) MyD88ko (N=5 for treated and N=4 for untreated) and (B) TLR4ko (N=6 for 40µm PTS pEV treated and untreated, N=5 for 100µm PTS pEV treated) mice (*, $p<0.05$; significance was determined via ANOVA or Kruskal-Wallis tests followed by Tukey or Conover-Iman posthoc tests respectively based on normality assessed by Shapiro-Wilk test, see 2.3.2.5: for details).

We next investigated the role of all TLR4 signaling (and therefore MyD88 independent signaling) in pEV-to-T cell communication by treating splenic T cells from TLR4 knockout mice with pEVs from 40μm and 100μm PTS. Treating TLR4 deficient splenic T cells with pEVs resulted in broad transcriptomic upregulation (**Figure 26B**). Treatment with pEVs from 40μm PTS caused an upregulation of FoxP3 (N=6 for 40μm PTS pEV treated and untreated, N=5 for 100μm PTS pEV treated, p=0.0132), IFN-γ (p=0.0357), TGF-β1 (p=0.00100), TNFα (p=0.00288), RORC (p=0.00552), TBX21 (p=0.00100), and GATA3 (p=0.00333). Conversely, treatment with pEVs from 100μm PTS caused a significant upregulation of TGF-β1 (p=0.0207), TNFα (p=0.0396), TBX21 (p=0.0358), and GATA3 (p=0.0278). TLR4 deficiency therefore drastically affected the regulation of pEV signaling to T cells, where pEVs from 40μm PTS exhibit the greatest transcriptomic impact.

Following the characterization of MyD88 dependent and MyD88 independent pEV mediated TLR4 signaling to affect $CD4^+$ T cell phenotype, we characterized the regulation of effectors downstream of TLR4 in T cells upon pEV treatment. In wild type splenic T cells, pEVs from both 40μm and 100μm PTS caused the downregulation of IFNα (**Figure 27A**) (N=5, p=0.00271). However, in MyD88 and TLR4 deficient splenic T cells, IFNα expression was not differentially regulated as a result of pEV treatment. Additionally, pEVs from 40μm PTS, but not 100μm PTS, also caused a downregulation of mTOR (N=5, p=0.0403 and p=0.0219 versus 100μm pEV treated and untreated respectively) and STAT3β (N=5, p=0.00741) in wild type splenic T cells. In MyD88 deficient splenic T cells, pEVs from 40μm PTS caused a downregulation of TRAF3 (**Figure 27B**) (N=5 for pEV treated and N=4 for untreated, p=0.00651). There was thus a distinct suppressive role for MyD88 mediated TLR4 signaling by pEVs in splenic T cells, especially by those pEVs from 40μm PTS.

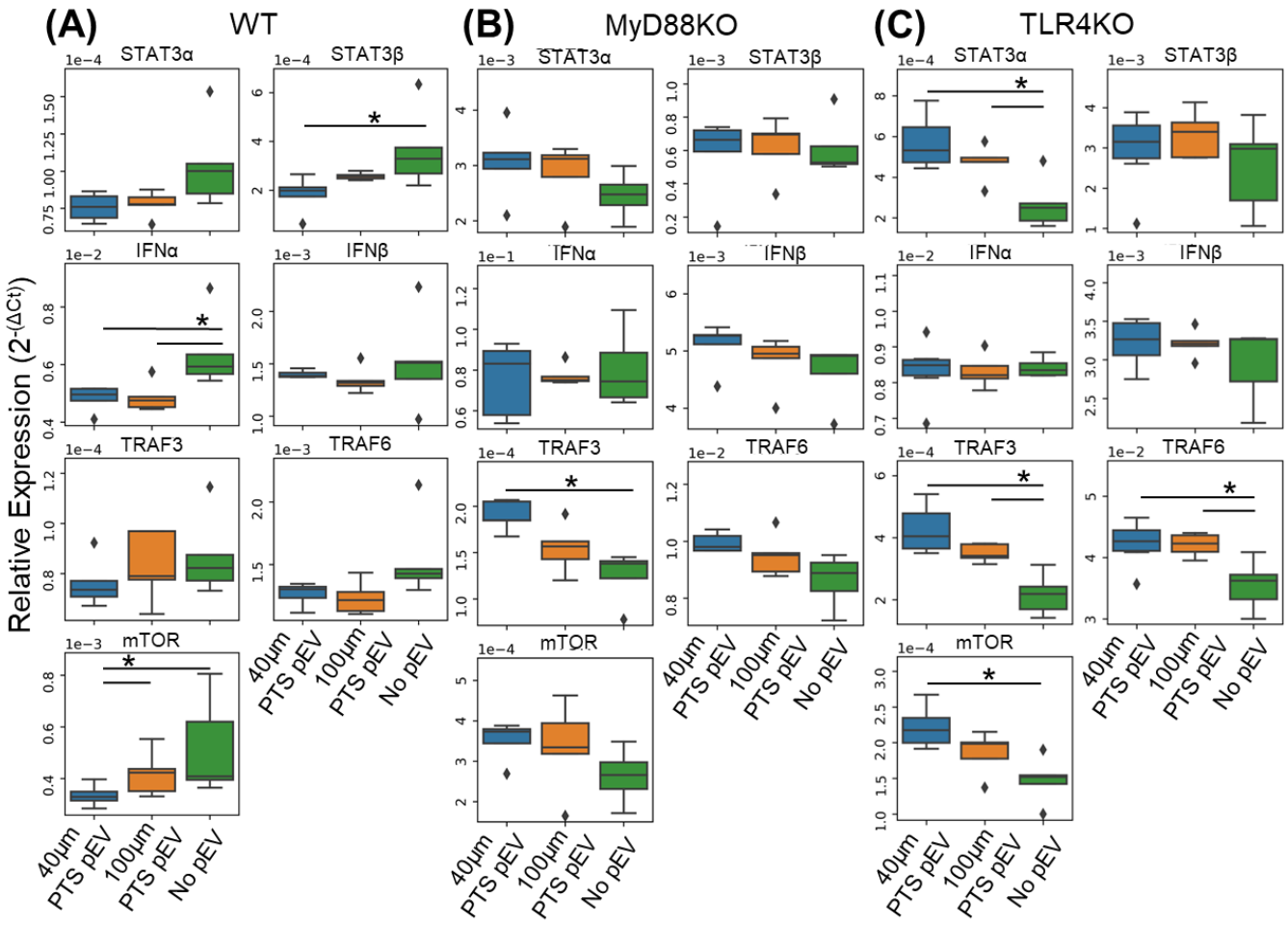

Figure 27: TLR4 effector expression in pEV treated primary T cells. TLR4 effector expression was measured via RT-qPCR (panel in **Table 3**) in pEV treated splenic T cells collected from (A) WT (N=5), (B) MyD88KO (N=5 for treated and N=4 for untreated), and (C) TLR4KO mice (N=6 for 40µm PTS pEV treated, N=5 for 100µm PTS pEV treated and untreated) (*, $p<0.05$; significance was determined via ANOVA or Kruskal-Wallis tests followed by Tukey or Conover-Iman posthoc tests respectively based on normality assessed by Shapiro-Wilk test, see 2.3.2.5: for details).

In TLR4 deficient splenic T cells, treatment with pEVs from both 40µm and 100µm PTS (**Figure 27C**) caused a significant upregulation of TRAF3 (N=6 for 40µm PTS pEV treated, N=5 for 100µm PTS pEV and untreated, p=0.00100 and p=0.0131 for 40µm and 100µm PTS pEV treated), TRAF6 (p=0.0170 and p=0.0245 for 40µm and 100µm PTS pEV treated), and STAT3α (p=0.00275 and p=0.0457 for 40µm and 100µm PTS pEV treated). mTOR was also upregulated only in T cells treated with pEVs from 40µm PTS (p=0.00386). These effects were not observed

in wild type or MyD88 deficient T cells treated with PTS cell-derived sEVs. MyD88 independent TLR4 signaling mediated by pEVs thus played a regulatory role in pEV-to-T cell signaling.

6.3: Discussion: The role of TLR4 in pEV mediated T cell signaling

TLR4 is involved in pEV-to-T cell signaling, and MyD88 dependent and independent pathways play unique roles. While MyD88 dependent TLR4 signaling by pEVs did not appear to affect $CD4^+$ T cell phenotype, it did play a role in the modulation of inflammation via the downregulation of type I interferon responses, as IFNα was downregulated as a result of pEV treatment in wild type T cells. Interestingly, type I interferons downregulate T_{reg} responses—so the downregulation of IFNα may have led to increased T_{reg} efficacy. Moreover, 40μm PTS pEVs downregulated mTOR to STAT3 signaling via MyD88 dependent TLR4 mediated signaling, which may have attenuated non-TH1 responses. Thus, pEV mediated MyD88 dependent TLR4 signaling modulated inflammatory responses in recipient T cells, and attenuated PI3K to MyD88 independent signaling in a pore size-dependent manner.

MyD88 independent TLR4 signaling by pEVs plays a key role in the regulation of $CD4^+$ T cell phenotype. While similar (though not identical) upregulations of T_{reg} and TH1 markers were observed in wild type, MyD88 deficient, and TLR4 deficient T cells, TLR4 deficient T cells also showed broad transcriptional upregulation as a result of pEV treatment. pEVs from both 40μm and 100μm PTS caused this broad transcriptional upregulation via the significantly increased expression of other TH1, TH2, and TH3 markers, although pEVs from 40μm PTS had additional cell signaling capabilities as demonstrated via additionally upregulated TH1 and TH17 markers. As this T cell activation took place only in TLR4 deficient T cells, we can conclude that TLR4 plays a regulatory role in pEV-to-T cell signaling. Moreover, as this did not occur in MyD88 deficient T cells, this regulatory aspect of pEV-to-T cell signaling is MyD88 independent. We may also conclude that the upregulation of specific T_{reg} and TH1 markers (FoxP3 and TBX21)

was independent of TLR4. Finally, we can conclude that pEVs from 40µm PTS are either more potent or contain different cell signaling cargo than pEVs from 100µm PTS.

The upregulation of STAT3 and the adaptor proteins for both MyD88 dependent (TRAF6) and independent (TRAF3) signaling upon pEV treatment in TLR4 deficient T cells was initially confounding. As this upregulation occurred only in TLR4 deficient T cells, this regulatory phenomenon was also MyD88 independent, but TLR4 mediated. However, many cell signaling pathways make use of TRAF3, TRAF6, and STAT3 signaling— for example, T cell receptor, other TLR (e.g. TLR2), and interleukin signaling pathways, respectively. When taken with the data demonstrating the transcriptional activation of pEV treated $CD4^+$ T cells, the differential expression of effector molecules downstream of TLR4 explains a potential mechanism of this regulatory MyD88 independent TLR4 signaling. More specifically, MyD88 independent TLR4 signaling appears to regulate pEV signaling—specifically with respect to other signaling pathways like TLR2 and the T cell receptor. This regulatory mechanism thus demonstrates that while pEVs directly signal to recipient T cells via TLR4, pEVs must also interact with multiple signaling pathways on and within recipient T cells. These studies therefore necessitated a comprehensive analysis of pEV cargo to further the understanding of other mechanisms of pEV-to-T cell signaling.

Chapter 7: Proteomic analysis of pEVs

7.1: Introduction: Characterizing pEV contents

sEVs contain a diverse, heterogeneous proteome necessary to their cell signaling potency. Exocarta and Vesiclepedia, curated databases of exosome and EV contents respectively, demonstrate that over 40,000 and 349,000 different proteins have been observed in these particles[185,186]. These proteins are involved in a massive variety of cell signaling pathways through many different methods of interaction (i.e. internalization, surface protein binding, etc.)[107]. However, the proteome of many different kinds of sEVs is still largely unknown, variable, and dependent on the condition of the parent cell. Thus, the examination of the sEV proteome is a key part of understanding yet undiscovered functions.

7.1.1: Methodology of EV protein identification

The characterization of EV proteomes has recently become a critical topic in EV research. Previous methods of EV proteomic characterization used as recently as 1999 were only able to quantify a small subset of highly abundant proteins within EVs, whereas recent methods have been able to identify hundreds to thousands[187]. High resolution mass spectrometry accompanied by liquid chromatography (LC-MS/MS) has recently been discovered as a new standard in EV proteomic characterization[187]. Not only is LC-MS/MS highly sensitive, it is also able to quantify non-abundant proteins label-free. Moreover, when combined with recent advances in proteomic analytical tools (e.g. PANTHER database) and statistical overrepresentation and enrichment analyses, functional cell signaling mechanisms of previously uncharacterized EVs can be mapped. LC-MS/MS has thus become a key tool in understanding EV function.

In addition to LC-MS/MS, more specific methods of EV protein characterization have recently been popularized. While western blotting remains a valuable tool in the identification of specific

EV protein cargo, imaging flow cytometry has recently been discovered as a tool to investigate EV surface proteins. Coupled with fluorescent antibody labeling and labeling of EVs with a lipophilic dye, individual EVs can be assessed for the presence of membrane bound and transmembrane proteins[188]. When combined with LC-MS/MS, these methods compose a powerful, high throughput toolset to examine the broad functions of an EV population and subsequently follow up with the identification of specific cell signaling molecules. We therefore used these methods to analyze the proteome and function of pEVs.

7.1.2: Hypothesized TLR4 agonists and signaling modulators

We proposed that two classes of cell signaling molecules were affecting TLR signaling pathways from the surface of pEVs: heat shock proteins (HSPs) and β –galactosidase binding lectins (Galectins) (**Table 4**). The HSP70 and HSP90 protein families have been implicated in TLR4 signal modulation: particularly HSPA5 (GRP78) and HSP90b1 (GRP94). However, studies characterizing EV-bound GRP78 and GRP94 are lacking. While the MISEV requirements officially list GRP78 and GRP94 as "*a priori* not enriched" in sEVs, other recent studies have identified them on the surface of sEVs in a variety of conditions via both western blot and electron microscopy[101,189]. Moreover, the abundance of membrane-bound and sEV-loaded GRP78 and GRP94 is upregulated during ER stress, which can be a consequence of a key part of the FBR: chronic inflammation[189–192]. Thus, both GRP78 and GRP94 may be plasma membrane-bound, contained in sEVs, and shuttle EV cargo synergistically[115,193–197].

Protein	Presence on EV Surface	Receptors	Affects
GRP78 (HSPA5)	Contentious	TLR4	TH1, TH2, TH17, T_{reg}
GRP94 (HSP90B1)	Contentious	TLR4	TH1, TH2, TH17, T_{reg}
Gal3 (Galectin 3)	Hypothesized	TLR4, LAG3	TH1, TH2, TH17, T_{reg}
Gal9 (Galectin 9)	Confirmed	LAG3, TIGIT, TIM-3, CD44	TH1, T_{reg}

Table 4: Summary of hypothesized pEV surface proteins and their signaling mechanisms that affect $CD4^+$ T cell phenotype.

Like GRP78 and GRP94, galectin-3 and galectin-9 (Gal3 & Gal9) are under-characterized molecules with respect to EV mediated $CD4^+$ T lymphocyte functional change. Moreover, GRPs and Galectins share binding targets and may act synergistically[115,198,199]. This is partially because Gal3 and Gal9 are highly promiscuous, which confounds the understanding of their roles in inflammation[200]. Gal9 is well characterized in a membrane-bound state, while Gal3 is best characterized as a soluble cytokine—though recent evidence demonstrates that non-monomeric Gal3 is expressed as a membrane-bound protein in other species[198,201–204]. Indeed, Gal3 is preferentially shuttled into EVs and localized to membranous lipid rafts (principal components of EV membranes)[199,205,206]. As EV bound Gal3, Gal9, GRP78, and GRP94 have the potential to influence $CD4^+$ T cell phenotype via TLR4, the specific roles of these proteins within the context of wound healing must be characterized in order to most effectively modulate the host immune response to foreign biomaterials.

Gal3 and GRP94 are TLR4 binding ligands we believed to be present on the surface of pEVs[195,198,199,203,205–207]. Both Gal3 and GRP94 have been implicated in MyD88 dependent TLR4 signaling by previous research to influence type I inflammatory responses[207,208]. Conversely, the highly pleiotropic GRP78 likely does not directly bind TLR4, but is still a key player in indirect

TLR signaling. GRP78 binds CD14: a TLR4 complexing protein principally expressed on macrophages present in both soluble and membrane bound forms[209–211]. CD14 is present on macrophage EVs, which were plentiful amongst pEV populations, but not natively expressed on T cells[209–211]. Previous studies show that the CD14/TLR4/GRP78 complex reduces effector molecule expression downstream of TLR4 signal transduction[209,212]. EV membrane bound GRP78 may then modulate the signal transduction initiated by direct binding of other GRP/Gal ligands. This phenomenon has not yet been investigated in T cells, but we hypothesize CD14/GRP78 complexes binding to TLR4 will reduce TH1 stimulation. TLR4 signaling via GRP/Gal proteins may thus be highly influential on T_{helper} phenotype, but $CD4^+$ T cell phenotype is also regulated by other surface receptor binding interactions with Gal proteins.

Gal3 and Gal9 bind a number of ligands that attenuate the effects of TLR4 binding at different stages of signal transduction. Interstitial Gal3 and Gal9 initiate LAG3 binding on the surface of T_{regs} and activated $CD4^+$ T cells[213,214]. LAG3 associates with CD4 at the plasma membrane to alter the KIEELE phosphorylation motif upon ligand binding, but the downstream effectors responsible for downstream signal transduction remain poorly understood[213,215]. Despite this poor mechanistic understanding, previous studies demonstrated that LAG3 binding downregulates TH1 activation and upregulates T_{reg} proliferation through elevated IL-10 secretion [213,215–217]. Gal9 also interacts with three more surface receptors of importance: Tim-3, TIGIT, and CD44. Gal9/Tim-3 binding can release Fyn binding Bat3 from the intracellular portion of Tim-3, repressing nucleated factor of activated T cell (NFAT) signaling[213,218,219]. Tim-3 binding at the $CD4^+$ T cell surface thus downregulates TH1 responses[218,220]. TIGIT binding yields ITIM or ITT tyrosine phosphorylation to cause Fyn/Lck activation, thereby enlisting SHIP-1 to attenuate the inflammatory signals of NF-κB signaling[213]. TIGIT binding on the surface of $CD4^+$ T cells thus upregulates T_{reg} efficacy while suppressing T cell activation to reduce effector proliferation and cytokine secretion[218,221–224]. Finally, Gal9-bound CD44 complexes with cell surface bound

TGF-βRI[225]. This phosphorylates Smad3, which initiates a positive feedback loop driving T_{reg} differentiation and viability, in turn reducing TH1 activation[225,226].

7.2: Large scale proteomic analysis of pEV cargo

7.2.1: Significance

While we have previously described the size, lineage, and select transcriptomic cargo of pEVs, the proteins on and within pEVs were yet uncharacterized. This lack of information was problematic, as key functional differences in pEV populations obtained from 40μm and 100μm PTS were unknown. Moreover, in addition to improving the understanding of biomaterial cues on sEV protein packaging, characterizing the proteome of pEVs is key to understanding the pEV-to-T cell signaling pathway. As TLR4 signaling modulates $CD4^+$ T cell activation and phenotype in a manner consistent with our previous findings, we hypothesized that protein-mediated TLR4 signaling by pEVs to T cells was the primary driver of this signaling pathway. We thus performed LC-MS/MS to characterize the proteomic cargo of pEVs to assess this hypothesis and better understand the potential of the PTS as an sEV engineering platform.

7.2.2: Materials and methods

7.2.2.1: *Liquid chromatography mass spectrometry*

Shotgun proteomic characterization by liquid chromatography mass spectrometry was performed by the Diabetes Research Center Quantitative and Functional Proteomics Core (The DRC is supported by grant P30 DK017047 from the NIH National Institute of Diabetes and Digestive and Kidney Diseases). Section written with assistance from Dr. Tomas Vaisar of DRC.

A BCA was run on pEVs isolated from WT mice and lysed as previously described in order to quantify the total protein per sample (**Figure 28**). Next, pEVs were lysed in 80 mM HEPES pH8.0, 8mM DTT, 4% SDS, 1X complete protease inhibitor, and 10μg was processed using the SP3 protocol using Sera-Mag carboxylate beads including protein cleanup, alkylation with

iodoacetamide, in-situ digestion with trypsin+LysC (1:20 w/w, Promega, WI) in 0.5% sodium deoxycholate, 100mM ammonium bicarbonate overnight at 37°C. The digestion was quenched with 0.1% TFA and samples were cleaned up on the beads.

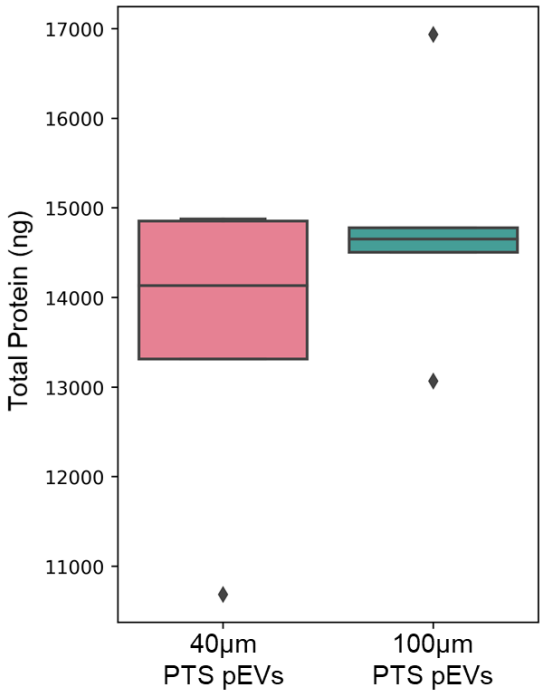

Figure 28: Total protein isolated from 20µL of pEVs isolated from PTS implanted in WT mice for 1 week measured by BCA.

The digested peptides were injected onto a trap column (40x0.1mm, Reprosil C18, 5µm, Dr. Maisch, Germany), desalted for 5 min at a flow of 4µL/min, and separated on a pulled tip analytical column (650 x 0.075mm, Reprosil C18, 5µm, Dr. Maisch, Germany) with a 3 segment linear gradient of acetonitrile, 0.1%FA (B) in water, 0.1%FA (A) as follows: 0-2 minutes 1-5%B, 2-150 minutes 5-25%B, 150-180 minutes 25-35%B followed by column wash at 80% B and re-equilibration at a flow rate 0.4 µL/minute (Thermo EasyLC 1200). Tandem MS/MS spectra were acquired on Orbitrap Fusion Lumos (Thermo Scientific) operated in data-dependent mode on charge states 2-4 with 2 second cycle time, dynamic exclusion of 30 seconds, HCD fragmentation (NCE 30%) and MS/MS acquisition in the Orbitrap. MS spectra were acquired at a resolution 120,000 and MS/MS spectra (precursor selection window 1.6Da) at a resolution of

15,000. The peptides and proteins were identified using the Comet search engine[227] with PeptideProphet and ProteinProphet validation. Search criteria included a 20ppm tolerance window for precursors and products, fixed Cys alkylation, and variable Met oxidation. Peptide identifications were filtered at 1% FDR and protein identifications at 5% FDR.

7.2.2.2: *Proteomic data analysis*

Proteins with at least 2 unique peptide spectral matches (PSMs) and present in at least 2 samples were considered valid proteins. For each valid protein, the normalized spectral abundance factor (NSAF) was calculated with the following equation as described by Zybailov et al. where SpC is the number of spectral counts and Length is the protein length (**Equation 1**)[228].

$$\mathrm{NSAF_k} = \frac{\left(\frac{SpC}{Length}\right)_k}{\sum_{i=0}^{N}\left(\frac{SpC}{Length}\right)_i}$$

Equation 1: Calculation of NSAF. Normalization accounts for protein length and total number of proteins per sample to allow more accurate comparisons across samples as described by Zybailov[228].

A list of all valid proteins found in pEVs from 40μm and 100μm PTS was compiled and checked against the ExoCarta and VesiclePedia databases to assess whether identified proteins in pEVs were known exosome or EV proteins. This list was input into a search of the Jensen Compartments database via ENRICHR[229–231]. Finally, this list was then run in a statistical overrepresentation test via PANTHER database query, specifically examining the PANTHER pathway analysis[232–235]. Statistical enrichment tests on the average NSAF from each protein in pEVs from 40μm or 100μm PTS were then separately run via PANTHER database query, again examining PANTHER pathway analysis[232–235].

Proteins identified in pEVs from 40μm and 100μm PTS were compared by pairwise statistical tests run on the NSAF values for each protein as previously described. The names of these

differentially regulated proteins were compiled and run in a statistical overrepresentation test via PANTHER database query, again examining the PANTHER pathway analysis[232,233,236].

7.2.3: Results

(Section adapted from Hady et. al, 2022 (in preparation))

LC-MS/MS was used to characterize the pEV proteome, elucidating the potential classifications, functions, and origins of pEVs. Of the 1560 proteins identified in pEVs from 40µm and 100µm PTS, 1247 proteins were considered to be EV proteins, as identified in the VesiclePedia database (**Figure 29A**). Moreover, 869 were associated with exosomes, as identified by the ExoCarta database (**Figure 29B**). Using Enrichr to query the Jensen Compartments database, we identified these proteins as most likely to be associated with EVs (**Figure 30**). These results thus indicated that the pEV isolation, pEV lysis, and protein digestion methods used in these studies were sound. The potential exosomal classification of pEVs was then explored via the expression of classical exosome markers CD9, CD63, CD81, and Syntenin-1; these proteins were identified in pEVs (**Figure 31A**), but so were proteins "*a priori* not enriched" in sEVs according to MISEV (calnexin and ER associated proteins) (**Figure 31B**)[101]. The presence of both of these sets of markers complicates the designation of pEVs as exosomes or non-exosomes. Finally, a statistical overrepresentation analysis of all 1560 proteins identified was performed using PANTHER. The top 5 results of the Panther Pathways database query were the "Integrin signaling", "Cytoskeletal regulation by Rho GTPase", "Inflammation mediated by chemokine and cytokine signaling", "Blood coagulation", and "Huntington disease" pathways (**Figure 32** and **Figure 33**). These results indicated potential functional mechanisms of pEV signaling.

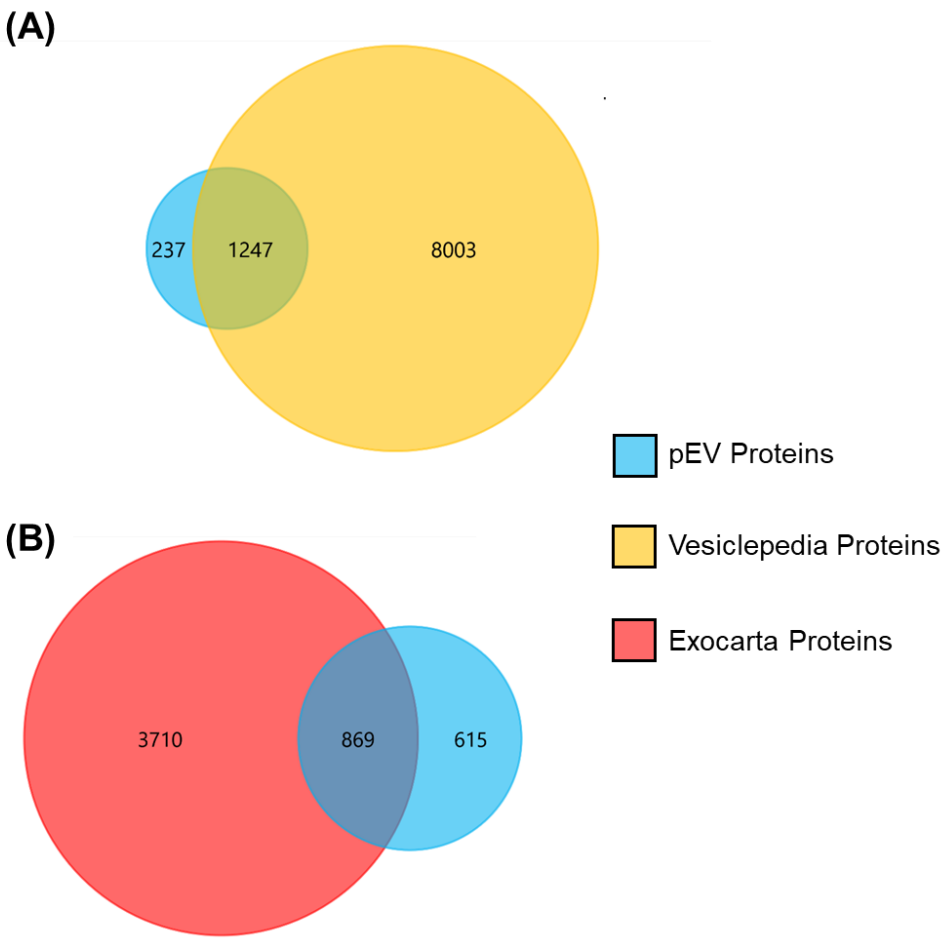

Figure 29: Known EV and Exosome proteins present in pEVs. Proteins identified from pEVs via LC-MS/MS were cross-referenced against (A) Vesiclepedia and (B) Exocarta databases to assess EV and exosome makeup.

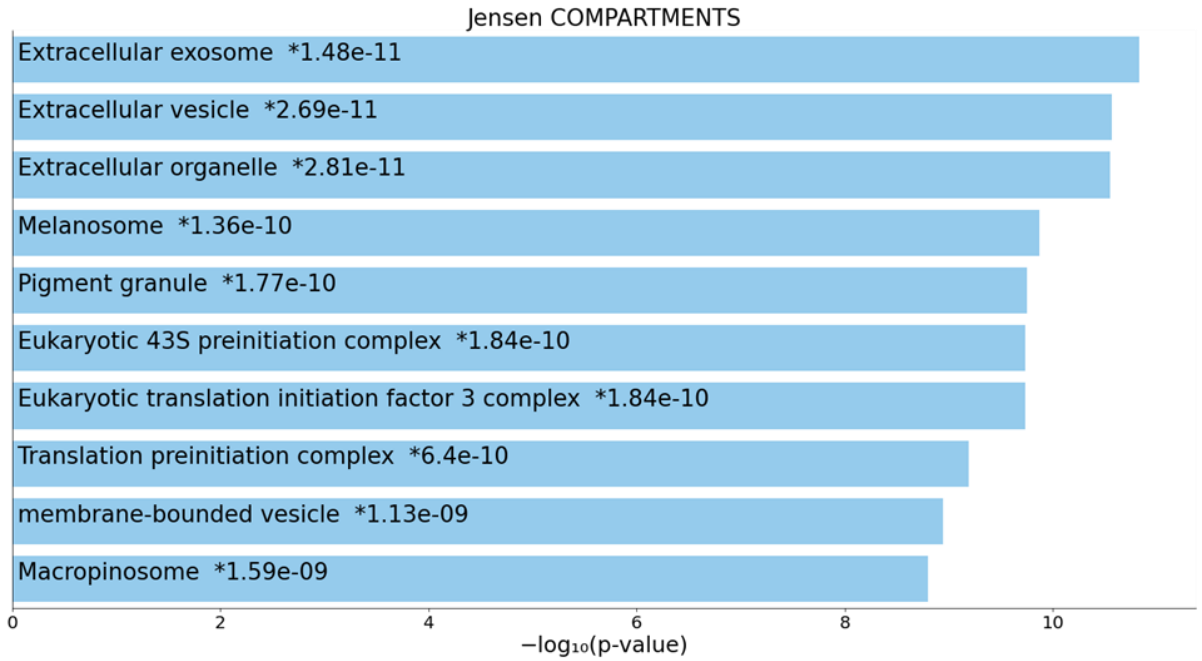

Figure 30: Cellular compartments associated with pEV proteins. Proteins identified from pEVs via LC-MS/MS were queried to Jensen Compartments database using ENRICHR tool (p-values are provided).

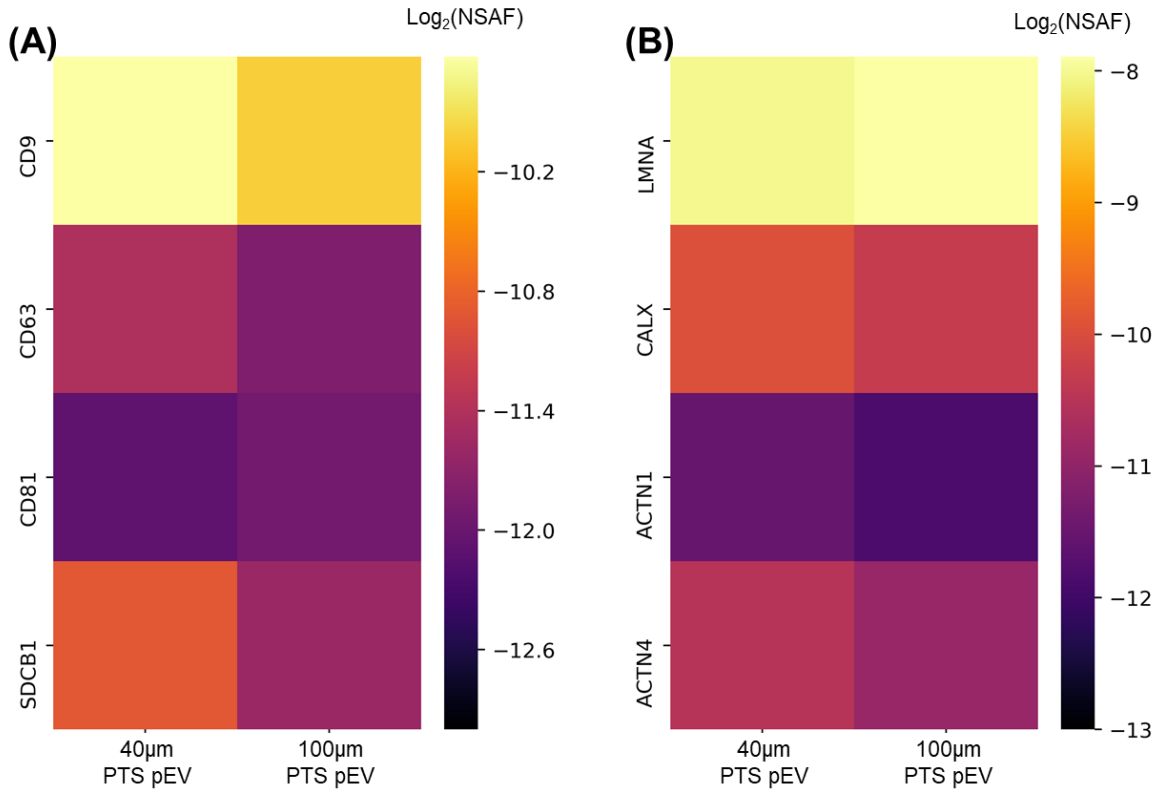

Figure 31: Exosome markers of pEVs. Abundance of (A) positive exosome/sEV markers and (B) markers usually (and according to MISEV, *a priori*) not enriched on sEVs/exosomes in proteins isolated from pEVs.

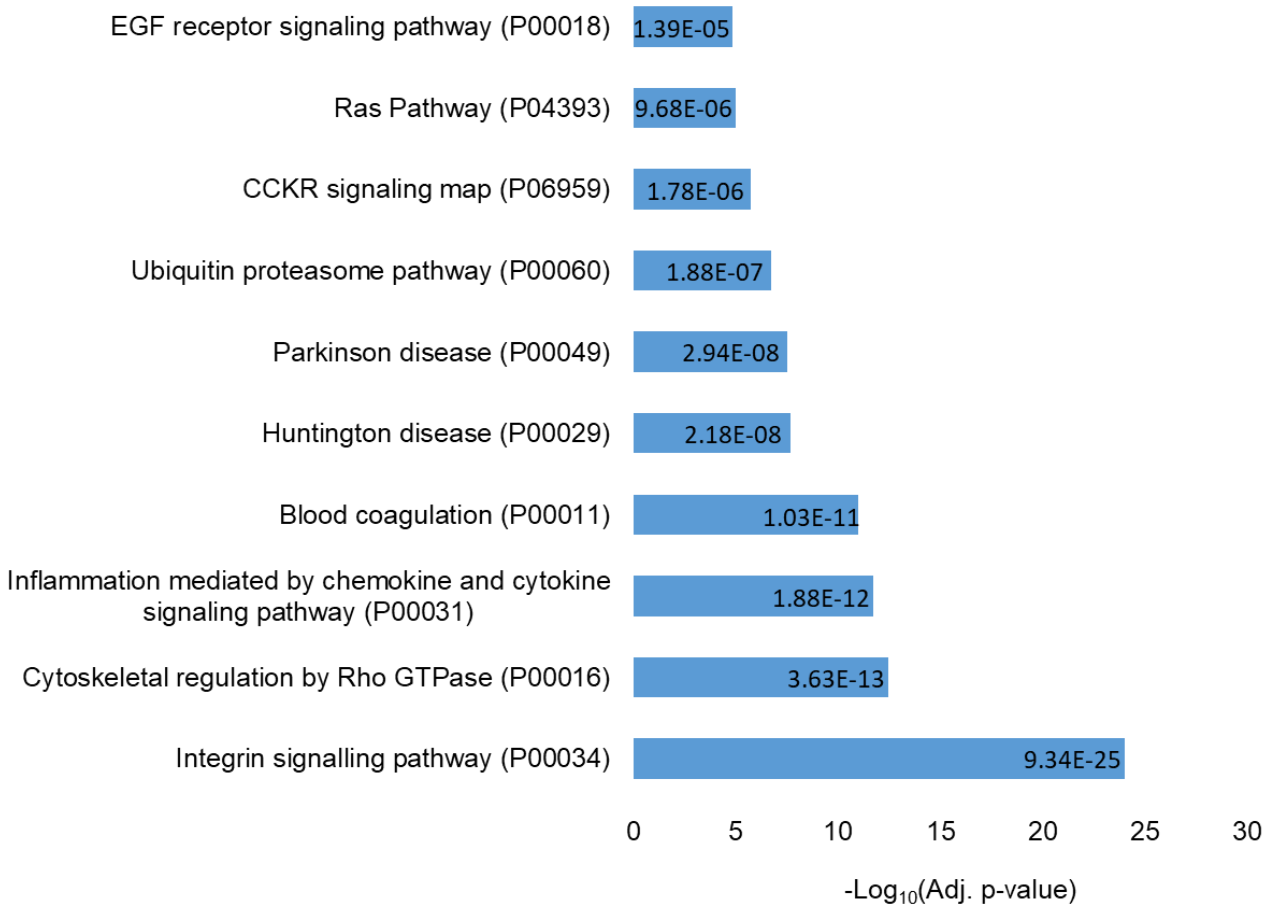

Figure 32: Statistical overrepresentation analysis of the 1560 identified proteins from pEVs. Analysis included all proteins from 40µm and 100µm PTS and was performed on the PANTHER database querying PANTHER pathways; p-values are provided.

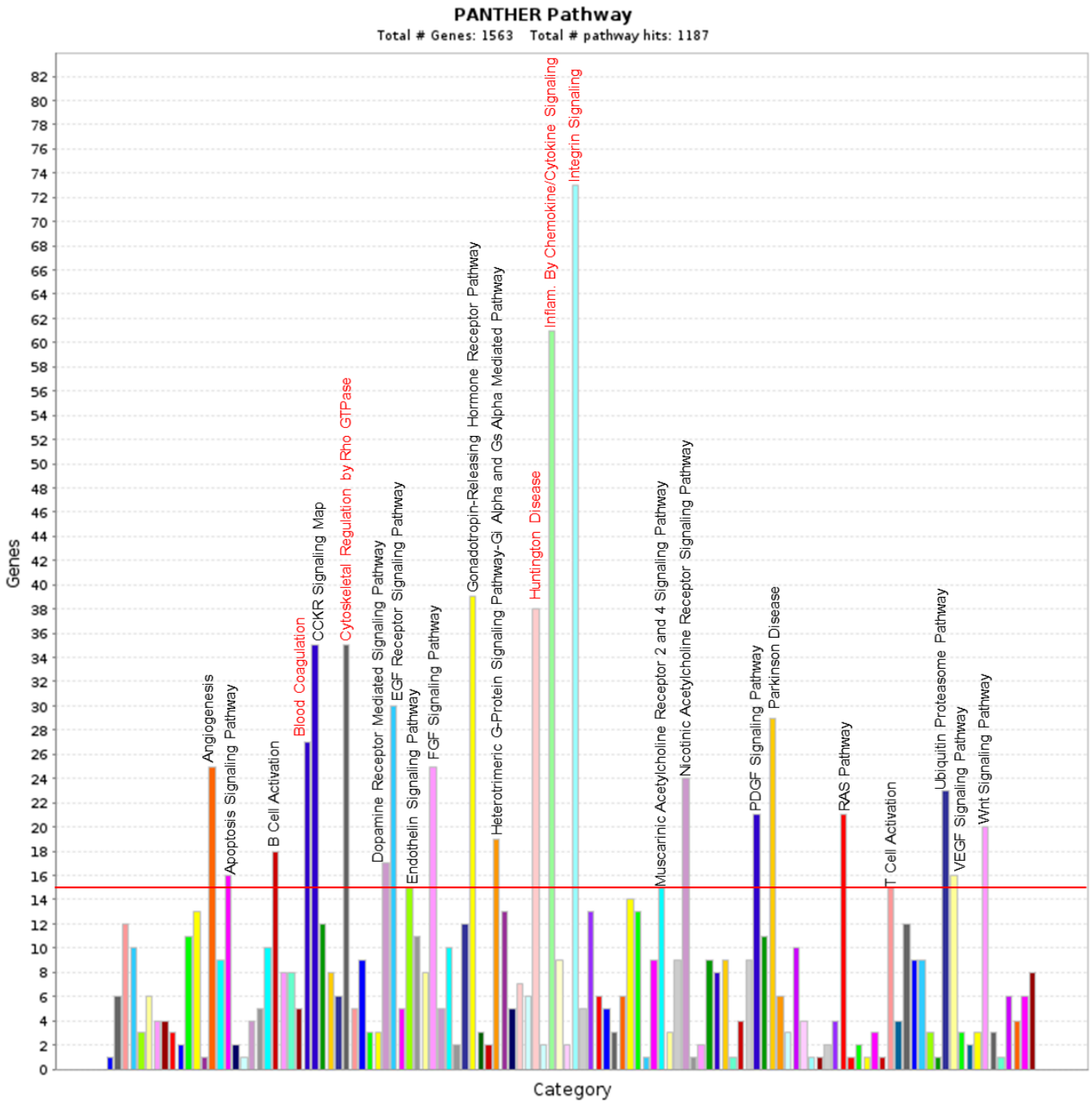

Figure 33: Plot of statistically overrepresented pEV pathways. All significantly overrepresented pathways with 15 or more genes identified in the statistical overrepresentation analysis of the 1560 identified proteins from pEVs from 40µm and 100µm PTS performed on the PANTHER database querying PANTHER pathways. The 5 indicated pathways in red were the most overrepresented results.

The cargo of pEVs from 40µm PTS was then compared to the cargo of pEVs from 100µm PTS. Using PCA (**Figure 34**), 60% of the differences in pEV proteome were captured in 3 dimensions. Based on the 95% confidence intervals of each cluster, there was differentiation

between pEVs from 40µm and 100µm PTS along PC2, with a high degree of similarity along PC1 and PC3. These data indicated that while the cargo of pEVs from 40µm and 100µm PTS were similar in some respects, there were also notable differences in protein composition between them. Upon further pair-wise statistical analysis, 201 of 1560 total proteins were differentially abundant between pEVs from 40µm PTS and 100µm PTS (**Figure 35**). Of note, the classic macrophage/monocyte markers CD11b/CD11c, CD44, CD14, CD180, CD36, and CD68 were differentially abundant as a function of PTS pore size (**Figure 36A**). Using PANTHER, a statistical overrepresentation analysis of these 201 proteins was performed in order to assess potential differences in pEV signaling ability as a function of PTS pore size. This analysis suggested that these differentially abundant proteins were involved in the “Integrin signaling pathway”, indicating functional differences between pEVs based on PTS pore size (**Figure 36B**). Using average pEV protein abundance data, a statistical enrichment analysis revealed that both sEVs from 40µm and 100µm PTS likely participated in the “Huntington disease” and “Glycolysis” Panther Pathways (**Figure 37**). A number of pEV proteins identified in Panther’s “Huntington disease” pathway were associated with vesicle endocytosis, namely: Rac, synaptojanin, dynein complexes, dynactin, components of the ARP2/3 complex, actins, β-tubulins, and Rab8 (**Figure 38**). This indicated a potential use of the endocytic pathway by pEVs.

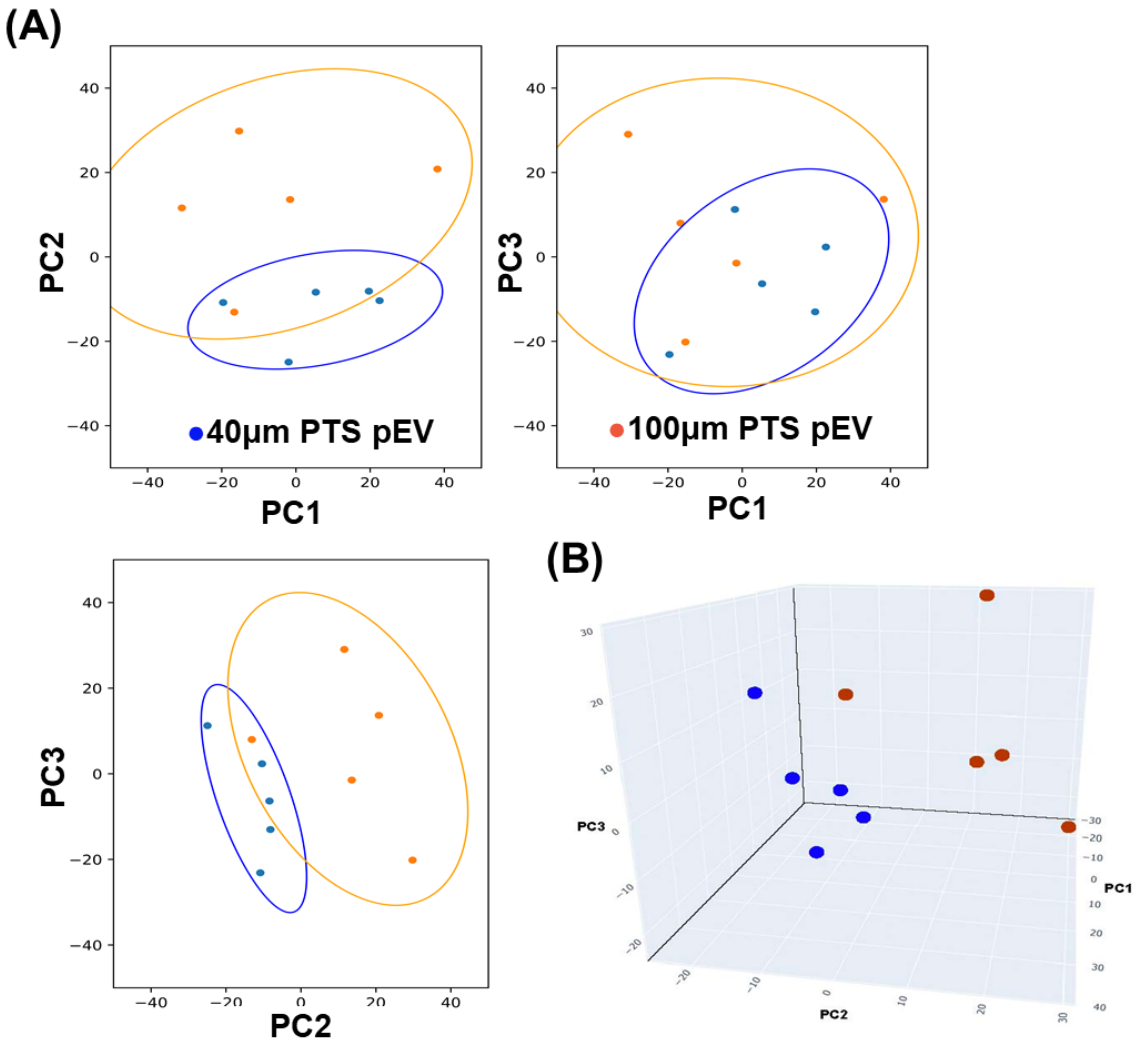

Figure 34: Three dimensional PCA of average protein abundance between pEVs isolated from 40μm and 100 μm PTS. 60% of the data was captured in 3 dimensions (PC1: 27.11%, PC2: 17.91%, PC3: 15.25%). Two dimensional views of the PCA are provided in (A), where circles represent 95% confidence intervals. A three dimensional representation is indicated in (B) (40μm PTS pEVs in blue, 100μm PTS pEVs in red).

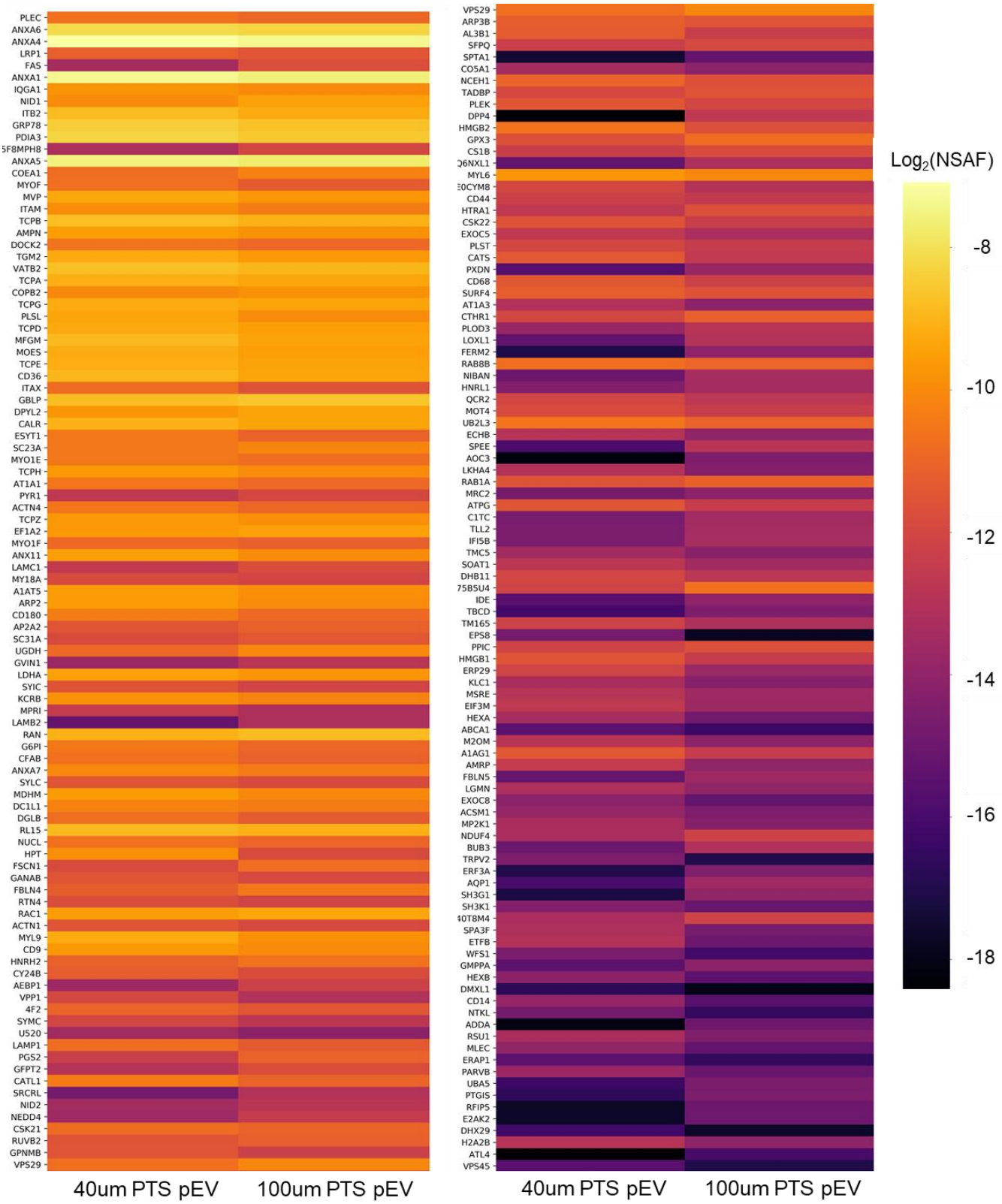

Figure 35: Heatmap of differentially abundant proteins in pEVs from 40µm and 100µm PTS (significance was determined via two-sided T or Mann-Whitney U test based on normality assessed by Shapiro-Wilk test, see 2.3.2.5: for details)**.**

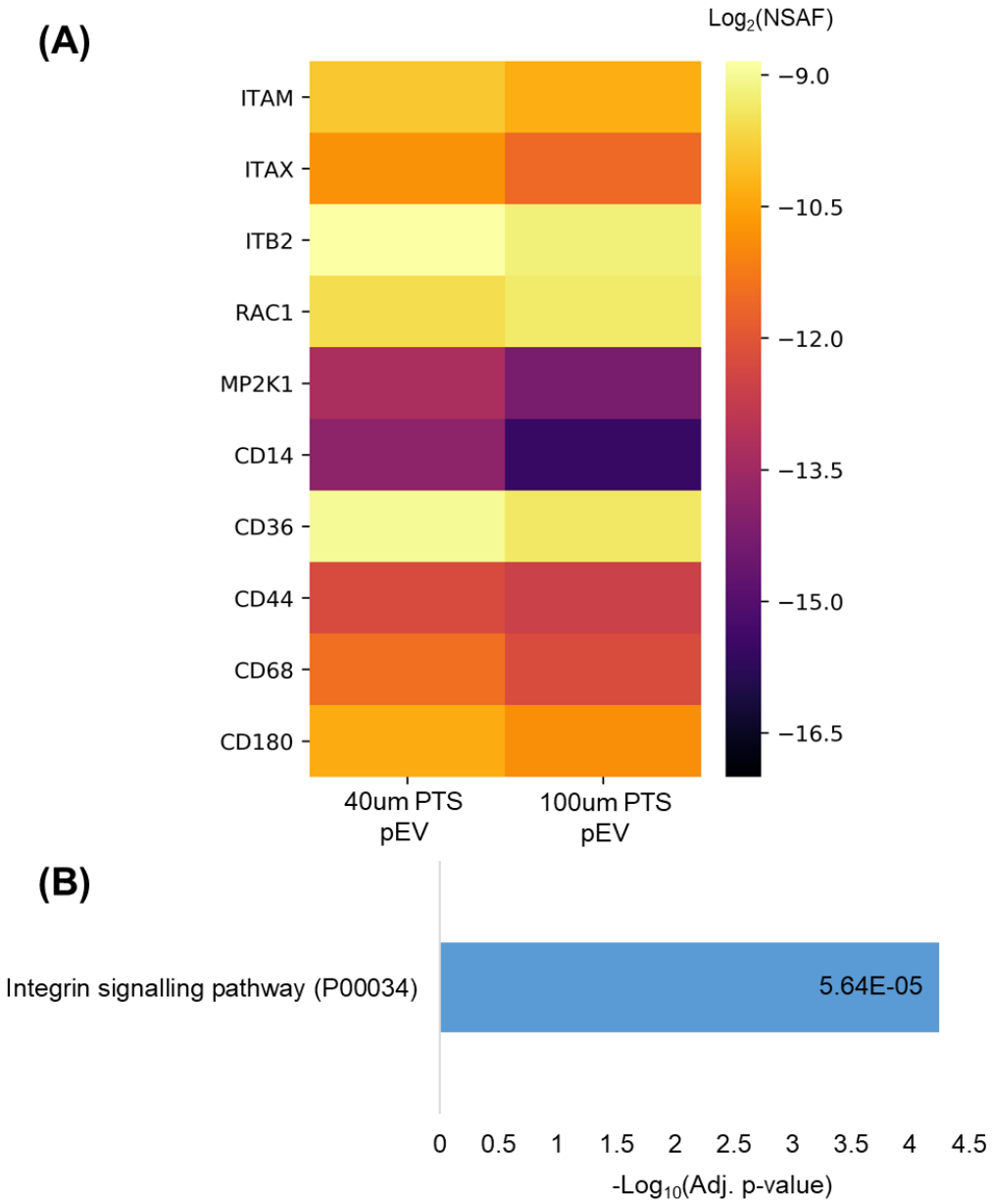

Figure 36: Key proteomic differences between pEVs from 40µm and 100µm PTS. (A) Key immunomodulatory proteins present in significantly differential abundance in pEVs as a function of PTS pore size (significance was determined via two-sided T or Mann-Whitney U test based on normality assessed by Shapiro-Wilk test, see 2.3.2.5: for details); (B) Statistical overrepresentation analysis of all differentially abundant proteins in pEVs performed on the PANTHER Database querying PANTHER Pathways.

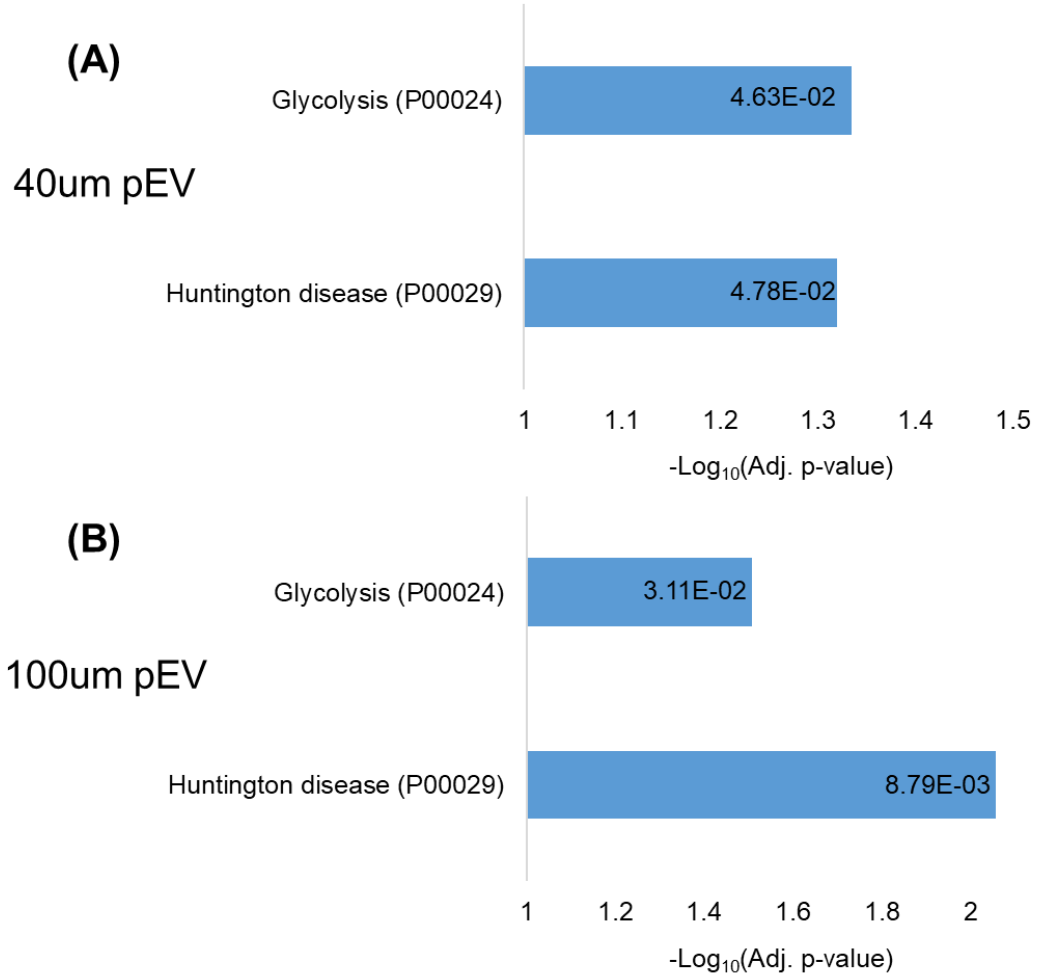

Figure 37: Statistical enrichment analyses of the function of pEVs from 40µm or 100µm PTS. A statistical enrichment analysis of the identified proteins from pEVs from (A) 40µm PTS or (B) 100µm PTS was performed on the PANTHER database querying PANTHER pathways.

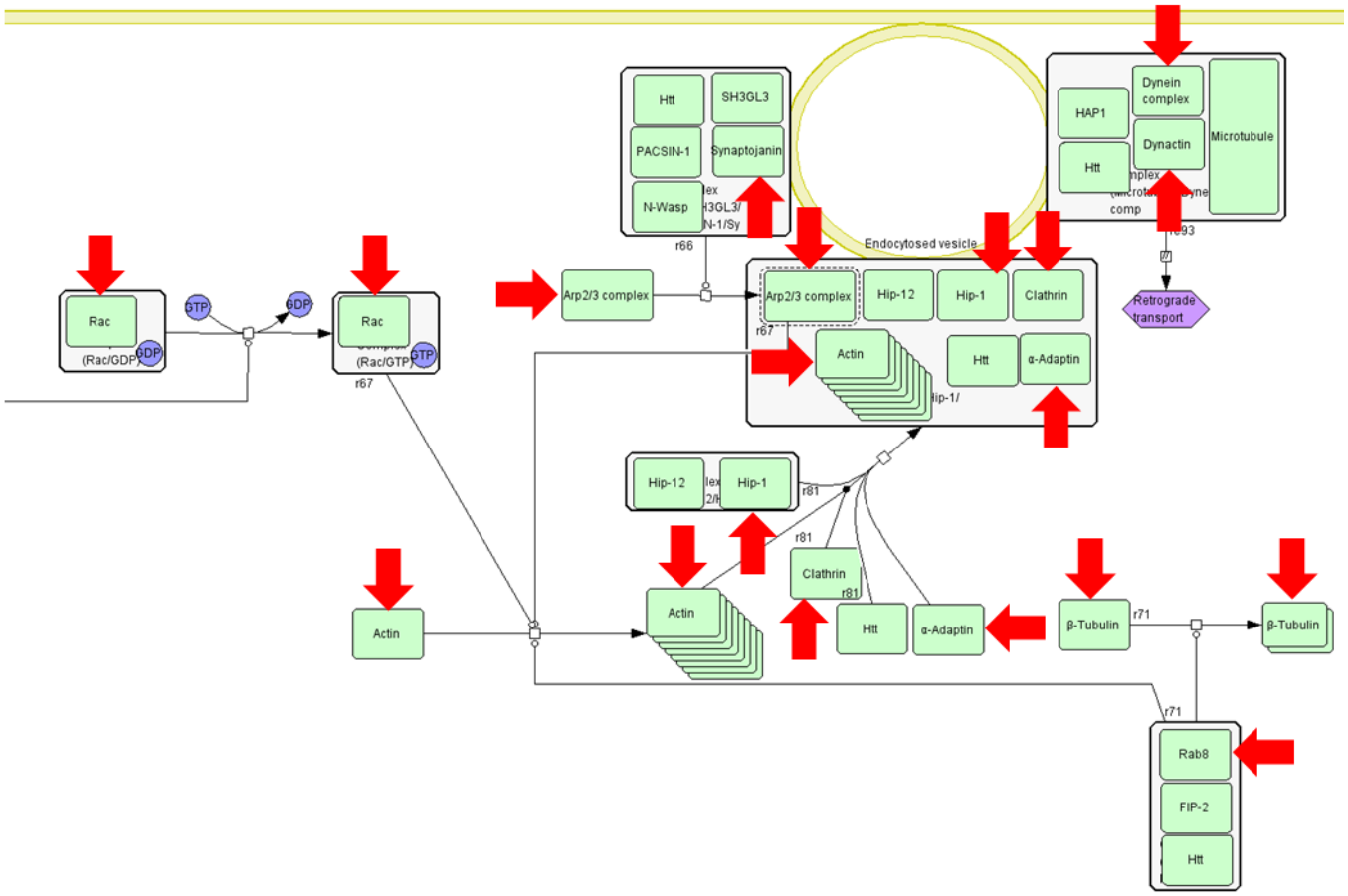

Figure 38: pEV proteins identified within a subset of the PANTHER Huntington Disease Pathway associated with vesicle endocytosis. Pathway diagram adapted from PANTHER database[235]. Proteins identified with red arrows were identified as pEV proteins.

7.3: Quantification of Gal3/9 and GRP78/94 on the pEV surface

7.3.1: Significance

Galectins 3 and 9 are potent cell signaling molecules, capable of modulating TLR4 signaling and $CD4^+$ T cell phenotype. However, Gal3 has not yet been characterized in a membrane-bound form in mammals, much less on the surface of EVs. Functional Gal9, on the other hand, has been characterized on the surface of sEVs, though few studies examine this pheneomenon[201]. GRP78 and GRP94 are highly contentious mediators of TLR4 signaling within the context of sEV and exosome research, thought by some to be not present in sEVs due to being endoplasmic reticulum-associated proteins, while also shown to be present on the surface

and inside of sEVs[101,189]. The characterization of Gal3, Gal9, GRP78, and GRP94 within the context of sEV research was therefore important. Moreover, the quantification of these potent immunomodulatory molecules on the surface of pEVs demonstrated their unique surfaceome and proteome to contribute to our understanding of the PTS as an sEV engineering platform.

7.3.2: Materials and methods

7.3.2.1: *Imaging flow cytometry data acquisition*

Two panels were used to assess GRP78, GRP94, Gal3, and Gal9 surface abundance on pEVs (**Table 5**). GRP78 polyclonal antibody (Cat #11587-1-AP, Proteintech/Thermo Fisher Scientific) was concentrated with a 0.5mL Amicon Ultra spin column to a concentration of 1.6mg/mL (Cat # UFC505024, Millipore Sigma) and then conjugated to Alexa Fluor 647 fluorophore with a direct antibody conjugation kit (APEX labeling kit, Cat # A10468, Thermo Fisher Scientific) as per the manufacturer's instructions. The final concentration of the GRP78 antibody was $5.6*10^{-7}$M with a degree of labeling of 4.7, and the labeled antibody was stored at -20°C. Four labeling reactions were prepared: one to label Gal3, Gal9, and GRP78 (reaction 1), one to label GRP94 (reaction 2), one CFSE only control (reaction 3), and one CFSE and secondary antibody only control (reaction 4). 3µL of pEVs at an average concentration of $1.39*10^{11}$ pEVs/mL were combined with PBS to yield a final reaction volume of 20µL. CFSE was diluted to a final concentration of 50µM. 2µL of diluted CFSE was added to each reaction and incubated for 10 minutes at room temperature. Antibodies were added to each reaction as follows: 5µL of labeled GRP78 antibody, 1µL of PE conjugated Gal3 antibody (Catalog # 12-5301-82, Thermo Fisher Scientific), and 1µL PE-Cy7 conjugated Gal9 antibody (Catalog # 25-921-180, Thermo Fisher Scientific) in reaction 1; 1µL of unconjugated GRP94 antibody (Catalog # 14700-1-AP, Proteintech/Thermo Fischer Scientific) to reaction 2. All reactions were then incubated at 37°C for 45 minutes. 15µL of PBS was added to reactions 1 and 3, which were then stored at 4°C until use. 1µL of goat anti-rabbit AF647 secondary antibody (Catalog #A21245, Thermo Fisher

Scientific) was then diluted 1:20 and added to reactions 2 and 4. These reactions were incubated at 37°C for 30 minutes, 15µL of PBS was added to each, and the reactions were stored at 4°C until use.

(A)

Antibody/Stain	Target	Fluorescence Channel	Function
CFSE	pEVs (Lipophilic Dye)	494ex/521em	pEV Gating
Anti-GRP94 pAb	GRP94	Unconjugated	GRP94 Label
Anti-Rabbit pAb	Anti-GRP94 Ab	AF647	GRP94 Fluorescence

(B)

Antibody/Stain	Target	Fluorescence Channel	Function
CFSE	pEVs (Lipophilic Dye)	494ex/521em	pEV Gating
Anti-GRP78 pAb	GRP78	AF647	GRP78 Label & Fluorescence
Anti-Gal3 mAb	Gal3	PE	Gal3 Label & Fluorescence
Anti-Gal9 mAb	Gal9	PE/Cy7	Gal9 Label & Fluorescence

Table 5: Fluorescent staining panels to measure the surface abundance of pEV proteins. (A) measured the surface abundance of GRP94 and (B) measured GRP78, Gal3, and Gal9 on pEVs with imaging flow cytometry.

Imaging flow cytometric analysis of the fluorescently labeled pEVs was performed on an Amnis ImageStream® (Luminex, Inc. Austin, TX). pEV events were gated on brightfield focus (Gradient RMS), CFSE intensity, and CFSE area versus aspect ratio. 12000 pEV events were captured per sample. Fluidics were set to slow, sensitivity to high, and observations were taken at 60x. Gating for fluorescent tags were determined by negative controls for each reaction: gates were

drawn where under 2% of the negative control population was positive for each marker. Reaction 3 was a negative control for reaction 1, and reaction 4 was a negative control for reaction 2. An example of gating strategies can be seen in **Figure 39**. The percentage of positive events in each channel of the corresponding negative control was subtracted from the percentage of positive pEV events in the stained samples. A representative image of stained pEVs can be seen in **Figure 40**.

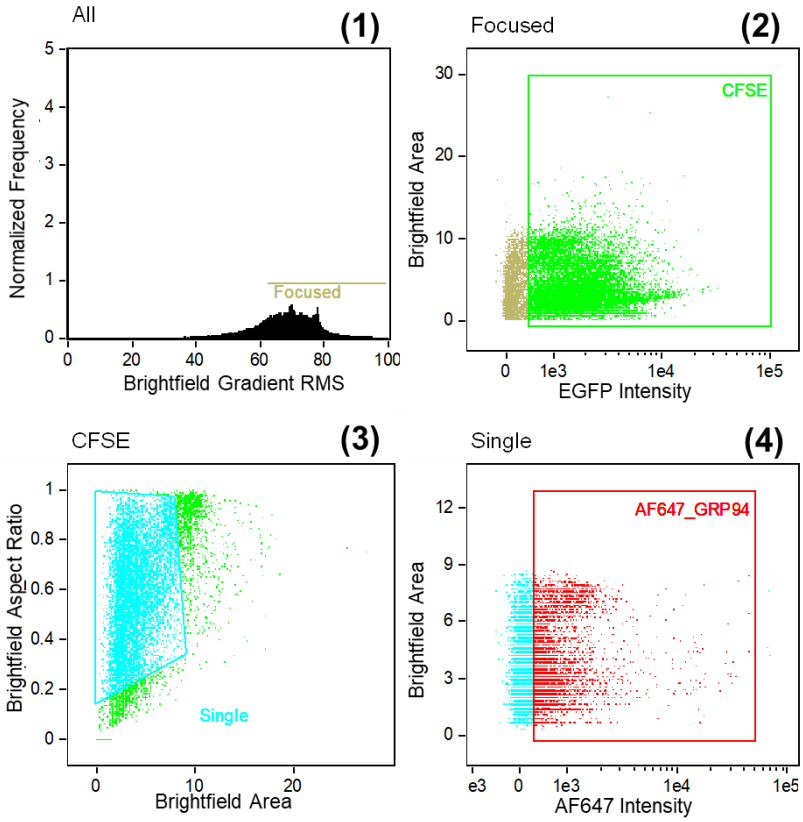

Figure 39: Gating strategy for the assessment of pEV surface markers via imaging flow cytometry. (1) Focused events were gated, (2) $CFSE^{+}$ events (i.e. lipid bilayer bound particles) were gated, (3) single sEVs were gated based on size and aspect ratio via brightfield, and (4) sEV marker positivity was gated on the fluorescence intensity of the corresponding fluorophore**.**

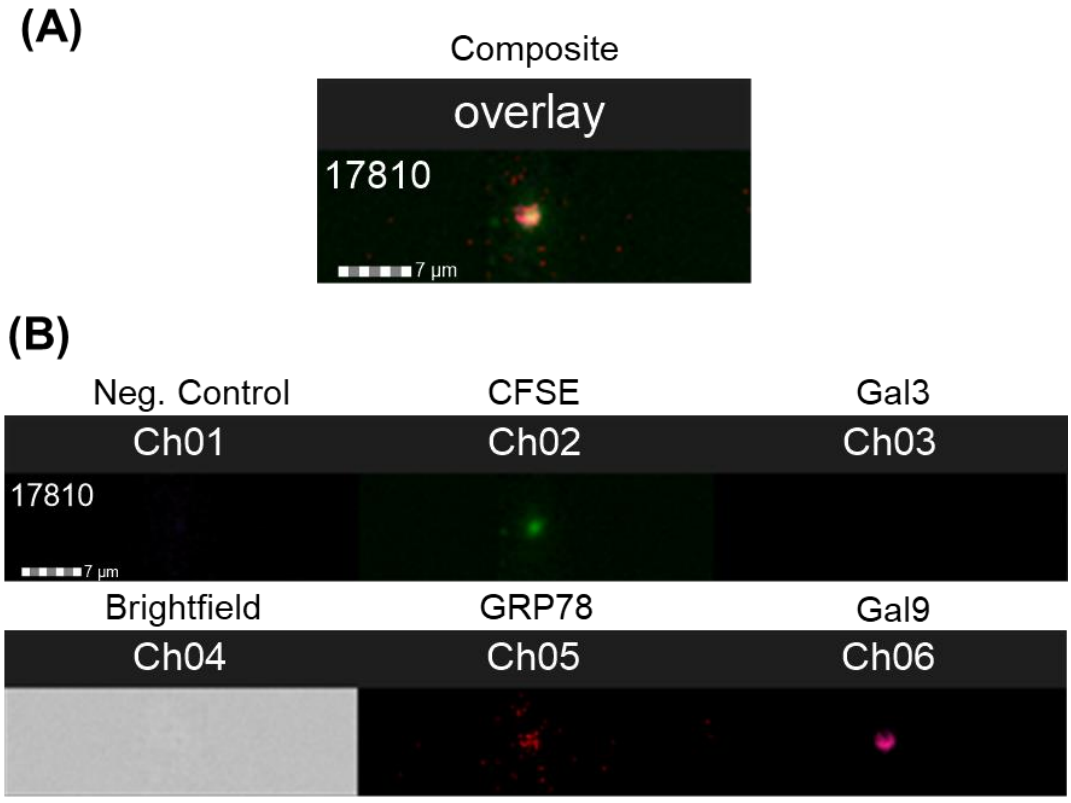

Figure 40: Representative images of pEV surface staining for Gal and GRP proteins. (A) shows a composite and (B) shows individual channel images of imaging flow cytometry performed on pEVs performed the panel from **Table 5B**. Ch01: pacific blue (negative control), Ch02: CFSE (lipophilic EV dye), Ch03: PE (Gal3), Ch04: Brightfield, Ch05: AF647 (GRP78), Ch06: PE-Cy7 (Gal9).

Fixed EL4 cells were used as positive controls to verify antibody efficacy. Briefly, 1 million cells were fixed in 300µL of 10% formalin for 15 minutes, 600µL of 1% horse serum in PBS was added to each sample, and the samples were centrifuged at 3000xg for 10 minutes. Each group was then resuspended in 200µL of PBS and stored in the dark at 4°C overnight. The cells were pelleted again and resuspended in 100µL of .1% saponin, 5% 5% nonfat dry milk, and 1% horse serum in hanks buffer for 10 minutes. 600µL of .1% saponin in 1% horse serum and hanks buffer was added to each reaction, and the cells were pelleted. Antibodies were then added to each reaction after resuspension in 100µL of the milk saponin solution, and were placed on ice for 30 minutes. 600µL of saponin in hanks buffer was added to each reaction, and the cells were pelleted. If secondary antibodies were added to each reaction, this process was repeated, beginning with resuspension in 100µL of the milk saponin solution. After the final pellet, 300µL

of 1% horse serum in PBS was used to resuspend the pellet. Flow cytometry was carried out on a CantoRuo, collecting 20000 events and gating on forward scatter and side scatter to isolate the cell population. Fluorescence was gated on the appropriate negative controls (i.e. unstained or secondary only EL4s).

7.3.3: Results

Gal9, GRP78, and GRP94 were all significantly present on the surface of pEVs from both 40μm and 100μm PTS (N=4, $p<0.05$) (**Figure 41**). The surface abundance of any of these markers on pEVs was not significantly different as a function of pore size. While the percentage of $GRP78^+$ pEVs appeared to be lower than the other markers, this was likely because the fluorescence intensity of the conjugated antibody was lower in positive control samples than the others. Gal3, contrary to our hypothesis, was not significantly present on the surface of pEVs from 40μm or 100μm PTS. However, Gal3, GRP78, and GRP94 were detected in the LC-MS/MS proteomic analysis performed on lysed pEVs, where GRP78 was significantly more abundant in 40μm PTS pEVs ($p=0.0380$, N=5) (**Figure 42**). Interestingly, Gal9 was only detected in trace amounts. Our results thus indicated that GRP78, GRP94, and Gal9 were present on the surface of pEVs regardless of pore size. They further indicated that Gal3 was likely present inside of pEVs, whereas Gal9 was not.

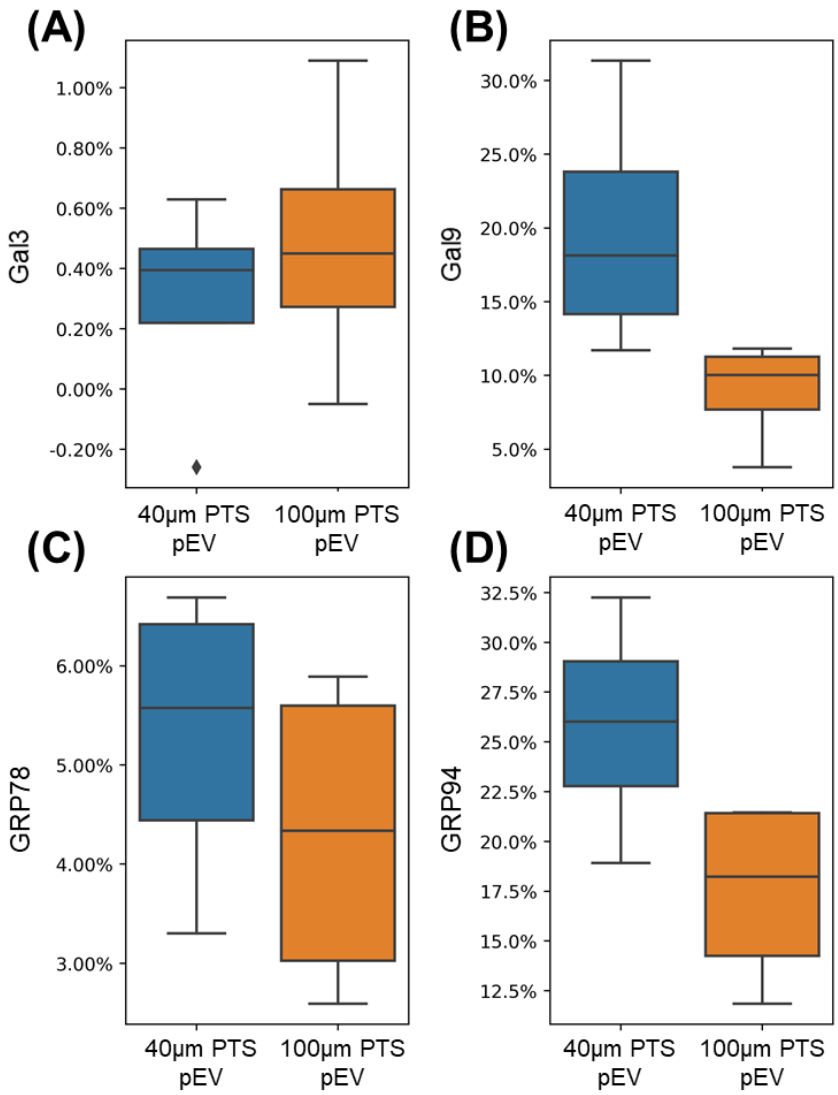

Figure 41: Percentage of pEVs with Gal and GRP proteins present on their surface. Imaging flow cytometry was used to quantify the number of pEVs from 40μm and 100μm PTS with surface bound (A) galectin-3, (B) galectin-9, (C) HSPA5, and (D) HSP90B1 on their surface (*,p<0.05, N=4; significance was determined via two-sided T or Mann-Whitney U test based on normality assessed by Shapiro-Wilk test, see 2.3.2.5: for details).

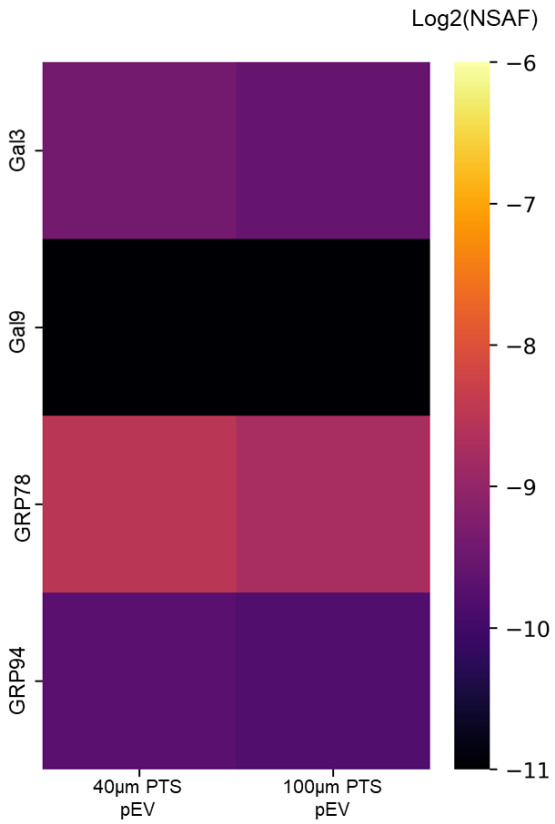

Figure 42: Abundance of Gal3, Gal9, HSPA5, and HSP90B1 in pEVs as determined by LC-MS/MS (N=5, significance was determined via two-sided T or Mann-Whitney U test based on normality assessed by Shapiro-Wilk test, see 2.3.2.5: for details)**.**

7.4: Discussion: Proteomic analysis of pEV cargo

(Section adapted from Hady et. al, 2022 (in preparation))

A general examination of the pEV proteome provided further insight as to their classification. As expected, most of the proteins identified in pEVs were considered EV proteins (79.9%). Further, the majority of the pEV proteome was comprised of exosome proteins (55.7%). Our Jensen Compartments database query corroborated these findings, indicating the efficacy of our pEV isolation and proteomic characterization methods. Additionally, we identified a number of exosome markers (i.e. tetraspanins and syntenin-1) in our population, as well as "*a priori* not enriched" sEV markers (calnexin and ER associated proteins)[101,237]. As demonstrated previously, pEVs are designated as sEVs based on their size classification alone. However, current MISEV requirements are contradictory: they state that EVs should be classified based

on their size, but also state that these "*a priori* not enriched" sEV markers should be analyzed in order to claim a population to be sEVs[101]. As pEVs clearly fit the more important size range requirements and therefore definition of small extracellular vesicles, we will continue to designate them as such. Further, while pEVs are sEVs based on their size, there is evidence both for and against their formal classification as exosomes[237]. These complications highlight a severe shortcoming of current EV and exosome research: the inherent heterogeneity and ambiguity in EV contents, regardless of particle size, is inadequately accounted for by current contradictory terminology requirements.

Our statistical overrepresentation PANTHER Pathway analysis indicated many potential biological roles for pEVs. However, the top results implicated pEVs in immunomodulatory signaling: the "Integrin signaling", "Cytoskeletal regulation by Rho GTPase", and "Inflammation mediated by chemokine and cytokine signaling" pathways all modulate inflammatory signals. The identification of these pathways provided insight to pEV functional signaling mechanisms that may induce immunomodulation in recipient cells, and allows us to consider potential mechanisms in pEV-to-T cell signaling. Integrin signaling specifically drives immune responses, including the activation of T cells, and recent evidence indicates that pEVs may induce horizontal integrin transfer to the recipient cells[238,239]. Moreover, the presence of functional ECM proteins in our pEV samples also may be explained by integrins on the surface of pEVs binding ECM proteins like fibronectin to coat their surface, which could also modulate $CD4^+$ T cell phenotype and activation[240–242]. These ECM proteins may affect cell adhesion molecules on the surface of recipient cells, which in turn may be playing a key role in immunomodulation. Rho GTPases that regulate the cytoskeleton also play a key role in inflammation, affecting phagocytosis, leukocyte recruitment, and leukocyte motility[243]. These proteins are explicitly involved in TLR4 signaling, with RhoA and RAC1 playing key roles in signal transduction, and leading to leukocyte recruitment and activation upon interactions with cell adhesion

molecules[243,244]. Integrins and the regulation of the cytoskeleton by Rho GTPases are thus important aspects of immunomodulatory pEV signaling that warrant further study. Moreover, these pathways may be partially involved with TLR4-mediated pEV-to-T cell signaling, although more experimentation is required to prove this definitively[232,245–247].

Some of these theorized aspects of pEV-to-T cell signaling (i.e. immunomodulatory proteins that act within the cytoplasm) would necessitate T cell endocytosis of pEVs. However, the current understanding of sEV endocytosis by T cells remains limited. While previous studies have demonstrated the uptake of dendritic cell sEVs by $CD4^+$ T cells, many potential mechanisms leading to these interactions remains unknown[148,149]. Our statistical enrichment analysis implicated the Huntington disease pathway in pEVs from both 40µm and 100µm PTS, which was initially confounding. However, this PANTHER Pathway contained a significant vesicular endocytosis component not strictly involved with the HTT protein. Additionally, we were able to map many of the pEV proteins identified as a part of this pathway to the vesicular endocytosis complex and effectors[232]. Thus, we believe that this analysis may indicate that pEVs are endocytosed by recipient cells, and it may demonstrate a key part of pEV biogenesis by way of the endocytic pathway. The further study of pEV endocytosis by T cells is therefore warranted, as it would provide a better understanding of both pEV-to-T cell signaling and general interactions of T cells with sEVs.

The proteomic comparison of pEVs from 40µm and 100µm PTS provided key information about differences in their potential functions. The PCA of pEVs from 40µm and 100µm PTS demonstrated distinct similarities between these two populations, indicating a degree of functional homology—this corroborated the consistent transcriptomic changes observed in pEV treated splenic T cells (T_{reg} and TH1 marker upregulation) upon pEV treatment regardless of pore size. However, comparison of proteins differentially abundant between pEVs from 40µm and 100µm PTS also revealed significant proteomic differences between the pEV populations,

which corroborated differences observed in pEV-to-T cell signaling as a function of PTS pore size. Specifically, the identification of differences in integrin signaling implicated differences in immunomodulatory signaling molecules. Moreover, macrophage/monocyte markers were differentially regulated between these two populations. These results imply two things: pEVs may contain differential immunomodulatory signaling payloads as a result of macrophage polarization that affect T cells, and that macrophage/monocyte recruitment and differentiation may be either be a reflection of or affected by pEVs. Recent evidence indicated that PTS pore size plays a role in the recruitment and activation of monocytes within the implant microenvironment, further corroborating this conclusion [248]. Finally, integrin signaling has been implicated in the modulation of TLR4 signaling, and all identified differentially regulated macrophage marker proteins are involved in TLR4 signaling[245,246,249–253].

Our studies confirmed the presence of the immunomodulatory ligands Gal3, Gal9, GRP78, and GRP94 on and within pEVs. As previously discussed, these proteins may have a wide variety of effects on immunomodulation, potentially impacting TLR4 signaling and drastically altering T cell phenotype. While controversial, our studies corroborate recent research that demonstrates the presence of GRP78 and GRP94 both on and within sEVs[189]. These proteins are highly potent signaling molecules, but also considered ER proteins—and are therefore "*a priori* not enriched" on sEVs by MISEV[101]. Our experiments proving the presence of GRP78 and GRP94 on and within pEVs thus lay the groundwork for and necessitate further study into these two poorly understood markers, particularly with regard to their regulation and function as sEV cargo. While less controversial, the presence of Gal3 within and Gal9 on the surface of pEVs also necessitates further research. As Gal3 and Gal9 play important roles in immunomodulation, experiments characterizing their cell signaling function within the context of sEV signaling are important, as they would further elucidate potential signaling roles played by galectins in pEV-to-T cell signaling.

Chapter 8: Limitations of the dissertation and suggestion of future works

8.1: Future work in the characterization of the host response to PTS

This work was able to broadly characterize PTS resident cells and pEVs, investigate the role of $CD4^+$ T cells within the PTS, and demonstrate novel pEV signaling to T cells. Although our work demonstrated the pore size-dependent polarization of macrophages and T cells in implanted PTS, the effect of PTS pore size as a biomechanical cue on $CD4^+$ T cell phenotype in isolation remains unstudied. Recent research has shown that engineered microporous biomaterials affect T cell activation differentially based on stiffness, indicating that T cells do respond to biomechanical cues in their microenvironment[254]. Thus, the characterization of PTS pore size on PTS seeded splenic T cells via microarray and RT-qPCR analysis would provide the opportunity for further understanding both T cell mechanoreceptors and the unique host response to implanted PTS.

While this work was able to address the necessity of $FoxP3^+$ T_{regs} in the unique host response to 40μm PTS, the roles of other cellular phenotypes in the FBR to PTS have yet to be uncovered. As the TH1 marker TBX21 was upregulated in $CD4^+$ T cells following pEV treatment, investigating the host response to PTS in TBX21 deficient mice through trichrome staining and RT-qPCR would characterize the potentially important role of TH1 cells in this phenomenon. Additionally, explanation of the effect of cellular phenotype on the host response to PTS is not limited to T cells; the role of macrophage polarization in the host response to PTS could also be determined via the same methods following PTS implantation in M2 deficient (IL-4Rα knockout) mice[255].

Although we provided a more detailed characterization of the phenotype and contents of PTS resident cells and pEVs than previously available, new technological advancements provide potentially important future experiments in this regard. Specifically, the use of singe cell RNA sequencing is a potentially powerful tool to further characterize PTS resident cells. Comparing

the transcriptomes of single cells resident to 40μm and 100μm PTS would allow for a more thorough characterization of leukocyte phenotype as a function of PTS pore size, and for the investigation of co-regulated genes therein to further address shortcomings in our understanding of macrophage polarization. Additionally, the use of single EV RNA characterization would be a useful tool to further evaluate pEV contents, and would aid in addressing the problems of EV heterogeneity currently inherent to the field. However, this technology is still in its early stages[256].

8.2: Future work in the characterization of pEV signaling within the PTS microenvironment

Our work implicated the use of the endocytic pathway by pEVs. However, further characterization of the endocytic pathway within the context of pEV biogenesis and cellular communication modalities would improve the understanding of these unique particles. In particular, an experiment to determine whether or not pEVs fuse to or are internalized by T cells would determine the primary utilization of the endocytic pathway by pEVs. This would be scientifically valuable, as the uptake of sEVs by T cells is currently not well characterized. Moreover, it would indicate whether or not pEV-to-T cell signaling is exclusively taking place via surface ligand binding or if vesicular internalization occurs. This phenomenon could be explained via an experiment wherein T cells isolated from a transgenic mTmG mouse model are treated with pEVs isolated from explanted PTS in mice universally expressing the CRE enzyme; this would yield T cells exhibiting spots of green fluorescence instead of red upon pEV internalization or fusion.

While our work demonstrated novel mechanisms of pEV-to-T cell signaling, the scope of our research did not allow for the study of pEV signaling to other PTS resident cells. This phenomenon is an excellent line of questioning for further experimentation, as pEVs may signal to other cells within the PTS to affect the unique host response upon implantation. As macrophage polarization has been demonstrated to play a role in the FBR to PTS, the role of

pEVs on macrophage phenotype is of particular interest, and could be characterized via further RT-qPCR. While recent research has clarified the role of PTS pore size in monocyte and macrophage recruitment within the scaffold microenvironment, the role of pEVs in cellular recruitment remains uncharacterized and a promising avenue for future experimentation as well[248].

Although our work clearly showed phenotypic differentiation and transcriptomic activation in T cells as a function of pEV signaling, the ability to generate an untreated control condition containing soluble factors while excluding pEVs within this context was impossible. This is because the total inhibition of sEV biogenesis and release is not yet feasible, and complete depletion of sEVs from conditioned medium is not possible. Ideally, we would have prepared an untreated control condition by subjecting conditioned medium from non-sEV producing PTS resident cells to the same sEV isolation procedure as the other conditions. This would have been optimal because while our sEV isolation was effective, there is still the possibility of other soluble factors released by PTS resident cells remaining within our sEV preparations. Progress has been made in the identification of drug candidates to reduce sEV release and biogenesis, but none of these candidates are able to completely inhibit sEV biogenesis and release[257]. Moreover, these drugs may affect other cellular and physiological processes beyond sEV signaling, making them inappropriate for the generation of a suitable untreated control condition. The second best alternative to blocking pEV production would have been a depletion of pEVs from the conditioned medium; however, a total depletion of sEVs from conditioned medium is not yet possible, even with ultracentrifugation[258]. Ultracentrifugation would also subject the conditioned medium of the untreated control condition to different isolation conditions than the pEV treated conditions, which may affect sample integrity or other soluble factors within the conditioned medium. Therefore, the generation of a true pEV-free untreated control condition subject to consistent isolation conditions was impossible due to a lack of total sEV-blocking and

depletion procedures.

8.3: Future work in the quantification of pEV-to-T cell signaling mechanisms

Data from our studies indicated that downstream effectors of TLR4 were affected by pEV signaling to T cells. Our chosen method of signal transduction measurement for these experiments was RT-qPCR, which probes the transcriptome, as this method was consistent with our assessment of $CD4^+$ T cell phenotype and allowed for a holistic investigation of many different key aspects of genes downstream of TLR4. Moreover, RT-qPCR provided more quantifiable data than other densitometry based methods. As mRNA abundance precedes protein abundance, RT-qPCR is generally accepted as a functional indicator of pathway activity. However, RT-qPCR did not allow for the investigation of protein phosphorylation. Although many proteins in our TLR4 downstream effector panel are not phosphorylated in the TLR4 signaling cascade, investigating the proteomic regulation of STAT3 and mTOR via western blotting would be an excellent follow-up experiment, as the measurement of phosphorylation of these proteins would provide valuable data further characterizing pEV-to-T cell signaling via TLR4.

In this work, we demonstrated that TLR4 played a role in pEV-to-T cell signaling. TLR4 was chosen because it can dramatically alter $CD4^+$ T cell phenotype, and because previous research has demonstrated the role of TLR4 and/or MyD88 in determination of macrophage phenotype based on biomaterial scaffold pore size and stiffness[53,54]. Moreover, current grants and unpublished data implicate TLR4 and MyD88 in the host response to PTS and sEV signaling within this context. Despite this, it is clear that other cell signaling pathways played a role in pEV-to-T cell signaling. Based on our results, we suggest that the exploration of the role of other TLRs (e.g. TLR2 and TLR3) and the TCR in pEV-to-T cell signaling would be valuable follow-up experiments. Specifically, RT-qPCR after pEV treatment of splenic T cells from mice with a non-functional TCR or other TLRs using our T cell panel would provide excellent initial

experiments to investigate this phenomenon.

Our studies demonstrated the abundance of Gal3, Gal9, GRP78, and GRP94 within or on the surface of pEVs. While the goal of these studies was to provide the groundwork demonstrating the abundance of these under studied proteins on and within pEVs, explication of the specific role of each of these proteins within pEV-to-T cell signaling would provide a compelling line of questioning for future experimentation. Specifically, treating splenic T cells with pEVs harvested from mice lacking Gal3 or Gal9 would improve the understanding of the roles of these signaling factors in pEV-to-T cell signaling. GRP78 and GRP94 knockout in mice, however, proves embryonically lethal—therefore, GRP78 or GRP94 heterozygotes (which thereby express lower quantities of GRP proteins) could be used to generate pEVs for T cell treatment[259,260]. These studies would further the understanding of these controversial and under characterized signaling factors within sEV research.

Chapter 9: References

1. Ratner BD, Bryant SJ. Biomaterials: Where We Have Been and Where We Are Going. *Annual Review of Biomedical Engineering*. 2004;6(1):41-75. doi:10.1146/annurev.bioeng.6.040803.140027

2. Lüscher TF, Steffel J, Eberli FR, et al. Drug-Eluting Stent and Coronary Thrombosis: Biological Mechanisms and Clinical Implications. *Circulation*. 2007;115(8):1051-1058. doi:10.1161/CIRCULATIONAHA.106.675934

3. Castagnola E, Maggiolini E, Ceseracciu L, et al. pHEMA Encapsulated PEDOT-PSS-CNT Microsphere Microelectrodes for Recording Single Unit Activity in the Brain. *Front Neurosci*. 2016;10. doi:10.3389/fnins.2016.00151

4. Tjellström A, Lindström J, Nylén O, Albrektsson T, Brånemark PI. Directly bone-anchored implants for fixation of aural epistheses. *Biomaterials*. 1983;4(1):55-57. doi:10.1016/0142-9612(83)90072-8

5. Lloyd AW, Faragher RGA, Denyer SP. Ocular biomaterials and implants. *Biomaterials*. 2001;22(8):769-785. doi:10.1016/S0142-9612(00)00237-4

6. Liang Y, Luan X, Liu X. Recent advances in periodontal regeneration: A biomaterial perspective. *Bioactive Materials*. 2020;5(2):297-308. doi:10.1016/j.bioactmat.2020.02.012

7. Hu CY, Yoon TR. Recent updates for biomaterials used in total hip arthroplasty. *Biomaterials Research*. 2018;22(1):33. doi:10.1186/s40824-018-0144-8

8. Metcalfe AD, Ferguson MWJ. Bioengineering skin using mechanisms of regeneration and repair. *Biomaterials*. 2007;28(34):5100-5113. doi:10.1016/j.biomaterials.2007.07.031

9. Sussman EM, Halpin MC, Muster J, Moon RT, Ratner BD. Porous implants modulate healing and induce shifts in local macrophage polarization in the foreign body reaction. *Ann Biomed Eng*. 2014;42(7):1508-1516. doi:10.1007/s10439-013-0933-0

10. Bryers JD, Giachelli CM, Ratner BD. Engineering Biomaterials to Integrate and Heal: The Biocompatibility Paradigm Shifts. *Biotechnol Bioeng*. 2012;109(8):1898-1911. doi:10.1002/bit.24559

11. Higgins DM, Basaraba RJ, Hohnbaum AC, Lee EJ, Grainger DW, Gonzalez-Juarrero M. Localized Immunosuppressive Environment in the Foreign Body Response to Implanted Biomaterials. *The American Journal of Pathology*. 2009;175(1):161-170. doi:10.2353/ajpath.2009.080962

12. Mooney JE, Rolfe BE, Osborne GW, et al. Cellular Plasticity of Inflammatory Myeloid Cells in the Peritoneal Foreign Body Response. *The American Journal of Pathology*. 2010;176(1):369-380. doi:10.2353/ajpath.2010.090545

13. Anderson JM, Rodriguez A, Chang DT. FOREIGN BODY REACTION TO BIOMATERIALS. *Semin Immunol*. 2008;20(2):86-100. doi:10.1016/j.smim.2007.11.004

14. Lee JM, Kim YJ. Foreign body granulomas after the use of dermal fillers: pathophysiology, clinical appearance, histologic features, and treatment. *Arch Plast Surg*. 2015;42(2):232-239. doi:10.5999/aps.2015.42.2.232

15. Witherel CE, Abebayehu D, Barker TH, Spiller KL. Macrophage and Fibroblast Interactions in Biomaterial-Mediated Fibrosis. *Adv Healthc Mater*. 2019;8(4):e1801451. doi:10.1002/adhm.201801451

16. Mosser DM, Edwards JP. Exploring the full spectrum of macrophage activation. *Nature Reviews Immunology*. 2008;8(12):958-969. doi:10.1038/nri2448

17. Spiller KL, Anfang RR, Spiller KJ, et al. The role of macrophage phenotype in vascularization of tissue engineering scaffolds. *Biomaterials*. 2014;35(15):4477-4488. doi:10.1016/j.biomaterials.2014.02.012

18. Braga TT, Agudelo JSH, Camara NOS. Macrophages During the Fibrotic Process: M2 as Friend and Foe. *Front Immunol*. 2015;6. doi:10.3389/fimmu.2015.00602

19. Hou J, Shi J, Chen L, et al. M2 macrophages promote myofibroblast differentiation of LR-MSCs and are associated with pulmonary fibrogenesis. *Cell Communication and Signaling*. 2018;16(1):89. doi:10.1186/s12964-018-0300-8

20. Brown BN, Londono R, Tottey S, et al. Macrophage phenotype as a predictor of constructive remodeling following the implantation of biologically derived surgical mesh materials. *Acta Biomater*. 2012;8(3):978-987. doi:10.1016/j.actbio.2011.11.031

21. Lotti F, Ranieri F, Vadalà G, Zollo L, Di Pino G. Invasive Intraneural Interfaces: Foreign Body Reaction Issues. *Front Neurosci*. 2017;11. doi:10.3389/fnins.2017.00497

22. O'Dwyer J, Wylie R, Cryan SA, Duffy GP, Dolan EB. Chapter 24 - Cardiac responses to biomaterials. In: Mozafari M, ed. *Handbook of Biomaterials Biocompatibility*. Woodhead Publishing Series in Biomaterials. Woodhead Publishing; 2020:573-599. doi:10.1016/B978-0-08-102967-1.00025-6

23. Anderson JM, Niven H, Pelagalli J, Olanoff LS, Jones RD. The role of the fibrous capsule in the function of implanted drug-polymer sustained release systems. *Journal of Biomedical Materials Research*. 1981;15(6):889-902. doi:https://doi.org/10.1002/jbm.820150613

24. Sutherland K, Mahoney JR, Coury AJ, Eaton JW. Degradation of biomaterials by phagocyte-derived oxidants. *Journal of Clinical Investigation*. 1993;92(5):2360-2367. doi:10.1172/JCI116841

25. Tang L, Eaton J. Inflammatory Responses to Biomaterials. *American Journal of Clinical Pathology*. 1995;103:466-471. doi:10.1093/ajcp/103.4.466

26. Ratner BD. A paradigm shift: biomaterials that heal. *Polym Int*. 2007;56(10):1183-1185. doi:10.1002/pi.2319

27. Narayan RJ. The next generation of biomaterial development. *Philosophical Transactions of the Royal Society A: Mathematical, Physical and Engineering Sciences*. 2010;368(1917):1831-1837. doi:10.1098/rsta.2010.0001

28. Ratner BD, Hoffman AS, Schoen FJ, Lemons JE. Introduction - Biomaterials Science: An Evolving, Multidisciplinary Endeavor. In: Ratner BD, Hoffman AS, Schoen FJ, Lemons JE, eds. *Biomaterials Science (Third Edition)*. Academic Press; 2013:xxv-xxxix. doi:10.1016/B978-0-08-087780-8.00153-4

29. Hench LL, Thompson I. Twenty-first century challenges for biomaterials. *J R Soc Interface*. 2010;7(Suppl 4):S379-S391. doi:10.1098/rsif.2010.0151.focus

30. Navarro M, Michiardi A, Castaño O, Planell JA. Biomaterials in orthopaedics. *Journal of The Royal Society Interface*. 2008;5(27):1137-1158. doi:10.1098/rsif.2008.0151

31. Meyers SR, Grinstaff MW. Biocompatible and bioactive surface modifications for prolonged in vivo efficacy. *Chem Rev*. 2012;112(3). doi:10.1021/cr2000916

32. Hench LL. Third-Generation Biomedical Materials. *Science*. 2002;295(5557):1014-1017. doi:10.1126/science.1067404

33. Zamecnik CR, Levy ES, Lowe MM, Zirak B, Rosenblum MD, Desai TA. An Injectable Cytokine Trap for Local Treatment of Autoimmune Disease. *Biomaterials*. 2020;230:119626. doi:10.1016/j.biomaterials.2019.119626

34. Hanson S, D'Souza RN, Hematti P. Biomaterial–Mesenchymal Stem Cell Constructs for Immunomodulation in Composite Tissue Engineering. *Tissue Engineering Part A*. 2014;20(15-16):2162-2168. doi:10.1089/ten.tea.2013.0359

35. Sackett SD, Tremmel DM, Ma F, et al. Extracellular matrix scaffold and hydrogel derived from decellularized and delipidized human pancreas. *Scientific Reports*. 2018;8(1):10452. doi:10.1038/s41598-018-28857-1

36. Dziki JL, Badylak SF. Immunomodulatory biomaterials. *Current Opinion in Biomedical Engineering*. 2018;6:51-57. doi:10.1016/j.cobme.2018.02.005

37. Sadtler K, Estrellas K, Allen BW, et al. Developing a pro-regenerative biomaterial scaffold microenvironment requires T helper 2 cells. *Science*. 2016;352(6283):366-370. doi:10.1126/science.aad9272

38. Marshall AJ, Ratner BD. Quantitative characterization of sphere-templated porous biomaterials. *AIChE Journal*. 2005;51(4):1221-1232. doi:10.1002/aic.10390

39. Fukano Y, Usui ML, Underwood RA, et al. Epidermal and dermal integration into sphere-templated porous poly(2-hydroxyethyl methacrylate) implants in mice. *J Biomed Mater Res A*. 2010;94(4):1172-1186. doi:10.1002/jbm.a.32798

40. Isenhath SN, Fukano Y, Usui ML, et al. A mouse model to evaluate the interface between skin and a percutaneous device. *J Biomed Mater Res A*. 2007;83(4):915-922. doi:10.1002/jbm.a.31391

41. Galperin A, Long TJ, Garty S, Ratner BD. Synthesis and fabrication of a degradable poly(N-isopropyl acrylamide) scaffold for tissue engineering applications. *J Biomed Mater Res A*. 2013;101(3):775-786. doi:10.1002/jbm.a.34380

42. Atzet S, Curtin S, Trinh P, Bryant S, Ratner B. Degradable poly(2-hydroxyethyl methacrylate)-co-polycaprolactone hydrogels for tissue engineering scaffolds. *Biomacromolecules*. 2008;9(12):3370-3377. doi:10.1021/bm800686h

43. Chen R, Ma H, Zhang L, Bryers JD. Precision-porous templated scaffolds of varying pore size drive dendritic cell activation. *Biotechnology and Bioengineering*. 2018;115(4):1086-1095. doi:10.1002/bit.26532

44. Teng W, Long TJ, Zhang Q, Yao K, Shen TT, Ratner BD. A tough, precision-porous hydrogel scaffold: ophthalmologic applications. *Biomaterials*. 2014;35(32):8916-8926. doi:10.1016/j.biomaterials.2014.07.013

45. Dryg I. *Modulating Neuroinflammation with Porous Templated Scaffolds*. Thesis. 2019. Accessed March 19, 2021. https://digital.lib.washington.edu:443/researchworks/handle/1773/44721

46. Prager J, Adams CF, Delaney AM, et al. Stiffness-matched biomaterial implants for cell delivery: clinical, intraoperative ultrasound elastography provides a ‘target’ stiffness for hydrogel synthesis in spinal cord injury. *J Tissue Eng*. 2020;11:2041731420934806. doi:10.1177/2041731420934806

47. Fukano Y, Knowles NG, Usui ML, et al. Characterization of an in vitro model for evaluating the interface between skin and percutaneous biomaterials. *Wound Repair Regen*. 2006;14(4):484-491. doi:10.1111/j.1743-6109.2006.00138.x

48. Thomson KS, Korte FS, Giachelli CM, Ratner BD, Regnier M, Scatena M. Prevascularized Microtemplated Fibrin Scaffolds for Cardiac Tissue Engineering Applications. *Tissue Eng Part A*. 2013;19(7-8):967-977. doi:10.1089/ten.tea.2012.0286

49. Galperin A, Oldinski RA, Florczyk SJ, Bryers JD, Zhang M, Ratner BD. Integrated Bi-Layered Scaffold for Osteochondral Tissue Engineering. *Advanced Healthcare Materials*. 2013;2(6):872-883. doi:10.1002/adhm.201200345

50. Bota PCS, Collie AMB, Puolakkainen P, et al. Biomaterial topography alters healing in vivo and monocyte/macrophage activation in vitro. *J Biomed Mater Res A*. 2010;95(2):649-657. doi:10.1002/jbm.a.32893

51. Madden LR, Mortisen DJ, Sussman EM, et al. Proangiogenic scaffolds as functional templates for cardiac tissue engineering. *Proc Natl Acad Sci USA*. 2010;107(34):15211-15216. doi:10.1073/pnas.1006442107

52. Tylek T, Blum C, Hrynevich A, et al. Precisely defined fiber scaffolds with 40 *μ* m porosity induce elongation driven M2-like polarization of human macrophages. *Biofabrication*. 2020;12(2):025007. doi:10.1088/1758-5090/ab5f4e

53. Garg K, Pullen NA, Oskeritzian CA, Ryan JJ, Bowlin GL. Macrophage functional polarization (M1/M2) in response to varying fiber and pore dimensions of electrospun scaffolds. *Biomaterials*. 2013;34(18):4439-4451. doi:10.1016/j.biomaterials.2013.02.065

54. Previtera ML, Sengupta A. Substrate Stiffness Regulates Proinflammatory Mediator Production through TLR4 Activity in Macrophages. *PLOS ONE*. 2015;10(12):e0145813. doi:10.1371/journal.pone.0145813

55. Marshall A, Irvin CA, Barker T, Sage EH, Hauch KD, Ratner B. Biomaterials with tightly controlled pore size that promote vascular in-growth. *Polym Prepr*. 2004;228:U386.

56. Ratner BD, Marshall A. Novel Porous Biomaterials. Published online March 27, 2008. Accessed February 12, 2019. https://patents.google.com/patent/US20080075752/en

57. Chen R. *Development of Biomaterial Porous Scaffolds for Dendritic Cell Modulation and MRNA Delivery*. Thesis. 2017. Accessed May 18, 2022. https://digital.lib.washington.edu:443/researchworks/handle/1773/40487

58. Long TJ, Takeno M, Sprenger CC, Plymate SR, Ratner BD. Capillary force seeding of sphere-templated hydrogels for tissue-engineered prostate cancer xenografts. *Tissue Eng Part C Methods*. 2013;19(9):738-744. doi:10.1089/ten.TEC.2012.0388

59. Pourcet B, Pineda-Torra I. Transcriptional regulation of macrophage arginase 1 expression and its role in atherosclerosis. *Trends in Cardiovascular Medicine*. 2013;23(5):143-152. doi:10.1016/j.tcm.2012.10.003

60. Pesce JT, Ramalingam TR, Mentink-Kane MM, et al. Arginase-1–Expressing Macrophages Suppress Th2 Cytokine–Driven Inflammation and Fibrosis. *PLOS Pathogens*. 2009;5(4):e1000371. doi:10.1371/journal.ppat.1000371

61. Qian F, Deng J, Lee YG, et al. The transcription factor PU.1 promotes alternative macrophage polarization and asthmatic airway inflammation. *Journal of Molecular Cell Biology*. 2015;7(6):557-567. doi:10.1093/jmcb/mjv042

62. Mariani E, Lisignoli G, Borzì RM, Pulsatelli L. Biomaterials: Foreign Bodies or Tuners for the Immune Response? *International Journal of Molecular Sciences*. 2019;20(3):636. doi:10.3390/ijms20030636

63. Sadtler K, Wolf MT, Ganguly S, et al. Divergent immune responses to synthetic and biological scaffolds. *Biomaterials*. 2019;192:405-415. doi:10.1016/j.biomaterials.2018.11.002

64. Rodriguez A, Voskerician G, Meyerson H, MacEwan SR, Anderson JM. T cell subset distributions following primary and secondary implantation at subcutaneous biomaterial implant

sites. *Journal of Biomedical Materials Research Part A*. 2008;85A(2):556-565. doi:10.1002/jbm.a.31562

65. Dievernich A, Achenbach P, Davies L, Klinge U. Characterization of innate and adaptive immune cells involved in the foreign body reaction to polypropylene meshes in the human abdomen. *Hernia*. Published online March 31, 2021. doi:10.1007/s10029-021-02396-7

66. Engelhardt E, Toksoy A, Goebeler M, Debus S, Bröcker EB, Gillitzer R. Chemokines IL-8, GROα, MCP-1, IP-10, and Mig Are Sequentially and Differentially Expressed During Phase-Specific Infiltration of Leukocyte Subsets in Human Wound Healing. *The American Journal of Pathology*. 1998;153(6):1849-1860. doi:10.1016/S0002-9440(10)65699-4

67. Blotnick S, Peoples GE, Freeman MR, Eberlein TJ, Klagsbrun M. T lymphocytes synthesize and export heparin-binding epidermal growth factor-like growth factor and basic fibroblast growth factor, mitogens for vascular cells and fibroblasts: differential production and release by CD4+ and CD8+ T cells. *PNAS*. 1994;91(8):2890-2894. doi:10.1073/pnas.91.8.2890

68. Julier Z, Park AJ, Briquez PS, Martino MM. Promoting tissue regeneration by modulating the immune system. *Acta Biomaterialia*. 2017;53:13-28. doi:10.1016/j.actbio.2017.01.056

69. Nosbaum A, Prevel N, Truong HA, et al. Cutting Edge: Regulatory T Cells Facilitate Cutaneous Wound Healing. *The Journal of Immunology*. 2016;196(5):2010-2014. doi:10.4049/jimmunol.1502139

70. Lin X, Chen M, Liu Y, et al. Advances in distinguishing natural from induced Foxp3+ regulatory T cells. *Int J Clin Exp Pathol*. 2013;6(2):116-123.

71. Sakaguchi S, Yamaguchi T, Nomura T, Ono M. Regulatory T Cells and Immune Tolerance. *Cell*. 2008;133(5):775-787. doi:10.1016/j.cell.2008.05.009

72. Murphy TJ, Ni Choileain N, Zang Y, Mannick JA, Lederer JA. CD4+CD25+ regulatory T cells control innate immune reactivity after injury. *J Immunol*. 2005;174(5):2957-2963. doi:10.4049/jimmunol.174.5.2957

73. Carbone F, Nencioni A, Mach F, Vuilleumier N, Montecucco F. Pathophysiological role of neutrophils in acute myocardial infarction. *Thromb Haemost*. 2013;110(3):501-514. doi:10.1160/TH13-03-0211

74. Weirather J, Hofmann UDW, Beyersdorf N, et al. Foxp3+ CD4+ T cells improve healing after myocardial infarction by modulating monocyte/macrophage differentiation. *Circ Res*. 2014;115(1):55-67. doi:10.1161/CIRCRESAHA.115.303895

75. Dombrowski Y, O'Hagan T, Dittmer M, et al. Regulatory T cells promote myelin regeneration in the central nervous system. *Nat Neurosci*. 2017;20(5):674-680. doi:10.1038/nn.4528

76. Castiglioni A, Corna G, Rigamonti E, et al. FOXP3+ T Cells Recruited to Sites of Sterile Skeletal Muscle Injury Regulate the Fate of Satellite Cells and Guide Effective Tissue Regeneration. *PLoS One*. 2015;10(6). doi:10.1371/journal.pone.0128094

77. Ali N, Zirak B, Rodriguez RS, et al. Regulatory T Cells in Skin Facilitate Epithelial Stem Cell Differentiation. *Cell*. 2017;169(6):1119-1129.e11. doi:10.1016/j.cell.2017.05.002

78. Lei H, Schmidt-Bleek K, Dienelt A, Reinke P, Volk HD. Regulatory T cell-mediated anti-inflammatory effects promote successful tissue repair in both indirect and direct manners. *Front Pharmacol*. 2015;6. doi:10.3389/fphar.2015.00184

79. Hotchkiss KM, Clark NM, Olivares-Navarrete R. Macrophage response to hydrophilic biomaterials regulates MSC recruitment and T-helper cell populations. *Biomaterials*. 2018;182:202-215. doi:10.1016/j.biomaterials.2018.08.029

80. Peloso A, Urbani L, Cravedi P, et al. THE HUMAN PANCREAS AS A SOURCE OF PRO-TOLEROGENIC EXTRACELLULAR MATRIX SCAFFOLD FOR A NEW GENERATION BIO-ARTIFICIAL ENDOCRINE PANCREAS. *Ann Surg*. 2016;264(1):169-179. doi:10.1097/SLA.0000000000001364

81. Shen P, Chen Y, Luo S, et al. Applications of biomaterials for immunosuppression in tissue repair and regeneration. *Acta Biomaterialia*. 2021;126:31-44. doi:10.1016/j.actbio.2021.03.019

82. Shah NJ, Mao AS, Shih TY, et al. An injectable bone marrow–like scaffold enhances T cell immunity after hematopoietic stem cell transplantation. *Nature Biotechnology*. 2019;37(3):293-302. doi:10.1038/s41587-019-0017-2

83. Allen JE, Wynn TA. Evolution of Th2 Immunity: A Rapid Repair Response to Tissue Destructive Pathogens. *PLOS Pathogens*. 2011;7(5):e1002003. doi:10.1371/journal.ppat.1002003

84. Wynn T. Cellular and molecular mechanisms of fibrosis. *J Pathol*. 2008;214(2):199-210. doi:10.1002/path.2277

85. Rodriguez A, MacEwan SR, Meyerson H, Kirk JT, Anderson JM. The Foreign Body Reaction in T cell deficient mice. *J Biomed Mater Res A*. 2009;90(1). doi:10.1002/jbm.a.32050

86. Shalev I, Schmelzle M, Robson SC, Levy G. Making Sense of Regulatory T Cell Suppressive Function. *Semin Immunol*. 2011;23(4):282-292. doi:10.1016/j.smim.2011.04.003

87. Beissert S, Schwarz A, Schwarz T. Regulatory T Cells. *Journal of Investigative Dermatology*. 2006;126(1):15-24. doi:10.1038/sj.jid.5700004

88. Brockmann L, Giannou AD, Gagliani N, Huber S. Regulation of TH17 Cells and Associated Cytokines in Wound Healing, Tissue Regeneration, and Carcinogenesis. *International Journal of Molecular Sciences*. 2017;18(5):1033. doi:10.3390/ijms18051033

89. Sheikh Z, Brooks PJ, Barzilay O, Fine N, Glogauer M. Macrophages, Foreign Body Giant Cells and Their Response to Implantable Biomaterials. *Materials*. 2015;8(9):5671-5701. doi:10.3390/ma8095269

90. Chung L, Maestas DR, Lebid A, et al. Interleukin 17 and senescent cells regulate the foreign body response to synthetic material implants in mice and humans. *Science Translational Medicine*. 2020;12(539). doi:10.1126/scitranslmed.aax3799

91. Sommerfeld SD, Cherry C, Schwab RM, et al. Interleukin-36γ–producing macrophages drive IL-17–mediated fibrosis. *Science Immunology*. 2019;4(40). doi:10.1126/sciimmunol.aax4783

92. Słomka A, Urban SK, Lukacs-Kornek V, Żekanowska E, Kornek M. Large Extracellular Vesicles: Have We Found the Holy Grail of Inflammation? *Front Immunol*. 2018;9. doi:10.3389/fimmu.2018.02723

93. Zhang X, Hubal MJ, Kraus VB. Immune cell extracellular vesicles and their mitochondrial content decline with ageing. *Immun Ageing*. 2020;17. doi:10.1186/s12979-019-0172-9

94. Quesenberry PJ, Aliotta J, Deregibus MC, Camussi G. Role of extracellular RNA-carrying vesicles in cell differentiation and reprogramming. *Stem Cell Res Ther*. 2015;6. doi:10.1186/s13287-015-0150-x

95. Lamichhane TN, Sokic S, Schardt JS, Raiker RS, Lin JW, Jay SM. Emerging Roles for Extracellular Vesicles in Tissue Engineering and Regenerative Medicine. *Tissue Engineering Part B: Reviews*. 2014;21(1):45-54. doi:10.1089/ten.teb.2014.0300

96. Mulcahy LA, Pink RC, Carter DRF. Routes and mechanisms of extracellular vesicle uptake. *Journal of Extracellular Vesicles*. 2014;3(1):24641. doi:10.3402/jev.v3.24641

97. de Gassart A, Geminard C, Fevrier B, Raposo G, Vidal M. Lipid raft-associated protein sorting in exosomes. *Blood*. 2003;102(13):4336-4344. doi:10.1182/blood-2003-03-0871

98. Boilard E. Extracellular vesicles and their content in bioactive lipid mediators: more than a sack of microRNA. *J Lipid Res*. 2018;59(11):2037-2046. doi:10.1194/jlr.R084640

99. Morhayim J, Ghebes CA, Erkeland SJ, et al. Identification of osteolineage cell-derived extracellular vesicle cargo implicated in hematopoietic support. *The FASEB Journal*. 2020;34(4):5435-5452. doi:10.1096/fj.201902610R

100. Álvarez V, Sánchez-Margallo FM, Macías-García B, et al. The immunomodulatory activity of extracellular vesicles derived from endometrial mesenchymal stem cells on CD4+ T cells is partially mediated by TGFbeta. *J Tissue Eng Regen Med*. 2018;12(10):2088-2098. doi:10.1002/term.2743

101. Théry C, Witwer KW, Aikawa E, et al. Minimal information for studies of extracellular vesicles 2018 (MISEV2018): a position statement of the International Society for Extracellular Vesicles and update of the MISEV2014 guidelines. *Journal of Extracellular Vesicles*. 2018;7(1):1535750. doi:10.1080/20013078.2018.1535750

102. Kim D ki, Nishida H, An SY, Shetty AK, Bartosh TJ, Prockop DJ. Chromatographically isolated CD63+CD81+ extracellular vesicles from mesenchymal stromal cells rescue cognitive impairments after TBI. *PNAS*. 2016;113(1):170-175. doi:10.1073/pnas.1522297113

103. Bjørge IM, Kim SY, Mano JF, Kalionis B, Chrzanowski W. Extracellular vesicles, exosomes and shedding vesicles in regenerative medicine – a new paradigm for tissue repair. *Biomater Sci*. 2017;6(1):60-78. doi:10.1039/C7BM00479F

104. Abels ER, Breakefield XO. Introduction to Extracellular Vesicles: Biogenesis, RNA Cargo Selection, Content, Release, and Uptake. *Cell Mol Neurobiol*. 2016;36(3):301-312. doi:10.1007/s10571-016-0366-z

105. Meldolesi J. Exosomes and Ectosomes in Intercellular Communication. *Current Biology*. 2018;28(8):R435-R444. doi:10.1016/j.cub.2018.01.059

106. Robbins PD, Morelli AE. Regulation of immune responses by extracellular vesicles. *Nat Rev Immunol*. 2014;14(3):195-208. doi:10.1038/nri3622

107. Urbanelli L, Magini A, Buratta S, et al. Signaling Pathways in Exosomes Biogenesis, Secretion and Fate. *Genes*. 2013;4(2):152-170. doi:10.3390/genes4020152

108. Lim JP, Gleeson PA. Macropinocytosis: an endocytic pathway for internalising large gulps. *Immunology & Cell Biology*. 2011;89(8):836-843. doi:https://doi.org/10.1038/icb.2011.20

109. Canton J. Macropinocytosis: New Insights Into Its Underappreciated Role in Innate Immune Cell Surveillance. *Front Immunol*. 2018;9. doi:10.3389/fimmu.2018.02286

110. Davis DM. Intercellular transfer of cell-surface proteins is common and can affect many stages of an immune response. *Nature Reviews Immunology*. 2007;7(3):238-243. doi:10.1038/nri2020

111. Rackov G, Garcia-Romero N, Esteban-Rubio S, Carrión-Navarro J, Belda-Iniesta C, Ayuso-Sacido A. Vesicle-Mediated Control of Cell Function: The Role of Extracellular Matrix and Microenvironment. *Front Physiol*. 2018;9. doi:10.3389/fphys.2018.00651

112. Zhou X, Xie F, Wang L, et al. The function and clinical application of extracellular vesicles in innate immune regulation. *Cellular & Molecular Immunology*. 2020;17(4):323-334. doi:10.1038/s41423-020-0391-1

113. Latifkar A, Hur YH, Sanchez JC, Cerione RA, Antonyak MA. New insights into extracellular vesicle biogenesis and function. *J Cell Sci*. 2019;132(13). doi:10.1242/jcs.222406

114. Nguyen DG, Booth A, Gould SJ, Hildreth JEK. Evidence That HIV Budding in Primary Macrophages Occurs through the Exosome Release Pathway. *J Biol Chem*. 2003;278(52):52347-52354. doi:10.1074/jbc.M309009200

115. Anand PK. Exosomal membrane molecules are potent immune response modulators. *Commun Integr Biol*. 2010;3(5):405-408. doi:10.4161/cib.3.5.12474

116. Yu B, Shao H, Su C, et al. Exosomes derived from MSCs ameliorate retinal laser injury partially by inhibition of MCP-1. *Scientific Reports*. 2016;6:34562. doi:10.1038/srep34562

117. Anderson JD, Johansson HJ, Graham CS, et al. Comprehensive Proteomic Analysis of Mesenchymal Stem Cell Exosomes Reveals Modulation of Angiogenesis via Nuclear Factor-KappaB Signaling. *STEM CELLS*. 34(3):601-613. doi:10.1002/stem.2298

118. Hajrasouliha AR, Jiang G, Lu Q, et al. Exosomes from Retinal Astrocytes Contain Antiangiogenic Components That Inhibit Laser-induced Choroidal Neovascularization. *J Biol Chem*. 2013;288(39):28058-28067. doi:10.1074/jbc.M113.470765

119. Papp K, Végh P, Prechl J, et al. B lymphocytes and macrophages release cell membrane deposited C3-fragments on exosomes with T cell response-enhancing capacity. *Mol Immunol*. 2008;45(8):2343-2351. doi:10.1016/j.molimm.2007.11.021

120. Agarwal A, Fanelli G, Letizia M, et al. Regulatory T Cell-Derived Exosomes: Possible Therapeutic and Diagnostic Tools in Transplantation. *Front Immunol*. 2014;5. doi:10.3389/fimmu.2014.00555

121. Okoye IS, Coomes SM, Pelly VS, et al. MicroRNA-containing T-regulatory-cell-derived exosomes suppress pathogenic T helper 1 cells. *Immunity*. 2014;41(1):89-103. doi:10.1016/j.immuni.2014.05.019

122. Shi R, Wang PY, Li XY, et al. Exosomal levels of miRNA-21 from cerebrospinal fluids associated with poor prognosis and tumor recurrence of glioma patients. *Oncotarget*. 2015;6(29):26971-26981.

123. Chan BD, Wong WY, Lee MML, et al. Exosomes in Inflammation and Inflammatory Disease. *PROTEOMICS*. 2019;19(8):1800149. doi:https://doi.org/10.1002/pmic.201800149

124. Jean-Toussaint R, Lin Z, Tian Y, et al. Therapeutic and prophylactic effects of macrophage-derived small extracellular vesicles in the attenuation of inflammatory pain. *Brain, Behavior, and Immunity*. 2021;94. doi:10.1016/j.bbi.2021.02.005

125. Console L, Scalise M, Indiveri C. Exosomes in inflammation and role as biomarkers. *Clinica Chimica Acta*. 2019;488:165-171. doi:10.1016/j.cca.2018.11.009

126. Fang SB, Zhang HY, Meng XC, et al. Small extracellular vesicles derived from human MSCs prevent allergic airway inflammation via immunomodulation on pulmonary macrophages. *Cell Death & Disease*. 2020;11(6):1-15. doi:10.1038/s41419-020-2606-x

127. Takeuchi S, Tsuchiya A, Iwasawa T, et al. Small extracellular vesicles derived from interferon-γ pre-conditioned mesenchymal stromal cells effectively treat liver fibrosis. *npj Regenerative Medicine*. 2021;6(1):1-14. doi:10.1038/s41536-021-00132-4

128. Toh WS, Zhang B, Lai RC, Lim SK. Immune regulatory targets of mesenchymal stromal cell exosomes/small extracellular vesicles in tissue regeneration. *Cytotherapy*. 2018;20(12):1419-1426. doi:10.1016/j.jcyt.2018.09.008

129. Wang Y, Zhao M, Liu S, et al. Macrophage-derived extracellular vesicles: diverse mediators of pathology and therapeutics in multiple diseases. *Cell Death & Disease*. 2020;11(10):1-18. doi:10.1038/s41419-020-03127-z

130. Lan J, Sun L, Xu F, et al. M2 Macrophage-Derived Exosomes Promote Cell Migration and Invasion in Colon Cancer. *Cancer Res*. 2019;79(1):146-158. doi:10.1158/0008-5472.CAN-18-0014

131. McDonald MK, Tian Y, Qureshi RA, et al. Functional significance of macrophage-derived exosomes in inflammation and pain. *PAIN*®. 2014;155(8):1527-1539. doi:10.1016/j.pain.2014.04.029

132. Cheng L, Wang Y, Huang L. Exosomes from M1-Polarized Macrophages Potentiate the Cancer Vaccine by Creating a Pro-inflammatory Microenvironment in the Lymph Node. *Mol Ther*. 2017;25(7):1665-1675. doi:10.1016/j.ymthe.2017.02.007

133. Wu J, Gao W, Tang Q, et al. M2 Macrophage–Derived Exosomes Facilitate HCC Metastasis by Transferring αMβ2 Integrin to Tumor Cells. *Hepatology*. 2021;73(4):1365-1380. doi:https://doi.org/10.1002/hep.31432

134. Du T, Yang CL, Ge MR, et al. M1 Macrophage Derived Exosomes Aggravate Experimental Autoimmune Neuritis via Modulating Th1 Response. *Front Immunol*. 2020;11. doi:10.3389/fimmu.2020.01603

135. Todorova Dilyana, Simoncini Stéphanie, Lacroix Romaric, Sabatier Florence, Dignat-George Françoise. Extracellular Vesicles in Angiogenesis. *Circulation Research*. 2017;120(10):1658-1673. doi:10.1161/CIRCRESAHA.117.309681

136. Atienzar-Aroca S, Flores-Bellver M, Serrano-Heras G, et al. Oxidative stress in retinal pigment epithelium cells increases exosome secretion and promotes angiogenesis in

endothelial cells. *Journal of Cellular and Molecular Medicine*. 2016;20(8):1457-1466. doi:https://doi.org/10.1111/jcmm.12834

137. Hettich BF, Greenwald MBY, Werner S, Leroux JC. Exosomes for Wound Healing: Purification Optimization and Identification of Bioactive Components. *Advanced Science*. 2020;7(23):2002596. doi:https://doi.org/10.1002/advs.202002596

138. Hoang DH, Nguyen TD, Nguyen HP, et al. Differential Wound Healing Capacity of Mesenchymal Stem Cell-Derived Exosomes Originated From Bone Marrow, Adipose Tissue and Umbilical Cord Under Serum- and Xeno-Free Condition. *Front Mol Biosci*. 2020;7. doi:10.3389/fmolb.2020.00119

139. Cardoso RMS, Rodrigues SC, Gomes CF, et al. Development of an optimized and scalable method for isolation of umbilical cord blood-derived small extracellular vesicles for future clinical use. *STEM CELLS Translational Medicine*. n/a(n/a). doi:https://doi.org/10.1002/sctm.20-0376

140. Zhou X, Brown BA, Siegel AP, et al. Exosome-Mediated Crosstalk between Keratinocytes and Macrophages in Cutaneous Wound Healing. *ACS Nano*. 2020;14(10):12732-12748. doi:10.1021/acsnano.0c03064

141. Nojima H, Freeman CM, Schuster RM, et al. Hepatocyte exosomes mediate liver repair and regeneration via sphingosine-1-phosphate. *J Hepatol*. 2016;64(1):60-68. doi:10.1016/j.jhep.2015.07.030

142. Liu Y, Ma Y, Zhang J, Yuan Y, Wang J. Exosomes: A Novel Therapeutic Agent for Cartilage and Bone Tissue Regeneration. *Dose Response*. 2019;17(4). doi:10.1177/1559325819892702

143. Wang J, Rong Y, Ji C, et al. MicroRNA-421-3p-abundant small extracellular vesicles derived from M2 bone marrow-derived macrophages attenuate apoptosis and promote motor function recovery via inhibition of mTOR in spinal cord injury. *Journal of Nanobiotechnology*. 2020;18(1). doi:10.1186/s12951-020-00630-5

144. Murali VP, Holmes CA. Biomaterial-based extracellular vesicle delivery for therapeutic applications. *Acta Biomaterialia*. 2021;124:88-107. doi:10.1016/j.actbio.2021.01.010

145. Liu L, Liu Y, Feng C, et al. Lithium-containing biomaterials stimulate bone marrow stromal cell-derived exosomal miR-130a secretion to promote angiogenesis. *Biomaterials*. 2019;192:523-536. doi:10.1016/j.biomaterials.2018.11.007

146. Rider MA, Hurwitz SN, Meckes DG. ExtraPEG: A Polyethylene Glycol-Based Method for Enrichment of Extracellular Vesicles. *Scientific Reports*. 2016;6(1):23978. doi:10.1038/srep23978

147. Théry C, Duban L, Segura E, Véron P, Lantz O, Amigorena S. Indirect activation of naïve CD4+ T cells by dendritic cell–derived exosomes. *Nat Immunol*. 2002;3(12):1156-1162. doi:10.1038/ni854

148. Hao S, Yuan J, Xiang J. Nonspecific CD4(+) T cells with uptake of antigen-specific dendritic cell-released exosomes stimulate antigen-specific CD8(+) CTL responses and long-term T cell memory. *J Leukoc Biol*. 2007;82(4):829-838. doi:10.1189/jlb.0407249

149. Undale AH, van den Elsen PJ, Celis E. Antigen-independent acquisition of MHC class II molecules by human T lymphocytes. *International Immunology*. 2004;16(10):1523-1533. doi:10.1093/intimm/dxh154

150. Bhatnagar S, Shinagawa K, Castellino FJ, Schorey JS. Exosomes released from macrophages infected with intracellular pathogens stimulate a proinflammatory response in vitro and in vivo. *Blood*. 2007;110(9):3234-3244. doi:10.1182/blood-2007-03-079152

151. Bhatnagar S, Schorey JS. Exosomes Released from Infected Macrophages Contain Mycobacterium avium Glycopeptidolipids and Are Proinflammatory. *J Biol Chem*. 2007;282(35):25779-25789. doi:10.1074/jbc.M702277200

152. Giri PK, Schorey JS. Exosomes Derived from M. Bovis BCG Infected Macrophages Activate Antigen-Specific CD4+ and CD8+ T Cells In Vitro and In Vivo. *PLOS ONE*. 2008;3(6):e2461. doi:10.1371/journal.pone.0002461

153. Zhou J, Li X, Wu X, et al. Exosomes Released from Tumor-Associated Macrophages Transfer miRNAs That Induce a Treg/Th17 Cell Imbalance in Epithelial Ovarian Cancer. *Cancer Immunol Res*. 2018;6(12):1578-1592. doi:10.1158/2326-6066.CIR-17-0479

154. Liu H, Liang Z, Wang F, et al. Intestinal CD14+ Macrophages Protect CD4+ T Cells From Activation-induced Cell Death via Exosomal Membrane TNF in Crohn's Disease. *Journal of Crohn's and Colitis*. 2020;14(11):1619-1631. doi:10.1093/ecco-jcc/jjaa083

155. Anel A, Gallego-Lleyda A, de Miguel D, Naval J, Martínez-Lostao L. Role of Exosomes in the Regulation of T-Cell Mediated Immune Responses and in Autoimmune Disease. *Cells*. 2019;8(2). doi:10.3390/cells8020154

156. Engela AU, Baan CC, Peeters AMA, Weimar W, Hoogduijn MJ. Interaction between adipose tissue-derived mesenchymal stem cells and regulatory T-cells. *Cell Transplant*. 2013;22(1):41-54. doi:10.3727/096368912X636984

157. Tone Y, Furuuchi K, Kojima Y, Tykocinski ML, Greene MI, Tone M. Smad3 and NFAT cooperate to induce Foxp3 expression through its enhancer. *Nat Immunol*. 2008;9(2):194-202. doi:10.1038/ni1549

158. Trinchieri G. Regulatory Role of T Cells Producing both Interferon γ and Interleukin 10 in Persistent Infection. *J Exp Med*. 2001;194(10):f53-f57.

159. Levine AG, Mendoza A, Hemmers S, et al. Stability and function of regulatory T cells expressing the transcription factor T-bet. *Nature*. 2017;546(7658):421-425. doi:10.1038/nature22360

160. MacLeod H, Wetzler LM. T cell activation by TLRs: a role for TLRs in the adaptive immune response. *Sci STKE*. 2007;2007(402):pe48. doi:10.1126/stke.4022007pe48

161. Okeke EB, Okwor I, Uzonna JE. Regulatory T cells restrain CD4+ T cells from causing unregulated immune activation and hypersensitivity to lipopolysaccharide challenge. *J Immunol*. 2014;193(2):655-662. doi:10.4049/jimmunol.1303064

162. Zanin-Zhorov A, Cohen IR. Signaling via TLR2 and TLR4 Directly Down-Regulates T Cell Effector Functions: The Regulatory Face of Danger Signals. *Front Immunol*. 2013;4. doi:10.3389/fimmu.2013.00211

163. Reynolds JM, Martinez GJ, Chung Y, Dong C. Toll-like receptor 4 signaling in T cells promotes autoimmune inflammation. *Proc Natl Acad Sci U S A*. 2012;109(32):13064-13069. doi:10.1073/pnas.1120585109

164. Lu YC, Yeh WC, Ohashi PS. LPS/TLR4 signal transduction pathway. *Cytokine*. 2008;42(2):145-151. doi:10.1016/j.cyto.2008.01.006

165. Bretz NP, Ridinger J, Rupp AK, et al. Body Fluid Exosomes Promote Secretion of Inflammatory Cytokines in Monocytic Cells via Toll-like Receptor Signaling *. *Journal of Biological Chemistry*. 2013;288(51):36691-36702. doi:10.1074/jbc.M113.512806

166. Honda K, Takaoka A, Taniguchi T. Type I Inteferon Gene Induction by the Interferon Regulatory Factor Family of Transcription Factors. *Immunity*. 2006;25(3):349-360. doi:10.1016/j.immuni.2006.08.009

167. Huber JP, Farrar JD. Regulation of effector and memory T-cell functions by type I interferon. *Immunology*. 2011;132(4):466-474. doi:10.1111/j.1365-2567.2011.03412.x

168. Gangaplara A, Martens C, Dahlstrom E, et al. Type I interferon signaling attenuates regulatory T cell function in viral infection and in the tumor microenvironment. *PLOS Pathogens*. 2018;14(4):e1006985. doi:10.1371/journal.ppat.1006985

169. Ying H, Da L, Yu-xiu S, et al. TLR4 Mediates MAPK–STAT3 Axis Activation in Bladder Epithelial Cells. *Inflammation*. 2013;36(5):1064-1074. doi:10.1007/s10753-013-9638-7

170. Brieger A, Rink L, Haase H. Differential Regulation of TLR-Dependent MyD88 and TRIF Signaling Pathways by Free Zinc Ions. *The Journal of Immunology*. 2013;191(4):1808-1817. doi:10.4049/jimmunol.1301261

171. Tsai MH, Pai LM, Lee CK. Fine-Tuning of Type I Interferon Response by STAT3. *Frontiers in Immunology*. 2019;10:1448. doi:10.3389/fimmu.2019.01448

172. Pallandre JR, Brillard E, Créhange G, et al. Role of STAT3 in CD4+CD25+FOXP3+ Regulatory Lymphocyte Generation: Implications in Graft-versus-Host Disease and Antitumor Immunity. *The Journal of Immunology*. 2007;179(11):7593-7604. doi:10.4049/jimmunol.179.11.7593

173. Gaddis DE, Michalek SM, Katz J. TLR4 Signaling via MyD88 and TRIF Differentially Shape the CD4+ T Cell Response to Porphyromonas gingivalis Hemagglutinin B. *The Journal of Immunology*. 2011;186(10):5772-5783. doi:10.4049/jimmunol.1003192

174. Stewart CA, Metheny H, Iida N, et al. Interferon-dependent IL-10 production by Tregs limits tumor Th17 inflammation. *J Clin Invest*. 2013;123(11):4859-4874. doi:10.1172/JCI65180

175. González-Navajas JM, Fine S, Law J, et al. TLR4 signaling in effector $CD4^+$ T cells regulates TCR activation and experimental colitis in mice. *J Clin Invest*. 2010;120(2):570-581. doi:10.1172/JCI40055

176. Deenick EK, Pelham SJ, Kane A, Ma CS. Signal Transducer and Activator of Transcription 3 Control of Human T and B Cell Responses. *Front Immunol*. 2018;9. doi:10.3389/fimmu.2018.00168

177. Deng Z bin, Poliakov A, Hardy RW, et al. Adipose Tissue Exosome-Like Vesicles Mediate Activation of Macrophage-Induced Insulin Resistance. *Diabetes*. 2009;58(11):2498-2505. doi:10.2337/db09-0216

178. Laird MHW, Rhee SH, Perkins DJ, et al. TLR4/MyD88/PI3K interactions regulate TLR4 signaling. *J Leukoc Biol*. 2009;85(6):966-977. doi:10.1189/jlb.1208763

179. Pourrajab F, Yazdi MB, Zarch MB, Zarch MB, Hekmatimoghaddam S. Cross talk of the first-line defense TLRs with PI3K/Akt pathway, in preconditioning therapeutic approach. *Mol Cell Ther*. 2015;3:4. doi:10.1186/s40591-015-0041-7

180. Zanin-Zhorov A, Tal-Lapidot G, Cahalon L, et al. Cutting Edge: T Cells Respond to Lipopolysaccharide Innately via TLR4 Signaling. *The Journal of Immunology*. 2007;179(1):41-44. doi:10.4049/jimmunol.179.1.41

181. Caramalho I, Lopes-Carvalho T, Ostler D, Zelenay S, Haury M, Demengeot J. Regulatory T Cells Selectively Express Toll-like Receptors and Are Activated by Lipopolysaccharide. *J Exp Med*. 2003;197(4):403-411. doi:10.1084/jem.20021633

182. Chapman NM, Chi H. mTOR signaling, Tregs and immune modulation. *Immunotherapy*. 2014;6(12):1295-1311. doi:10.2217/imt.14.84

183. Da-wa ZX, Jun M, Chao-Zheng L, et al. Exosomes Derived from M2 Macrophages Exert a Therapeutic Effect via Inhibition of the PI3K/AKT/mTOR Pathway in Rats with Knee Osteoarthritic. *BioMed Research International*. 2021;2021:e7218067. doi:10.1155/2021/7218067

184. Hady TF, Hwang B, Pusic AD, et al. Uniform 40-μm-pore diameter precision templated scaffolds promote a pro-healing host response by extracellular vesicle immune communication. *Journal of Tissue Engineering and Regenerative Medicine*. 2021;15(1):24-36. doi:10.1002/term.3160

185. Kalra H, Simpson RJ, Ji H, et al. Vesiclepedia: A Compendium for Extracellular Vesicles with Continuous Community Annotation. *PLOS Biology*. 2012;10(12):e1001450. doi:10.1371/journal.pbio.1001450

186. Keerthikumar S, Chisanga D, Ariyaratne D, et al. ExoCarta: A Web-Based Compendium of Exosomal Cargo. *Journal of Molecular Biology*. 2016;428(4):688-692. doi:10.1016/j.jmb.2015.09.019

187. Pocsfalvi G, Stanly C, Vilasi A, et al. Mass spectrometry of extracellular vesicles. *Mass Spectrometry Reviews*. 2016;35(1):3-21. doi:10.1002/mas.21457

188. Mastoridis S, Bertolino GM, Whitehouse G, Dazzi F, Sanchez-Fueyo A, Martinez-Llordella M. Multiparametric Analysis of Circulating Exosomes and Other Small Extracellular

Vesicles by Advanced Imaging Flow Cytometry. *Front Immunol*. 2018;9. doi:10.3389/fimmu.2018.01583

189. Furmanik M, van Gorp R, Whitehead M, et al. Endoplasmic Reticulum Stress Mediates Vascular Smooth Muscle Cell Calcification via Increased Release of Grp78 (Glucose-Regulated Protein, 78 kDa)-Loaded Extracellular Vesicles. *Arteriosclerosis, Thrombosis, and Vascular Biology*. 2021;41(2):898-914. doi:10.1161/ATVBAHA.120.315506

190. Hasnain SZ, Lourie R, Das I, Chen ACH, McGuckin MA. The interplay between endoplasmic reticulum stress and inflammation. *Immunol Cell Biol*. 2012;90(3):260-270. doi:10.1038/icb.2011.112

191. Chaumonnot K, Masson S, Sikner H, et al. The HSP GRP94 interacts with macrophage intracellular complement C3 and impacts M2 profile during ER stress. *Cell Death Dis*. 2021;12(1):1-15. doi:10.1038/s41419-020-03288-x

192. Vig S, Buitinga M, Rondas D, et al. Cytokine-induced translocation of GRP78 to the plasma membrane triggers a pro-apoptotic feedback loop in pancreatic beta cells. *Cell Death Dis*. 2019;10(4):1-13. doi:10.1038/s41419-019-1518-0

193. Chanteloup G, Cordonnier M, Isambert N, et al. Membrane-bound exosomal HSP70 as a biomarker for detection and monitoring of malignant solid tumours: a pilot study. *Pilot and Feasibility Studies*. 2020;6(1):35. doi:10.1186/s40814-020-00577-2

194. Gonzalez-Begne M, Lu B, Han X, et al. Proteomic Analysis of Human Parotid Gland Exosomes by Multidimensional Protein Identification Technology (MudPIT). *J Proteome Res*. 2009;8(3):1304-1314. doi:10.1021/pr800658c

195. Taha EA, Ono K, Eguchi T. Roles of Extracellular HSPs as Biomarkers in Immune Surveillance and Immune Evasion. *International Journal of Molecular Sciences*. 2019;20(18):4588. doi:10.3390/ijms20184588

196. Marzec M, Eletto D, Argon Y. GRP94: an HSP90-like protein specialized for protein folding and quality control in the Endoplasmic Reticulum. *Biochim Biophys Acta*. 2012;1823(3):774-787. doi:10.1016/j.bbamcr.2011.10.013

197. Radons J, Multhoff G. Immunostimulatory functions of membrane-bound and exported heat shock protein 70. *Exerc Immunol Rev*. 2005;11:17-33.

198. Burguillos MA, Svensson M, Schulte T, et al. Microglia-Secreted Galectin-3 Acts as a Toll-like Receptor 4 Ligand and Contributes to Microglial Activation. *Cell Reports*. 2015;10(9):1626-1638. doi:10.1016/j.celrep.2015.02.012

199. Hsu DK, Chernyavsky AI, Chen HY, Yu L, Grando SA, Liu FT. Endogenous Galectin-3 Is Localized in Membrane Lipid Rafts and Regulates Migration of Dendritic Cells. *Journal of Investigative Dermatology*. 2009;129(3):573-583. doi:10.1038/jid.2008.276

200. Henderson NC, Sethi T. The regulation of inflammation by galectin-3. *Immunol Rev*. 2009;230(1):160-171. doi:10.1111/j.1600-065X.2009.00794.x

201. Klibi J, Niki T, Riedel A, et al. Blood diffusion and Th1-suppressive effects of galectin-9–containing exosomes released by Epstein-Barr virus–infected nasopharyngeal carcinoma cells. *Blood*. 2009;113(9):1957-1966. doi:10.1182/blood-2008-02-142596

202. Liu FT, Hsu DK, Zuberi RI, Kuwabara I, Chi EY, Henderson WR. Expression and function of galectin-3, a beta-galactoside-binding lectin, in human monocytes and macrophages. *Am J Pathol*. 1995;147(4):1016-1028.

203. Gorski JP, Liu FT, Artigues A, Castagna LF, Osdoby P. New Alternatively Spliced Form of Galectin-3, a Member of the β-Galactoside-binding Animal Lectin Family, Contains a Predicted Transmembrane-spanning Domain and a Leucine Zipper Motif. *J Biol Chem*. 2002;277(21):18840-18848. doi:10.1074/jbc.M109578200

204. Stillman BN, Hsu DK, Pang M, et al. Galectin-3 and Galectin-1 Bind Distinct Cell Surface Glycoprotein Receptors to Induce T Cell Death. *The Journal of Immunology*. 2006;176(2):778-789. doi:10.4049/jimmunol.176.2.778

205. Bänfer S, Schneider D, Dewes J, et al. Molecular mechanism to recruit galectin-3 into multivesicular bodies for polarized exosomal secretion. *PNAS*. 2018;115(19):E4396-E4405. doi:10.1073/pnas.1718921115

206. Flores-Ibarra A, Vértesy S, Medrano FJ, Gabius HJ, Romero A. Crystallization of a human galectin-3 variant with two ordered segments in the shortened N-terminal tail. *Scientific Reports*. 2018;8(1):9835. doi:10.1038/s41598-018-28235-x

207. Warger T, Hilf N, Rechtsteiner G, et al. Interaction of TLR2 and TLR4 Ligands with the N-terminal Domain of Gp96 Amplifies Innate and Adaptive Immune Responses. *J Biol Chem*. 2006;281(32):22545-22553. doi:10.1074/jbc.M502900200

208. Zhou W, Chen X, Hu Q, Chen X, Chen Y, Huang L. Galectin-3 activates TLR4/NF-κB signaling to promote lung adenocarcinoma cell proliferation through activating lncRNA-NEAT1 expression. *BMC Cancer*. 2018;18:580. doi:10.1186/s12885-018-4461-z

209. Qin K, Ma S, Li H, et al. GRP78 Impairs Production of Lipopolysaccharide-Induced Cytokines by Interaction with CD14. *Front Immunol*. 2017;8. doi:10.3389/fimmu.2017.00579

210. Shive CL, Jiang W, Anthony DD, Lederman MM. Soluble CD14 is a nonspecific marker of monocyte activation. *AIDS*. 2015;29(10):1263-1265. doi:10.1097/QAD.0000000000000735

211. Chettimada S, Lorenz DR, Misra V, et al. Exosome markers associated with immune activation and oxidative stress in HIV patients on antiretroviral therapy. *Scientific Reports*. 2018;8(1):7227. doi:10.1038/s41598-018-25515-4

212. Burel JG, Pomaznoy M, Lindestam Arlehamn CS, et al. Circulating T cell-monocyte complexes are markers of immune perturbations. *eLife*. 8. doi:10.7554/eLife.46045

213. Anderson AC, Joller N, Kuchroo VK. Lag-3, Tim-3, and TIGIT: Co-inhibitory Receptors with Specialized Functions in Immune Regulation. *Immunity*. 2016;44(5):989-1004. doi:10.1016/j.immuni.2016.05.001

214. Corthay A. How do Regulatory T Cells Work? *Scand J Immunol*. 2009;70(4):326-336. doi:10.1111/j.1365-3083.2009.02308.x

215. Andrews LP, Marciscano AE, Drake CG, Vignali DAA. LAG3 (CD223) as a Cancer Immunotherapy Target. *Immunol Rev*. 2017;276(1):80-96. doi:10.1111/imr.12519

216. Huang CT, Workman CJ, Flies D, et al. Role of LAG-3 in Regulatory T Cells. *Immunity*. 2004;21(4):503-513. doi:10.1016/j.immuni.2004.08.010

217. Maruhashi T, Okazaki I mi, Sugiura D, et al. LAG-3 inhibits the activation of CD4 + T cells that recognize stable pMHCII through its conformation-dependent recognition of pMHCII. *Nature Immunology*. 2018;19(12):1415-1426. doi:10.1038/s41590-018-0217-9

218. Zhu C, Anderson AC, Schubart A, et al. The Tim-3 ligand galectin-9 negatively regulates T helper type 1 immunity. *Nature Immunology*. 2005;6(12):1245-1252. doi:10.1038/ni1271

219. Tomkowicz B, Walsh E, Cotty A, et al. TIM-3 Suppresses Anti-CD3/CD28-Induced TCR Activation and IL-2 Expression through the NFAT Signaling Pathway. *PLoS One*. 2015;10(10). doi:10.1371/journal.pone.0140694

220. Das M, Zhu C, Kuchroo VK. Tim-3 and its role in regulating anti-tumor immunity. *Immunological Reviews*. 2017;276(1):97-111. doi:10.1111/imr.12520

221. Joller N, Hafler JP, Brynedal B, et al. Cutting Edge: TIGIT Has T Cell-Intrinsic Inhibitory Functions. *The Journal of Immunology*. 2011;186(3):1338-1342. doi:10.4049/jimmunol.1003081

222. Chen F, Xu Y, Chen Y, Shan S. TIGIT enhances CD4+ regulatory T-cell response and mediates immune suppression in a murine ovarian cancer model. *Cancer Med*. 2020;9(10):3584-3591. doi:10.1002/cam4.2976

223. Zhao W, Dong Y, Wu C, Ma Y, Jin Y, Ji Y. TIGIT overexpression diminishes the function of CD4 T cells and ameliorates the severity of rheumatoid arthritis in mouse models. *Exp Cell Res*. 2016;340(1):132-138. doi:10.1016/j.yexcr.2015.12.002

224. Mao L, Hou H, Wu S, et al. TIGIT signalling pathway negatively regulates CD4+ T-cell responses in systemic lupus erythematosus. *Immunology*. 2017;151(3):280-290. doi:10.1111/imm.12715

225. Cummings RD. T Cells Are Smad'ly in Love with Galectin-9. *Immunity*. 2014;41(2):171-173. doi:10.1016/j.immuni.2014.08.001

226. Wu C, Thalhamer T, Franca RF, et al. Galectin-9-CD44 interaction enhances stability and function of adaptive regulatory T cells. *Immunity*. 2014;41(2):270-282. doi:10.1016/j.immuni.2014.06.011

227. Eng JK, Hoopmann MR, Jahan TA, Egertson JD, Noble WS, MacCoss MJ. A Deeper Look into Comet—Implementation and Features. *J Am Soc Mass Spectrom*. 2015;26(11):1865-1874. doi:10.1007/s13361-015-1179-x

228. Zybailov BL, Florens L, Washburn MP. Quantitative shotgun proteomics using a protease with broad specificity and normalized spectral abundance factors. *Mol BioSyst*. 2007;3(5):354-360. doi:10.1039/B701483J

229. Chen EY, Tan CM, Kou Y, et al. Enrichr: interactive and collaborative HTML5 gene list enrichment analysis tool. *BMC Bioinformatics*. 2013;14:128. doi:10.1186/1471-2105-14-128

230. Kuleshov MV, Jones MR, Rouillard AD, et al. Enrichr: a comprehensive gene set enrichment analysis web server 2016 update. *Nucleic Acids Res*. 2016;44(W1):W90-97. doi:10.1093/nar/gkw377

231. Xie Z, Bailey A, Kuleshov MV, et al. Gene Set Knowledge Discovery with Enrichr. *Current Protocols*. 2021;1(3):e90. doi:10.1002/cpz1.90

232. Thomas PD, Kejariwal A, Guo N, et al. Applications for protein sequence–function evolution data: mRNA/protein expression analysis and coding SNP scoring tools. *Nucleic Acids Research*. 2006;34(suppl_2):W645-W650. doi:10.1093/nar/gkl229

233. Thomas PD, Campbell MJ, Kejariwal A, et al. PANTHER: A Library of Protein Families and Subfamilies Indexed by Function. *Genome Res*. 2003;13(9):2129-2141. doi:10.1101/gr.772403

234. Mi H, Ebert D, Muruganujan A, et al. PANTHER version 16: a revised family classification, tree-based classification tool, enhancer regions and extensive API. *Nucleic Acids Research*. 2021;49(D1):D394-D403. doi:10.1093/nar/gkaa1106

235. Mi H, Thomas P. PANTHER Pathway: an ontology-based pathway database coupled with data analysis tools. *Methods Mol Biol*. 2009;563:123-140. doi:10.1007/978-1-60761-175-2_7

236. Mi H, Dong Q, Muruganujan A, Gaudet P, Lewis S, Thomas PD. PANTHER version 7: improved phylogenetic trees, orthologs and collaboration with the Gene Ontology Consortium. *Nucleic Acids Research*. 2010;38(suppl_1):D204-D210. doi:10.1093/nar/gkp1019

237. Kugeratski FG, Hodge K, Lilla S, et al. Quantitative proteomics identifies the core proteome of exosomes with syntenin-1 as the highest abundant protein and a putative universal biomarker. *Nat Cell Biol*. 2021;23(6):631-641. doi:10.1038/s41556-021-00693-y

238. Bertoni A, Alabiso O, Galetto AS, Baldanzi G. Integrins in T Cell Physiology. *Int J Mol Sci*. 2018;19(2):485. doi:10.3390/ijms19020485

239. Shimaoka M, Kawamoto E, Gaowa A, Okamoto T, Park EJ. Connexins and Integrins in Exosomes. *Cancers (Basel)*. 2019;11(1). doi:10.3390/cancers11010106

240. Buzás EI, Tóth EÁ, Sódar BW, Szabó-Taylor KÉ. Molecular interactions at the surface of extracellular vesicles. *Semin Immunopathol*. 2018;40(5):453-464. doi:10.1007/s00281-018-0682-0

241. Nishikimi A, Koyama YI, Ishihara S, et al. Collagen-derived peptides modulate CD4+ T-cell differentiation and suppress allergic responses in mice. *Immun Inflamm Dis*. 2018;6(2):245-255. doi:10.1002/iid3.213

242. Nojima Y, Humphries MJ, Mould AP, et al. VLA-4 mediates CD3-dependent CD4+ T cell activation via the CS1 alternatively spliced domain of fibronectin. *Journal of Experimental Medicine*. 1990;172(4):1185-1192. doi:10.1084/jem.172.4.1185

243. Bokoch GM. Regulation of innate immunity by Rho GTPases. *Trends in Cell Biology*. 2005;15(3):163-171. doi:10.1016/j.tcb.2005.01.002

244. Chirathaworn C, Kohlmeier JE, Tibbetts SA, Rumsey LM, Chan MA, Benedict SH. Stimulation Through Intercellular Adhesion Molecule-1 Provides a Second Signal for T Cell Activation. *The Journal of Immunology*. 2002;168(11):5530-5537. doi:10.4049/jimmunol.168.11.5530

245. Ling GS, Bennett J, Woollard KJ, et al. Integrin CD11b positively regulates TLR4-induced signalling pathways in dendritic cells but not in macrophages. *Nat Commun*. 2014;5(1):3039. doi:10.1038/ncomms4039

246. Lukácsi S, Gerecsei T, Balázs K, et al. The differential role of CR3 (CD11b/CD18) and CR4 (CD11c/CD18) in the adherence, migration and podosome formation of human macrophages and dendritic cells under inflammatory conditions. *PLoS One*. 2020;15(5):e0232432. doi:10.1371/journal.pone.0232432

247. Tauseef M, Newaz M, Al-Ghoul W, Aqil M, Fazal N. TLR4 Activation of Small GTPase RhoA Signaling Mediates Endotoxin-Induced Endothelial Barrier Dysfunction. *The Journal of Immunology*. 2017;198(1 Supplement):206.27-206.27.

248. Chan NR, Hwang B, Ratner BD, Bryers JD. Monocytes contribute to a pro-healing response in 40 μm diameter uniform-pore, precision-templated scaffolds. *Journal of Tissue Engineering and Regenerative Medicine*. n/a(n/a). doi:10.1002/term.3280

249. Muto J, Yamasaki K, Taylor KR, Gallo RL. Engagement of CD44 by hyaluronan suppresses TLR4 signaling and the septic response to LPS. *Molecular immunology*. 2009;47(2-3):449. doi:10.1016/j.molimm.2009.08.026

250. Zanoni I, Ostuni R, Marek LR, et al. CD14 controls the LPS-induced endocytosis of Toll-like Receptor 4. *Cell*. 2011;147(4):868-880. doi:10.1016/j.cell.2011.09.051

251. Bastiaansen AJNM, Karper JC, Wezel A, et al. TLR4 Accessory Molecule RP105 (CD180) Regulates Monocyte-Driven Arteriogenesis in a Murine Hind Limb Ischemia Model. *PLoS One*. 2014;9(6):e99882. doi:10.1371/journal.pone.0099882

252. Cao D, Luo J, Chen D, et al. CD36 regulates lipopolysaccharide-induced signaling pathways and mediates the internalization of Escherichia coli in cooperation with TLR4 in goat mammary gland epithelial cells. *Sci Rep*. 2016;6(1):23132. doi:10.1038/srep23132

253. Pushpakumar S, Ren L, Kundu S, Gamon A, Tyagi SC, Sen U. Toll-like Receptor 4 Deficiency Reduces Oxidative Stress and Macrophage Mediated Inflammation in Hypertensive Kidney. *Sci Rep*. 2017;7(1):6349. doi:10.1038/s41598-017-06484-6

254. Shi L, Lim JY, Kam LC. Substrate Stiffness Modulates Human Regulatory T Cell Induction and Metabolism. In: *Published Abstracts*. Society for Biomaterials; 2022:95. Accessed March 22, 2022. http://abstracts.biomaterials.org/data/2022_js/sfb_js.pdf

255. Massie A, Boland E, Kapás L, Szentirmai É. Mice Lacking Alternatively Activated (M2) Macrophages Show Impairments in Restorative Sleep after Sleep Loss and in Cold Environment. *Sci Rep*. 2018;8(1):8625. doi:10.1038/s41598-018-26758-x

256. Iqbal F, Lupieri A, Aikawa M, Aikawa E. Harnessing Single-Cell RNA Sequencing to Better Understand How Diseased Cells Behave the Way They Do in Cardiovascular Disease. *Arteriosclerosis, Thrombosis, and Vascular Biology*. 2021;41(2):585-600. doi:10.1161/ATVBAHA.120.314776

257. Catalano M, O'Driscoll L. Inhibiting extracellular vesicles formation and release: a review of EV inhibitors. *J Extracell Vesicles*. 9(1):1703244. doi:10.1080/20013078.2019.1703244

258. Shelke GV, Lässer C, Gho YS, Lötvall J. Importance of exosome depletion protocols to eliminate functional and RNA-containing extracellular vesicles from fetal bovine serum. *J Extracell Vesicles*. 2014;3:10.3402/jev.v3.24783. doi:10.3402/jev.v3.24783

259. Luo S, Mao C, Lee B, Lee AS. GRP78/BiP Is Required for Cell Proliferation and Protecting the Inner Cell Mass from Apoptosis during Early Mouse Embryonic Development. *Mol Cell Biol*. 2006;26(15):5688-5697. doi:10.1128/MCB.00779-06

260. Mao C, Wang M, Luo B, et al. Targeted Mutation of the Mouse Grp94 Gene Disrupts Development and Perturbs Endoplasmic Reticulum Stress Signaling. *PLoS One*. 2010;5(5):e10852. doi:10.1371/journal.pone.0010852